

FINAL REPORT FOR GRANT

Composition Measurements at the Magnetopause and in the Plasma Mantle

Grant NAGW-4049

(for the period from 15 August 1994 ending 31 January 1998)

This final report describes activities under NASA grant NAGW-4049 to Lockheed Missiles and Space Company. The report covers the entire period of the grant from 15 August 1994 to 31 January 1998. The original grant was for 3 years ending in August 1997; however the grant was extended 6 months to accomodate additional data analysis that added significantly to the scientific results. This is a grant under the NASA Supporting Research and Technology Program for the analysis and interpretation of the combined scientific data from the ISEE-1 Plasma Composition Experiment and the AMPTE/CCE Hot Plasma Composition Experiment. These combined data sets were used in a study of the Earth's magnetopause to develop a fundamental understanding of plasma entry and dynamics at the boundary and formation and maintenance of the low latitude boundary layer under a variety of solar wind and magnetospheric conditions and at a wide range of local times.

The first part of this final report contains a summary of the data analysis activities. Appendix A contains preprints of publications submitted during the lifetime of the grant.

DATA ANALYSIS ACTIVITIES

The analysis of the composition data under this grant proceeded along two different lines. Magnetopause crossings in the ISEE-1 Plasma Composition Data were processed into a usable data set. The AMPTE/CCE hot plasma composition data were already in a usable form and were simply analyzed. In the next two sections, the analysis of these two data sets is described separately.

ISEE-1 Plasma Composition Data

The ISEE-1 plasma composition data for this study consists of approximately 100 magnetopause crossings which span local times from pre-dawn to pre-dusk. These magnetopause crossings occurred during intervals when the plasma composition experiment was in its high time resolution mode. During the 3 year study, data from other experiments were accumulated and analyzed. These data included the magnetometer plots and 1 min time resolution Fast Plasma Experiment data and needed to interpret the lower time resolution (~30 s to 1 min) composition data. Finally, in the last months of the study, an additional set of data were accumulated looking specifically at the dusk flank magnetopause in relatively low time resolution. Again, the high resolution FPE data were used as a guide to determine the location of the spacecraft.

These data were analyzed for the first of several studies concerning plasma entry and dynamics at the Earth's magnetopause. This first study started with the accumulation of the higher time resolution data. The focus of the first study was the entry of solar wind plasma into the low latitude boundary layer. In this study, the He^{2+} density change across the magnetopause was evaluated to determine when and where changes in the solar wind composition occur in the transition from the magnetosheath to the magnetosphere. The results of this study were summarized in a paper submitted to the Journal of Geophysical Research entitled Solar wind composition changes across the Earth's magnetopause. This paper was published in the Journal of Geophysical Research and appears in the reference list.

In addition to the gathering of supporting data for the ISEE plasma composition experiment, the data from this experiment was used in two more studies of the magnetopause. These studies demonstrate the importance of the composition data in understanding magnetopause dynamics. These papers were also published and also appear in the reference list below.

A second study that directly involved the composition observations is the study of kinetic aspects of magnetopause crossings during times when reconnection was occurring. Specifically, reflected magnetosheath and magnetospheric ions are observed outside and inside of the magnetosphere, respectively. Using data from several crossings, a reflection coefficient for the magnetosheath ions and for the magnetospheric ions was estimated to be ~30%. Specific events near the subsolar region were used. A paper discussing the results of this study was published in the second year and is listed in the reference list below.

AMPTE/CCE Hot Plasma Composition Data

The AMPTE hot plasma composition data for this study consists of a small group of magnetopause crossings (~27 crossings or groups of crossings) that was used to study plasma entry into the magnetosphere under high solar wind dynamic pressure conditions. The specific study of these data concerned a follow-on study of the magnetopause structure during northward IMF conditions. In particular, this study focused on the different ion signatures observed in the low latitude boundary layer under these IMF conditions. Two types of ion distributions were observed. The first was a distribution that appeared to convect into the low latitude boundary layer when the field line the ions were on reconnected at high latitudes. These ion distributions were distinguished by their low energy component and lack of a low energy cutoff velocity. A second type of distribution was observed where the low energy ion distribution had a low energy cutoff in one direction along the magnetic field. These distributions may have been the result of reconnection equatorward of the cusp. The low energy cutoff in the ion distribution allowed an estimate of the location of the reconnection site. This site appeared to be far from the spacecraft but clearly equatorward of the cusp. A paper summarizing these results was submitted to the Journal of

Geophysical Research in the second year. It was published in the third year of the study and appears in the reference list.

Finally, the last months of the contract were used to provide a part of a chapter of a book that will be entitled *Source and Loss Processes in the Magnetosphere*. This book will appear in early 1999 when other contributions are accumulated and the book editor has revised these contributions.

In addition to this last work, another study was started that focuses on the dusk flank magnetopause. The dusk flank magnetosphere exhibits significant structure. The mantle density on the flanks can range over several orders of magnitude. It is sometimes difficult to distinguish the dusk flank magnetopause on the basis of ion data alone because the magnetosheath and mantle plasmas often have nearly similar densities, temperatures, and bulk flow velocities at the magnetopause. However, the mantle can often be distinguished by the presence of O⁺ that originates from the ionosphere or plasmasphere. We have used ISEE Fast Plasma Experiment and Plasma Composition Experiment data to examine the composition of the mantle and to study a set of transitions from the mantle to the plasma sheet where mantle-like and plasma sheet-like plasmas overlap. In this mixed region the mantle-like plasma typically has almost zero convection speed. The results of this investigation indicate that the variability of the mantle density is entirely due to variability in the solar wind component (H⁺ and He²⁺): the ionospheric plasma (O⁺) density is usually roughly constant in the mantle. Similarly, the mantle-like, but non-flowing, plasma found in the mixed region is entirely of solar wind origin. These results have important implications for the origin and transport of plasma at the flank magnetosphere. A paper describing these results will be submitted to the Geophysical Research Letters in the near future.

SUMMARY OF PUBLICATIONS

The following papers were published during the 3 year study. Reprints of all papers are attached:

Gary, S. P., D. Winske, M. E. McKean, S. A. Fuselier, R. E. Denton, and B. J. Anderson, Proton Anisotropies upstream of the magnetopause, in *Physics of the Magnetopause*, ed. P. Song, B. U. Ö Sonnerup, M. F. Thomsen and M. Scholer, *Geophysical Monograph Series 90*, p. 181-187, AGU, Washington D.C., 1995.

Fuselier, S. A., Kinetic aspects of reconnection at the magnetopause, in *Physics of the Magnetopause*, ed. P. Song, B. U. Ö Sonnerup, M. F. Thomsen and M. Scholer, *Geophysical Monograph Series 90*, p. 181-187, AGU, Washington D.C., 1995.

Eastman, T. E., S. A. Fuselier, and J. T. Gosling, Local time dependence of magnetopause microstructure, *J. Geophys. Res.*, *101*, 49-57, 1996.

Fuselier, S. A., B. J. Anderson, T. G. Onsager, Electron and ion signatures of field line topology at the low shear magnetopause, *J. Geophys. Res.*, *102*, 4847-4863, 1997

Fuselier, S. A., E. G. Shelley, and O. W. Lennartsson, Solar wind composition changes across the Earth's magnetopause, *J. Geophys. Res.*, *102*, 275-283, 1997.

Anderson, B. J., T.-D. Phan, and S. A. Fuselier, Relationships between plasma depletion and subsolar reconnection, *J. Geophys. Res.*, *102*, 9531-9542, 1997.

SUMMARY OF PRESENTATIONS

Fuselier, S. A., Particle Signatures of Magnetic Topology at the Magnetopause, AMPTE/CCE Observations, 27 October, 1994, Palo Alto, CA.

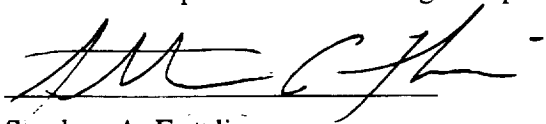
Fuselier, S. A., B. J. Anderson, and T. G. Onsager, Particle Signatures of Magnetic Topology at the Magnetopause, AMPTE/CCE Observations, Fall AGU, San Francisco, CA, 1995.

Fuselier, S. A., E. G. Shelley, and O. W. Lennartsson, Solar wind composition changes across the Earth's magnetopause, Spring AGU, Baltimore, MD, 1996.

FINAL SUMMARY AND FUTURE WORK

The work in the last few months of this grant indicated that the ISEE and AMPTE composition data is still an important asset to the space physics community. With the loss of Cluster, these data still represent the only composition data at the low latitude magnetopause. The recent launch of Equator-S will provide exciting new high resolution data. However, this spacecraft had a difficult start and is not tracked 100% of the time. Furthermore, it is currently in the tail and will not provide new composition measurements at the magnetopause for another 8 months. Even when it does, it will not match the breath of the ISEE data set which spans over 5 years and contains hundreds of magnetopause crossings. Thus, the ISEE and AMPTE data sets should be analyzed further. Our hope is to submit a new proposal for supporting research and technology funds so that this research can be continued. With a favorable review, issues such as the ultimate fate of the

plasma in the low latitude boundary layer will be addressed. This will close the loop of the entry of solar wind plasma into the magnetosphere.

A handwritten signature in black ink, appearing to read 'SAF', written over a horizontal line.

Stephen A. Fuselier

APPENDIX A: PUBLICATIONS

Proton Anisotropies Upstream of the Magnetopause

S. Peter Gary,¹ Dan Winske,¹ Michael E. McKean,² Stephen A. Fuselier,³

Richard E. Denton,⁴ and Brian J. Anderson⁵

Boundary conditions for magnetopause processes such as reconnection can be understood by studying the properties of magnetosheath plasma as it flows toward this transition. This paper reviews the role of electromagnetic ion cyclotron instabilities in constraining ion temperature anisotropies in the magnetosheath. Linear Vlasov theory and hybrid computer simulations have demonstrated that the upper bound on the proton temperature anisotropy observed in the subsolar magnetosheath and which is represented by an inverse correlation between that anisotropy and the parallel proton β is due to wave-particle scattering by ion cyclotron anisotropy instabilities. Recent research on this topic is reviewed and the application of this upper bound to a successful model of proton temperature evolution in the sheath is described.

1. INTRODUCTION

This paper describes a recent development in the theory of microscopic, i.e., kinetic physics upstream of the Earth's magnetopause. Although the primary thrust here will be the same as in my invited talk at the Conference, some of the details will be different. In particular magnetosheath observations of magnetic fluctuations near the proton cyclotron frequency are addressed in Anderson [this volume] and will not be treated in detail here.

¹Los Alamos National Laboratory, Los Alamos, New Mexico.

²Now at: Department of ECE, University of California, San Diego.

³Lockheed Palo Alto Research Laboratory, Palo Alto, California.

⁴Dartmouth College, Hanover, New Hampshire.

⁵Applied Physics Laboratory, Johns Hopkins University, Laurel, Maryland.

The context of my presentation and of this paper can be established by quoting several other speakers at this Conference. George Siscoe said that, in order that an issue be regarded as of critical importance to future magnetopause studies, it should meet at least one of several criteria. One of these criteria was that "microphysics sets qualitative macrophysics." The concept that small scale physics determines a condition on plasma parameters characterizing the large scale magnetosheath is indeed central to the research presented here. Harry Petschek noted that, to get drag in fluid dynamics, viscosity is necessary, but that its value is not important in subsonic flow. Similarly, although the plasma physics described here depends in a detailed way on the small-scale processes of fluctuation growth and wave-particle scattering, the result, an upper bound on the proton temperature anisotropy, is independent of microscopic quantities such as wave amplitudes or transport coefficients. Finally, Rick Elphic, speaking about a different problem, said, "This is something we should have done in 1980." Indeed, the theoretical tools for the solution of the problem we will describe have been available since the publication of Kennel and Petschek [1966]. What we have done is to use the linear theory formalism and the instability threshold concept of that pioneering paper in a new way which, we believe, can be applied not only to magnetospheric and magnetosheath plasmas, but to any relatively homogeneous space plasma in which microinstabilities are driven to sufficiently large amplitude.

It is well established that heating at the bow shock and magnetic field line draping against the magnetopause imply the development of a proton temperature anisotropy $T_{\perp p}/T_{\parallel p} > 1$, where \perp and \parallel refer, respectively, to directions perpendicular and parallel to the background magnetic field \mathbf{B}_0 . Such an anisotropy has been observed frequently in the Earth's magnetosheath [Tsurutani *et al.*, 1982; Schopke *et al.*, 1990; Anderson *et al.*, 1991].

In the terrestrial magnetosheath this nonthermal property leads to the growth of two distinct instabilities and the observation of corresponding enhanced magnetic fluctuations at frequencies below the proton cyclotron frequency Ω_p [Schopke *et al.*, 1990; Song *et al.*, 1993; Anderson, this volume]. Mirror-like magnetic fluctuations arise from the growth of the mirror instability [Price *et al.*, 1986], have frequencies ω_r much less than Ω_p , and are primarily compressive, that is, $\delta\mathbf{B} \parallel \mathbf{B}_0$. In contrast growth of the proton cyclotron anisotropy instability leads to enhanced proton-cyclotron-like fluctuations at $\omega_r \lesssim \Omega_p$ with predominantly transverse fluctuating fields, i.e., $\delta\mathbf{B} \perp \mathbf{B}_0$. The relatively tenuous, hot, anisotropic doubly ionized helium in the sheath can drive the helium cyclotron anisotropy instability; its magnetic fluctuations are observed in the sheath at frequencies below the helium cyclotron frequency [Anderson *et al.*, 1994]. Here we will primarily address the first two modes and refer the reader to Denton *et al.* [1994a] and Gary *et al.* [1994b] for further discussions of the theoretical properties of the helium cyclotron instability.

Anderson and Fuselier [1993] and Anderson *et al.* [1994] used AMPTE/CCE observations to study the subsolar magnetosheath downstream of quasi-perpendicular bow shocks during times when the magnetosphere was strongly compressed by the solar wind. These observations showed that proton-cyclotron-like fluctuation spectra were predominant at $\beta_{\parallel p} \lesssim 1$, but mirror-like spectra constituted the majority of observations at β values large compared to unity. These authors also showed that the proton temperature anisotropies exhibited a relatively small variation for a given value of $\beta_{\parallel p}$ and that a least-squares fit to the data over the range $0.02 \lesssim \beta_{\parallel p} \lesssim 10.0$ yielded the result

$$\frac{T_{\perp p}}{T_{\parallel p}} - 1 = \frac{0.85}{\beta_{\parallel p}^{0.48}} \quad (1)$$

where $\beta_{\parallel p} \equiv 8\pi n_p T_{\parallel p}/B_0^2$. Similar anisotropy/ β inverse correlations in the magnetosheath have been observed by Phan *et al.* [1994] and Fuselier *et al.* [1994], and Hau *et al.* [1993] have shown that Equation (1) corresponds to an approximate upper bound for the proton temperature anisotropy as observed in the magnetosheath by AMPTE/IRM.

We have used both linear Vlasov theory and hybrid simulations to interpret these observations in terms of an upper bound on the proton temperature anisotropy imposed by ion cyclotron anisotropy instabilities. I will first discuss linear theory results using the formalism and notation of Chapter 7 of Gary [1993].

2. LINEAR THEORY

It has long been known that the thresholds of both the proton cyclotron anisotropy instability and the mirror instability qualitatively satisfy the same type of inverse correlation between proton temperature anisotropy and parallel β that is represented by Equation (1) [Gary *et al.*, 1976]. To quantify this relationship, we assumed that γ_m , the instability growth rate maximized over all wavevectors, held a constant value of $0.01\Omega_p$ at the thresholds of both growing modes, and used computer evaluations of the unapproximated linear Vlasov dispersion equation for a homogeneous plasma to determine the corresponding temperature anisotropies. For each of these instabilities we then plotted these threshold anisotropies as functions of $\beta_{\parallel p}$ and, in both cases, used a standard least-squares fitting procedure to obtain analytic expressions for the corresponding relationships. Our results for the range $0.01 \leq \beta_{\parallel p} \leq 10.0$ are shown in Figure 1; for the mirror instability

$$\frac{T_{\perp p}}{T_{\parallel p}} - 1 = \frac{0.97}{\beta_{\parallel p}^{0.81}} \quad (2)$$

and for the proton cyclotron anisotropy instability

$$\frac{T_{\perp p}}{T_{\parallel p}} - 1 = \frac{0.64}{\beta_{\parallel p}^{0.40}} \quad (3)$$

Although the $\beta_{\parallel p}$ value of the crossover point of the two threshold curves in Figure 1 can vary with different choices of γ_m and inclusion of the range of He^{++} densities observed in the sheath [Gary *et al.*, 1993a], it is generally true that the proton cyclotron instability has the lower threshold anisotropy at $\beta_{\parallel p} \lesssim 1$ and the mirror instability has the lower threshold at β values considerably larger than unity. Thus, if a strong anisotropy were suddenly imposed on a plasma as, for example, at the quasi-perpendicular shock, the system would be unstable to both modes and both types of fluctuations might be observed. On the other hand, if the proton anisotropy were relatively weak so that the plasma was stable to the growth of both modes and that anisotropy were gradually increased, as might happen under the more slowly changing sheath conditions downstream of the shock, Figure 1 suggests that the local β value would determine which instability would

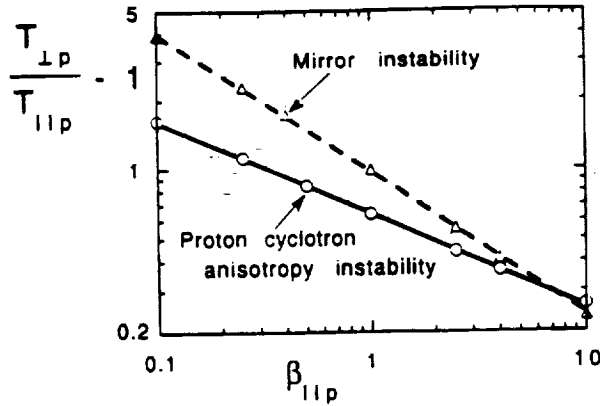


Fig. 1. Proton temperature anisotropies at the thresholds of the proton cyclotron and mirror instabilities as a function of $\beta_{\parallel p}$. The solid symbols represent numerical solutions of the linear Vlasov dispersion equation [Gary, 1993] at $\gamma_m = 0.01\Omega_p$ for the proton cyclotron instability (circles) and for the mirror instability (triangles). The lines represent analytic expressions fitting these results: the dashed line is Equation (2) and the solid line is Equation (3). Anisotropies greater than threshold correspond to faster instability growth; anisotropies less than threshold imply slower growth or stability. The model here is that of an electron-proton plasma with bi-Maxwellian zeroth order distribution functions and $T_e = 0.25T_p$ (After Gary *et al.*, 1994c).

first arise. The presumption that that growing mode would also dominate the magnetic fluctuation spectrum leads to the interpretation that proton-cyclotron-like spectra should primarily be observed at low β and mirror-like spectra at high β , in agreement with the observations.

3. HYBRID SIMULATIONS

The identification of enhanced fluctuations from a particular instability in either spacecraft data or computer simulations does not necessarily imply that that instability dominates the wave-particle processes which help determine plasma properties. The simulations of McKean *et al.* [1992b, 1994] have shown that, even at relatively high β , the mirror instability may be less effective than the proton cyclotron anisotropy at reducing $T_{\perp p}/T_{\parallel p}$ under conditions characteristic of the magnetosheath.

This result has been illustrated in a different way by Figure 2 which plots late-time results from a series of initial-value hybrid simulations [Winske and Omid, 1993]. Each run was begun with ion tempera-

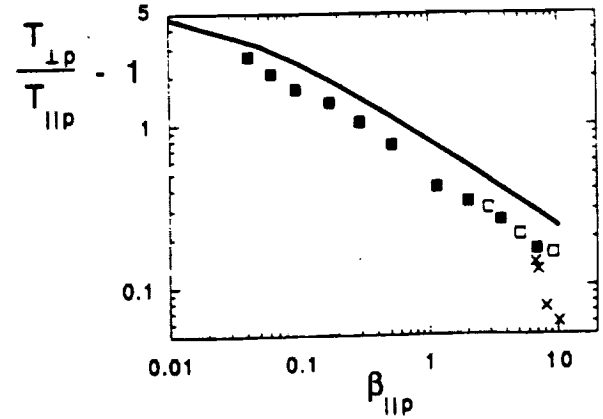


Fig. 2. Proton temperature anisotropy as a function of $\beta_{\parallel p}$; results from the asymptotic states of initial-value hybrid computer simulations using the magnetosheath parameter model of Gary *et al.* [1993b]. Here the solid squares represent results from one-dimensional simulations of ion cyclotron anisotropy instabilities, the 'x' symbols show results from one-dimensional simulations of the mirror instability, and the open squares represent results from two-dimensional simulations in which both instability types may arise. The solid line represents an approximate fit to the AMPTE/CCE observations (From Gary *et al.*, 1993b).

ture anisotropies large enough to excite rapid instability growth; the individual points in the figure correspond to late-time results reflecting the proton heating and reduction of the temperature anisotropy to the condition of relatively weak instability growth. The solid squares represent the results of one-dimensional simulations at $\mathbf{k} \times \mathbf{B}_0 = 0$, a condition permitting only ion cyclotron instabilities to grow. The 'x' symbols represent results of one-dimensional simulations allowing only wavevectors strongly oblique to the background magnetic field; in these simulations only the mirror instability was able to increase in amplitude. The open squares illustrate late-time anisotropies from two-dimensional hybrid simulations which permit a broad range of wavevector direction and which therefore have allowed both ion cyclotron and mirror instabilities to grow. The simulations which involve growth of ion cyclotron instabilities yield late-time results which show the same proton anisotropy/ β inverse correlation as the observations, whereas the one-dimensional computations which permit the growth of only the mirror instability do not resemble the observed results. This result supports the hypothesis that ion cyclotron instabilities are the source of the inverse correlation; the picture is that the relatively short wavelengths of these instabili-

ties are very efficient at scattering and reducing the proton temperature anisotropy to the threshold condition, whereas the mirror-like fluctuations are less efficient at producing wave-particle interactions and, when they do interact with the protons, produce changes that are not readily characterized as a reduction of $T_{\perp p}/T_{\parallel p}$.

Initial value simulations provide insight into the wave-particle interactions associated with ion cyclotron anisotropy instabilities, and provide a useful model for the study of plasma evolution downstream of a quasi-perpendicular shock, where ion temperature anisotropies are suddenly introduced and instabilities lead to a subsequent reduction of those anisotropies. In the magnetosheath close to the magnetopause, by contrast, macroscopic forces lead to a more gradual compression of the magnetic field and to a consequent increase in ion anisotropies. In such a situation, we believe that the model of *Kennel and Petschek* [1966] and *Manheimer and Boris* [1977] is appropriate: a macroscopic driving force which continually pushes the plasma toward increased anisotropy is balanced by the consequences of microscopic effects reducing this anisotropy so that a quasi-steady condition is established which corresponds to an instability threshold.

To represent the conditions of this balance between macroscopic and microscopic effects, we have modified the one-dimensional hybrid simulation code of *Winske and Omid* [1993] to include a recycle algorithm which acts primarily on superthermal superparticles. The resulting simulations, which are generally similar to the "recycled" simulations of *Ambrosiano and Brecht* [1987] and *McKean et al.* [1992a] or the "refreshed" simulations of *Denton et al.* [1993], are described in detail in *Gary et al.* [1994a]. The recycle algorithm reduces the magnetic-field-aligned velocity of all ions, but provides a greater reduction to those particles with the largest such speeds. If our recycling algorithm does not strongly perturb the ions, ion anisotropy instabilities will continue to grow and the quasi-steady balance we seek will be established.

Figure 3 shows results from one such simulation. The growth of the fluctuating magnetic field energy density to saturation indicates that the instability is indeed flourishing here. In contrast, the late-time response of $\beta_{\parallel p}$ shows a gradual diminuation; because n_p and B_0 are constant in these simulations, the decrease in β reflects the result that the recycling procedure not only reduces $T_{\parallel p}$ but also removes ion kinetic energy from the system. The value of $T_{\perp p}$ (not shown) also gradually decreases in time, so that the proton temperature anisotropy, after an initial phase in which the system develops its response to the recycling process, eventually attains a quasi-steady state.

Figure 4 exhibits results from an ensemble of fifteen driven simulations. The solid circles represent the anisotropy values corresponding to the early-time max-

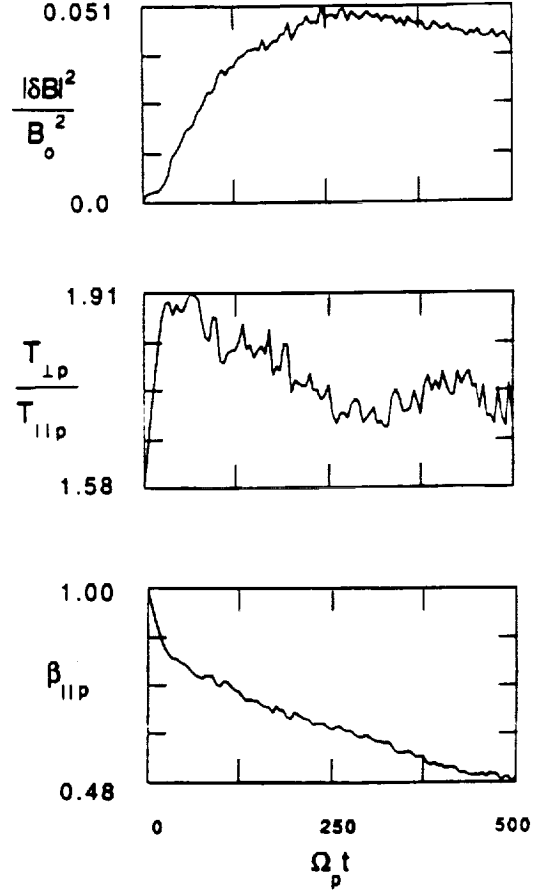


Fig. 3. Results from a driven simulation of the proton cyclotron anisotropy instability in an electron/proton plasma. The initial parameters here are $\beta_{\parallel p} = 1.00$ and $T_{\perp p}/T_{\parallel p} = 1.58$. The three panels here represent the total fluctuating magnetic field energy, the proton temperature anisotropy, and the proton parallel β (From *Gary et al.*, 1994a).

imum of the proton temperature anisotropy (See Figure 3), whereas the solid squares show late-time values of the anisotropy from the same runs. A detailed discussion of these results is given in *Gary et al.* [1994a]; the solid line of Figure 4 represents the least-squares fit of the late-time results:

$$\frac{T_{\perp p}}{T_{\parallel p}} - 1 = \frac{0.55}{\beta_{\parallel p}^{0.52}} \quad (4)$$

The similarity between the late-time results of the initial value and the recycled simulations is strong evidence that our recycle algorithm has not disturbed the wave-particle scattering process which drives the plasma toward instability threshold.

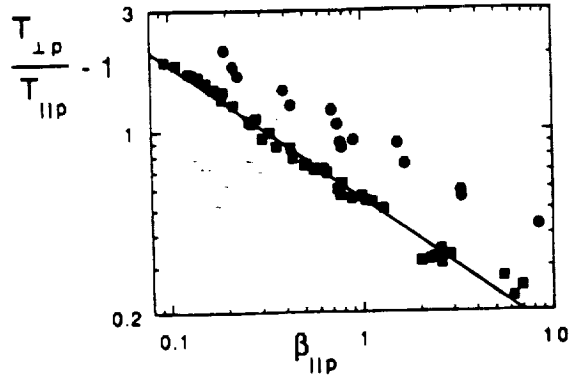


Fig. 4. The proton anisotropy from an ensemble of driven simulations of the proton cyclotron anisotropy instability in an electron/proton plasma as a function of $\beta_{\parallel p}$. For this ensemble of runs, the initial values of $\beta_{\parallel p}$ ranged from 0.25 to 10.0. The solid circles represent the maximum early-time value of the anisotropy from each simulation; the solid squares show corresponding late-time anisotropies. The line represents the least-squares fit to the late-time results, Equation (4) (From Gary *et al.*, 1994a).

The proton anisotropy/ β inverse correlation corresponds to special plasma conditions; that is, a quasi-steady state in which the anisotropy is maintained close to instability threshold. A broader set of physical conditions corresponding to the AMPTE/IRM sheath observations of Hau *et al.* [1993] and Phan *et al.* [1994] indicate that Equation (1) represents an approximate upper bound to the proton temperature anisotropy, and an ensemble of simulations which include weak anisotropies which do not excite the proton cyclotron instability show that Equation (4) provides a similar interpretation for the computational results [Gary *et al.*, 1994a]. Thus, we agree with Phan *et al.* [1994] that there is no single, universal relationship between $T_{\perp p}/T_{\parallel p}$ and $\beta_{\parallel p}$ which may be applied to each magnetosheath transit of a spacecraft. Rather, our interpretation of the proton anisotropy/ β inverse correlation, which is a weak function of local parameters such as the helium ion relative density [Gary *et al.*, 1994b], is that it represents a broadly applicable upper bound for $T_{\perp p}/T_{\parallel p}$ which should be approximately valid for all terrestrial magnetosheath observations.

4. BOUNDED ANISOTROPY MODEL

Denton *et al.* [1994b] have developed a bounded anisotropy model for describing the evolution of proton temperatures in the magnetosheath. This model is a one-fluid representation for the evolution of $T_{\perp p}$

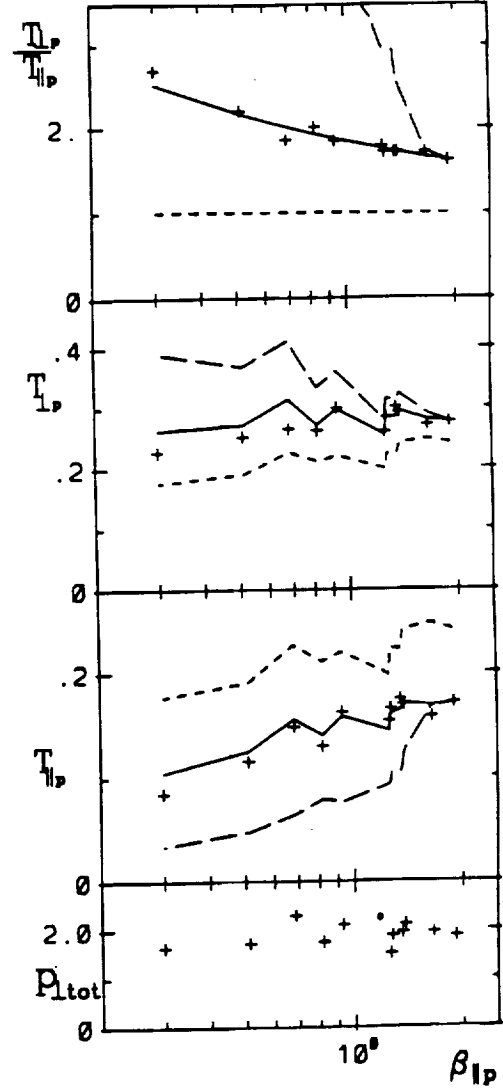


Fig. 5. The proton temperature anisotropy, the perpendicular proton temperature (in keV), the parallel proton temperature (in keV), and the total (plasma plus magnetic) perpendicular pressure (in units of 10^{-6} dyne/cm²) as functions of $\beta_{\parallel p}$. The curves represent predictions of three theories: isotropic adiabatic theory (small dashes), double adiabatic theory (large dashes), and the bounded anisotropy model (solid lines). Observations from CCE are plotted as plus signs (From Denton *et al.*, 1994b).

and $T_{\parallel p}$ in a collisionless plasma which is similar to the double adiabatic theory of Chew *et al.* [1956] except that it uses Equation (1) to provide an upper bound on the proton temperature anisotropy. Figure 5, which is taken from Denton *et al.* [1994b], illustrates several relevant quantities observed from AMPTE/CCE as the

spacecraft made a single crossing of the sheath. Here the quantities are plotted as a function of $\beta_{\parallel p}$ so that data from sheath regions closer to the bow shock appear toward the right and data from regions closer to the magnetopause appear toward the left. The approximate constancy of $p_{\perp tot}$ in the bottom panel of this figure indicates that conditions in the subsolar magnetosheath were approximately constant during this spacecraft transit.

Three curves are shown in the top three panels of Figure 5 for comparison against the data (crosses). The short dashed lines represent the predictions of adiabatic theory in which $T_{\perp p} = T_{\parallel p}$; this approach obviously predicts a $T_{\perp p}$ which is smaller than that observed and a $T_{\parallel p}$ which is larger than observations. In contrast, the long dashed lines illustrate the predictions of double adiabatic theory in which there is no coupling between the parallel and perpendicular proton temperatures. In this case the opposite result obtains; $T_{\perp p}$ is too large and $T_{\parallel p}$ is too small to match the observations. The solid lines in Figure 5 represent the results of the bounded anisotropy theory in which the proton anisotropy may not be larger than the observed value (See the top panel). This model yields quite good agreement with the observed evolution of both the perpendicular and parallel proton temperatures. The model even reproduces the temperature fluctuations observed as the spacecraft traversed the magnetosheath.

5. SUMMARY

Observations from AMPTE/CCE have found an inverse correlation between the proton temperature anisotropy and $\beta_{\parallel p}$ in the highly compressed terrestrial magnetosheath (Equation (1)). We have obtained similar correlations from the linear theory threshold condition of the proton cyclotron anisotropy instability (Equation (3)), from initial-value hybrid simulations of this instability, and from driven hybrid simulations of the same growing mode (Equation (4)). The theory and simulations show that the observations may be interpreted as an upper bound for the proton anisotropy, imposed by the growth and wave-particle scattering of the proton cyclotron instability. The successful application of this bound to the prediction of $T_{\perp p}$ and $T_{\parallel p}$ observed during an AMPTE/CCE sheath crossing implies that this relationship represents a limited closure relation for the equations of anisotropic MHD that should provide more accurate descriptions of sheath flow as well as more accurate boundary conditions for magnetopause dynamics including reconnection. Although this closure relation is limited in the sense that it applies only if the protons have a bi-Maxwellian distribution with $T_{\perp p}$ sufficiently larger than $T_{\parallel p}$, it is quite general in the sense

that it should be valid in any such plasma in which the field-aligned gradient scale lengths are long compared to an instability wavelength. Thus with minor modifications it should also be applicable to anisotropic MHD models of the terrestrial magnetosphere, Earth's magnetotail, and other planetary magnetosheaths.

Acknowledgments. The Los Alamos portion of this work was performed under the auspices of the U.S. Department of Energy (DOE) and was supported by the DOE Office of Basic Energy Sciences, Division of Engineering and Geosciences, and the Space Plasma Theory Program of the National Aeronautics and Space Administration (NASA). The Dartmouth College portion of this work was supported with funding from NASA grants NAGW-1652 and NAGW-3052-1992. Research at Lockheed was funded through NASA contract NAS5-30565. Work at the Johns Hopkins University Applied Physics Laboratory was supported by NASA under the AMPTE Missions Operations and Data Analysis Program.

REFERENCES

- Ambrosiano, J., and S. H. Brecht, A simulation study of the Alfvén ion-cyclotron instability in high-beta plasmas, *Phys. Fluids*, **30**, 108, 1987.
- Anderson, B. J., ULF signals observed near the magnetopause, this volume.
- Anderson, B. J., and S. A. Fuselier, Magnetic pulsations from 0.1 to 4.0 Hz and associated plasma properties in the Earth's subsolar magnetosheath and plasma depletion layer, *J. Geophys. Res.*, **98**, 1461, 1993.
- Anderson, B. J., S. A. Fuselier, and D. Murr, Electromagnetic ion cyclotron waves observed in the plasma depletion layer, *Geophys. Res. Lett.*, **18**, 1955, 1991.
- Anderson, B. J., S. A. Fuselier, S. P. Gary and R. E. Denton, Magnetic spectral signatures in the Earth's magnetosheath and plasma depletion layer, *J. Geophys. Res.*, **99**, 5877, 1994.
- Chew, G. F., M. L. Goldberger, and F. E. Low, The Boltzmann equation and the one-fluid hydromagnetic equations in the absence of particle collisions, *Proc. Roy. Soc., Ser. A*, **236**, 112, 1956.
- Denton, R. E., M. K. Hudson, S. A. Fuselier, and R. J. Anderson, Electromagnetic ion cyclotron waves in the magnetosheath plasma depletion layer, *J. Geophys. Res.*, **98**, 13,477, 1993.
- Denton, R. E., S. P. Gary, B. J. Anderson, S. A. Fuselier, and M. K. Hudson, Low-frequency magnetic fluctuation spectra in the magnetosheath and plasma depletion layer, *J. Geophys. Res.*, **99**, 5893, 1994a.
- Denton, R. E., B. J. Anderson, S. P. Gary, and S. A. Fuselier, Bounded anisotropy fluid model, *J. Geophys. Res.*, **99**, 11,225, 1994b.
- Fuselier, S. A., B. J. Anderson, S. P. Gary, and R. E. Denton, Ion anisotropy/beta correlations in the Earth's quasi-

- parallel magnetosheath, *J. Geophys. Res.*, **99**, 14,931, 1994.
- Gary, S. P., *Theory of Space Plasma Microinstabilities*, Cambridge University Press, Cambridge, 1993.
- Gary, S. P., M. D. Montgomery, W. C. Feldman, and D. W. Forslund, Proton temperature anisotropy instabilities in the solar wind, *J. Geophys. Res.*, **81**, 1241, 1976.
- Gary, S. P., S. A. Fuselier, and B. J. Anderson, Ion anisotropy instabilities in the magnetosheath, *J. Geophys. Res.*, **98**, 1481, 1993a.
- Gary, S. P., B. J. Anderson, R. E. Denton, S. A. Fuselier, M. E. McKean, and D. Winske, Ion anisotropies in the magnetosheath, *Geophys. Res. Lett.*, **18**, 1767, 1993b.
- Gary, S. P., M. E. McKean, D. Winske, B. J. Anderson, R. E. Denton, and S. A. Fuselier, The proton cyclotron instability and the anisotropy/ β correlation, *J. Geophys. Res.*, **99**, 5903, 1994a.
- Gary, S. P., P. D. Convery, R. E. Denton, S. A. Fuselier, and B. J. Anderson, Proton and helium cyclotron anisotropy instability thresholds in the magnetosheath, *J. Geophys. Res.*, **99**, 5915, 1994b.
- Gary, S. P., B. J. Anderson, R. E. Denton, S. A. Fuselier, and M. E. McKean, A limited closure relation for anisotropic plasmas from the Earth's magnetosheath, *Phys. Plasmas*, **1**, 1676, 1994c.
- Hau, L.-N., T.-D. Phan, B. U. Ö. Sonnerup, and G. Paschmann, Double-polytropic closure in the magnetosheath, *Geophys. Res. Lett.*, **20**, 2255, 1993.
- Kennel, C. F., and H. E. Petschek, Limit on stably trapped particle fluxes, *J. Geophys. Res.*, **71**, 1, 1966.
- Manheimer, W., and J. P. Boris, Marginal stability analysis—A simpler approach to anomalous transport in plasmas, *Comments Plasma Phys. Cont. Fusion*, **9**, 15, 1977.
- McKean, M. E., D. Winske, and S. P. Gary, Kinetic properties of mirror waves in magnetosheath plasmas, *Geophys. Res. Lett.*, **19**, 1331, 1992a.
- McKean, M. E., D. Winske, and S. P. Gary, Mirror and ion cyclotron anisotropy instabilities in the magnetosheath, *J. Geophys. Res.*, **97**, 19,421, 1992b.
- McKean, M. E., D. Winske, and S. P. Gary, Two-dimensional simulations of ion anisotropy instabilities in the magnetosheath, *J. Geophys. Res.*, **99**, 11,141, 1994.
- Phan, T.-D., G. Paschmann, W. Baumjohann, N. Skopke, and H. Lühr, The magnetosheath region adjacent to the dayside magnetopause: AMPTE/IRM observations, *J. Geophys. Res.*, **99**, 121, 1994.
- Price, C. P., D. W. Swift, and L.-C. Lee, Numerical simulation of nonoscillatory mirror waves at the Earth's magnetosheath, *J. Geophys. Res.*, **91**, 101, 1986.
- Skopke, N., G. Paschmann, A. L. Brinca, C. W. Carlson, and H. Lühr, Ion thermalization in quasi-perpendicular shocks involving reflected ions, *J. Geophys. Res.*, **95**, 6337, 1990.
- Song, P., C. T. Russell, and C. Y. Huang, Wave properties near the subsolar magnetopause: Pc 1 waves in the sheath transition layer, *J. Geophys. Res.*, **98**, 5907, 1993.
- Tsurutani, B. T., E. J. Smith, R. R. Anderson, K. W. Ogilvie, J. D. Scudder, D. N. Baker, and S. J. Barne, Lion roars and nonoscillatory drift mirror waves in the magnetosheath, *J. Geophys. Res.*, **87**, 6060, 1982.
- Winske, D., and N. Omid, Hybrid codes: Methods and applications, in *Computer Space Plasma Physics: Simulation Techniques and Software*, Edited by H. Matsumoto and Y. Omura, p. 103, Terra Scientific Publishers, Tokyo, 1993.

B. J. Anderson, Applied Physics Laboratory, Johns Hopkins University, Johns Hopkins Road, Laurel, MD 20723-6099. (Internet: anderson@ampete.dnet.nasa.gov)

R. E. Denton, Department of Physics and Astronomy, Dartmouth College, 6127 Wilder Laboratory, Hanover, NH 03755-3528 (Internet: denton@comet.dartmouth.edu)

S. A. Fuselier, Department 91-20, Building 225, Lockheed Palo Alto Research Laboratory, 3251 Hanover Street, Palo Alto, CA 94304-1191 (Internet: fuselier@lockhd-dnet.nasa.gov)

S. P. Gary, M. S. D466, Los Alamos National Laboratory, Los Alamos, NM 87545 (Internet: pgary@lanl.gov)

M. E. McKean, Department of ECE, University of California, San Diego, La Jolla, CA 92093-0407. (Internet: mmckean@ece.ucsd.edu)

D. Winske, M. S. F645, Los Alamos National Laboratory, Los Alamos, NM 87545 (Internet: dw@demons.lanl.gov)

Kinetic Aspects of Reconnection at the Magnetopause

Stephen A. Fuselier

Lockheed Palo Alto Research Laboratory, Palo Alto, California

Observations presented here support the kinetic (or single particle) description of quasi-steady reconnection where ions interacting with the magnetopause conserve their pitch angles or change them by equal amounts as in adiabatic motion. These observations include ion reflection and transmission at the magnetopause and time of flight effects associated with the magnetopause layers, with an emphasis here on ion reflection. Velocities of the reflected distributions predicted from this kinetic description are in good agreement with observed velocities. However, predicted velocities for the transmitted distributions are often higher than observed ones. Reflected distributions are also heated at the magnetopause; however, this heating is less important than the large scale ion motion. Reflection coefficients at the magnetopause are high (averaging 30%), appear to be the same on either side of the magnetopause, and have little or no dependence on ion mass. Time of flight effects result from the finite extent of the reconnection layers and are best observed at the edges of the layers.

INTRODUCTION

Early modelers of the magnetopause suggested that a field free cavity could exist around a stagnation point in the subsolar region when the interplanetary magnetic field (IMF) was nearly radial [e.g., *Beard*, 1964]. It was suggested that solar wind ions convecting along the Earth-sun line could enter this field free region, ballistically reflect off the magnetopause, and return in the sunward direction. This type of reflection at the magnetopause has not been observed. In the current understanding of the magnetopause and magnetosheath, such a field free cavity cannot form even for radial IMF because the field rotates across the bow shock and in the magnetosheath [e.g., *Phan et al.*, 1994].

Although the concept of magnetic reconnection was introduced about the same time as these early magnetopause models [*Dungey*, 1961], the possibility of particle reflection (and transmission) in association with magnetic reconnection was first considered in the mid 1970's [*Sonnerup*, 1976]. Later, ion reflection at the magnetopause was treated in detail independently by *Cowley* [1980; 1982] and *Sonnerup et al.* [1981]. This consideration was motivated by the physics of single particle motion in thin current sheets that had already been applied to other regions such as the Earth's magnetotail and the bow shock [e.g., *Sonnerup*, 1969]. In this regard, ion reflection off the magnetopause during reconnection

is a manifestation of kinetic (or single particle) processes at the open boundary.

A qualitative sketch of the reflection and transmission process is shown in Figure 1 (from *Gosling et al.* [1990a]). For southward interplanetary magnetic field, reconnection most likely occurs in the subsolar region. Magnetosheath ions will either reflect off the magnetopause or cross the boundary and enter the magnetosphere. Similarly, both high energy ring current ions and low energy ionospheric ions will either reflect off the magnetopause or cross the boundary and enter the magnetosheath. The reflected and transmitted ions remain within the separatrices S1 and S2 in Figure 1 and the edges of the electron and ion layers (E1, I1 and E2, I2) can be offset due to time of flight effects (see *Gosling et al.* [1990a]). Transmitted magnetosheath ions and reflected magnetospheric ions form the low latitude boundary layer (LLBL) on the magnetospheric side of the magnetopause. Similarly, transmitted magnetospheric and reflected magnetosheath ions form the magnetosheath boundary layer (MSBL) on the magnetosheath side of the magnetopause.

The reflection and transmission process as discussed by *Cowley* [1982] and *Sonnerup et al.* [1981] does not specify whether an ion incident on the magnetopause will reflect or be transmitted. However, it does describe ion motion upon reflection or transmission. After specifying a reflection coefficient at the magnetopause, three primary assumptions are needed to determine the collective motion of reflected and transmitted ions at the magnetopause. The first assumption is the existence of a time stationary deHoffman-Teller (dHT) frame [*deHoffman and Teller*, 1950; *Sonnerup et al.* this volume]. In this frame, the electric field on both sides of the

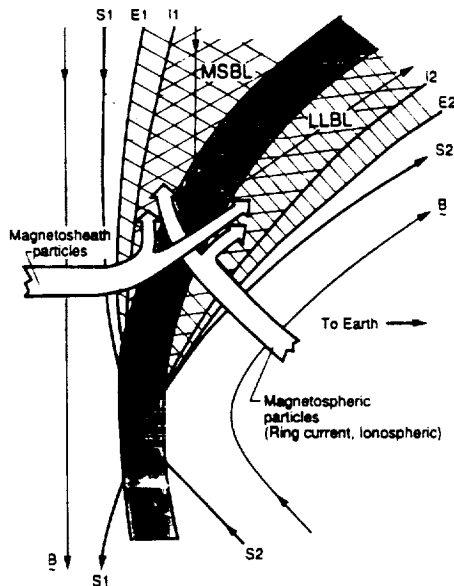


Fig. 1. Qualitative sketch of the magnetopause region for quasi-stationary reconnection (from Gosling *et al.* [1990a]). Magnetospheric (magnetospheric) ions either reflect off the magnetopause and enter the MSBL (LLBL) or cross the magnetopause and enter the LLBL (MSBL).

magnetopause is zero. This is a particularly important assumption for the multi-component plasma at the magnetopause because it requires that all ion distributions on each side of the magnetopause have the same $E \times B$ drift speed (i.e., that magnetic field gradients are not important). Indeed, $E \times B$ drifts for the individual plasma components in the LLBL are nearly the same and this is also true for the plasma components in the MSBL [e.g., Gosling *et al.*, 1990b; Fuselier *et al.*, 1991; 1993].

The second assumption is that the magnetopause is a one-dimensional rotational discontinuity. Under this assumption, the bulk flow velocity of the center of mass of the distribution in the dHT frame is the local Alfvén speed. This assumption will be discussed later and is also discussed in other articles in this Monograph. Finally, the third assumption is that ions either do not change their pitch angles upon reflection or transmission or change their pitch angles in a constant way as in adiabatic motion (i.e., ions conserve the first adiabatic invariant). Under this assumption, stochastic processes such as wave particle interactions are less important than the kinematic processes of ion motion in the large scale magnetic and electric fields. A consequence of this assumption is that ions with the same incident velocity but different mass/charge will have the same velocity upon transmission across the magnetopause. This is indeed the case; transmitted magnetosheath H^+ and He^{2+} bulk flow velocities in the LLBL were found to be nearly the same [Paschmann *et al.*, 1989].

With these three primary assumptions, Figure 2 shows cuts through the ion distributions in the MSBL (a) and the LLBL (b)

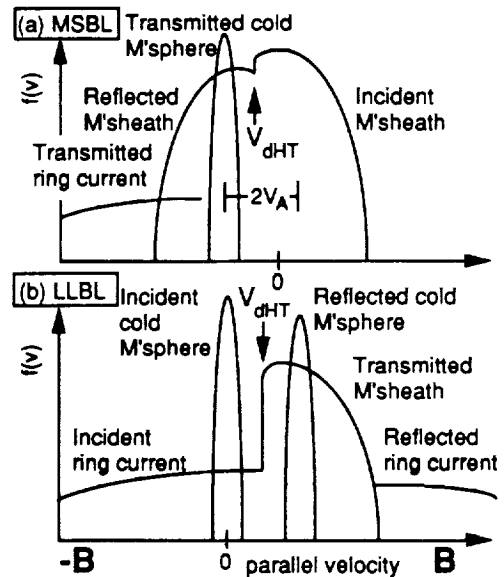


Fig. 2. Qualitative sketch of the ion distributions expected in the MSBL (a) and the LLBL (b) for a magnetopause crossing north of the reconnection line. If V_{dHT} is small and the magnetosheath temperature is large, then the incident and reflected magnetosheath distributions in the MSBL will not be distinguished. Also, reflection is difficult to observe in the LLBL because the transmitted magnetosheath distribution dominates there.

for a magnetopause crossing north of the reconnection site during southward IMF (adapted from Cowley *et al.* [1982] and Fuselier *et al.* [1991]). These cuts are along the magnetic field in the $E \times B$ frame of the plasma. The separation between the incident and reflected distributions is twice the local Alfvén velocity ($2V_A$). The velocity changes upon reflection and transmission are related to the energy gain individual ions experience in their interaction with the rotational discontinuity and are discussed in detail elsewhere [e.g., Sonnerup *et al.*, 1981; Cowley, 1982; Paschmann *et al.*, 1989]. For a crossing south of the reconnection site, the reflected and transmitted distributions are mirror imaged about zero parallel velocity. Time of flight effects (discussed later) become important as the observation point moves away from the magnetopause. Therefore, it is assumed that the distributions in Figure 2 are measured in the respective boundary layers very near the magnetopause current layer so that the cutoff velocity is at the dHT velocity [Smith and Rodgers, 1991]. Also, additional assumptions needed to produce Figure 2 are that the velocities of the inflowing plasma parallel to the magnetic field in the frame at rest with the magnetopause are small on both sides of the magnetopause and that the incident solar wind H^+ distribution dominates the plasma density in the MSBL and LLBL. These assumptions are valid for the subsolar region [e.g., Fuselier *et al.*, 1993; Phan *et al.*, 1994] and result in the special case where the dHT velocity (V_{dHT} in Figure 2) bisects the incident and reflected ion distributions and the transmitted and reflected distributions have the same velocity (the local Alfvén velocity) in this frame.

The purpose of this paper is to present and interpret observations of the kinetic aspects of quasi-steady reconnection at the magnetopause. (Time dependent reconnection and fluid aspects of reconnection are discussed separately in other papers in this volume.) The kinetic aspects discussed here are ion reflection and transmission at the magnetopause and time of flight effects, with an emphasis on reflection. Interpretation of these aspects will include (1) reflection and transmission as evidence for reconnection (2) the relative importance of heating and other stochastic effects compared to kinematic processes (3) the determination of the dHT frame (4) the relationship between incident and reflected ion distributions (5) time of flight effects on the distributions and (6) the difference between ion reflection at the bow shock and at the magnetopause.

OBSERVATIONS

Ion reflection and transmission

Figure 2 shows two features of the magnetopause region that make it difficult to distinguish incident, reflected, and transmitted ion distributions. First, if the component of the dHT velocity parallel to the magnetic field is small compared to the thermal speed of the incident solar wind distribution, then it is difficult to distinguish the incident and reflected magnetosheath components in the MSBL (Figure 2a). In the subsolar region, the several hundred km/s thermal speeds of the incident H^+ and He^{2+} distributions usually limit the observation of reflected ions to cases where the dHT velocity is also a few hundred km/s. For lower dHT velocities, the incident and reflected distributions merge and can be misinterpreted as parallel heating in the MSBL.

A second feature that causes difficulties is that the transmitted magnetosheath H^+ population dominates the LLBL. Typical H^+ densities are 10 to 100 times larger than magnetospheric ion densities in the LLBL [Fuselier *et al.*, 1993]. This dominance and also heating of the reflected distribution (discussed below), make it very difficult to observe ion reflection in the LLBL without ion composition instruments that resolve individual ion species.

Despite these difficulties, magnetosheath ion reflection in the MSBL has been observed at low latitudes [Sonnerup *et al.*, 1981; Gosling *et al.*, 1990c; Fuselier *et al.*, 1991] and at high latitudes [Gosling *et al.*, 1991]. Magnetospheric ion reflection in the LLBL has also been observed for the cold low energy component [Fuselier *et al.*, 1991] and the high energy ring current component [Scholer and Ipavich, 1983].

An example of ion reflection and transmission in the MSBL is shown in Figure 3. This event from the ISEE-1 data was the first reported evidence of solar wind proton reflection and low energy magnetospheric ion transmission in the MSBL [Sonnerup *et al.*, 1981]. For this crossing in the subsolar region (1140 local time and $+26^\circ$ GSM latitude), the stress balance test indicated that the magnetopause was approximately consistent with a one-dimensional rotational discontinuity although the predicted velocity change across the magnetopause was somewhat higher than the observed one [Sonnerup *et al.*, 1981]. Figure 3 shows solar wind He^{2+} and magnetospheric He^+ distributions measured

by the plasma composition experiment on ISEE-1. The B_z component of the magnetic field (from the ISEE-1 magnetometer) is shown in the lower left hand corner. The spacecraft was in the magnetosphere/LLBL at 0040 UT and in the magnetosheath at 0100 UT. Magnetic field rotations at 0044, 0046, and 0051 UT are magnetopause crossings. Short bars indicate where the He^{2+} and He^+ distributions were measured. The upper panels show contours of constant phase space density (two contours per decade of phase space) in 2-dimensional velocity space. The measurement plane is nearly centered on the ecliptic with V_x toward the sun and V_y toward dusk. The magnetic field direction is shown by the arrow and is approximately in the instrument field of view (i.e., within 19° of the ecliptic plane).

The distribution in the left hand panel in Figure 3 was measured in the magnetosheath well after the final outbound magnetopause crossing. It is a typical anisotropic magnetosheath He^{2+} distribution with very low bulk flow velocity both toward the magnetopause (in the $-V_x$ direction) and perpendicular to the magnetopause (in the $\pm V_y$ direction). The two distributions in the middle panel were measured in the MSBL near the magnetopause current layer. The distribution near zero velocity is the incident magnetosheath distribution and the one displaced along the magnetic field is the reflected magnetosheath distribution. The cut parallel to the magnetic field below this panel shows that the incident and reflected distributions are separated by twice the local Alfvén speed ($2V_A$) in the layer, as predicted in Figure 2. The reflected distribution contains approximately 6% of the total He^{2+} density and is heated (note the wider spaced contours of the reflected distribution when compared to the incident magnetosheath distribution). Comparing the incident magnetosheath distributions in the left and middle panels, there is little evidence of heating of this distribution in the MSBL.

The He^+ distribution in the right hand panel of Figure 3 was also measured in the MSBL near the magnetopause. This is the transmitted cold magnetospheric He^+ distribution (Figure 2a) (first noted by Sonnerup *et al.* [1981] for this event). The magnetospheric distribution was originally near zero drift velocity in the LLBL but, upon crossing the magnetopause, gained significant energy so that it had a bulk flow velocity along the magnetic field that was somewhat smaller than, but comparable to that of the reflected He^{2+} distribution in the middle panel.

An example of ion reflection and transmission in the LLBL is shown in Figure 4. The event in Figure 4 is from the AMPTE/Charge Composition Explorer data and has not been reported previously. Low energy magnetospheric He^+ and magnetosheath He^{2+} measured by the hot plasma composition experiment (HPCE) on the CCE spacecraft are shown in a format similar to that in Figure 3. The B_z component of the magnetic field in the lower left hand panel (from the CCE magnetometer experiment) shows that the spacecraft was in the magnetosheath at 0015 UT ($B_z < 0$) and in the magnetosphere at 0030 UT ($B_z > 0$). The single magnetopause crossing for this event (also in the subsolar region) was at 0020 UT. Short bars show where the He^+ and He^{2+} distributions were measured. The top panels show contours of constant phase space density similar to those in Figure 3. The measurement plane of the AMPTE instrument was tilted nearly 90° from that of the ISEE-1 instrument in Figure 3. Thus, the

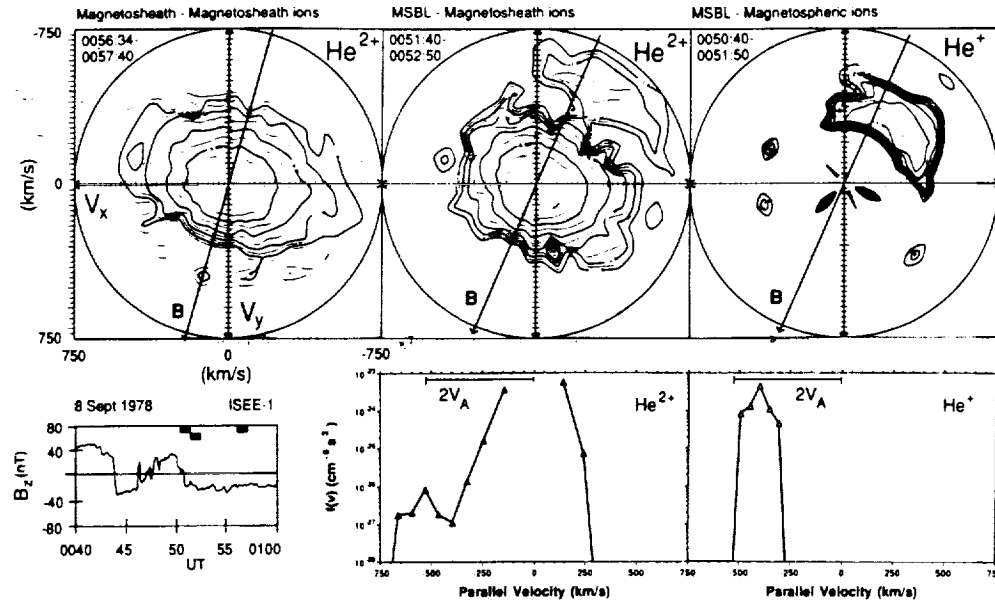


Fig. 3. An example of ion reflection and transmission in the MSBL. The upper panels show contours of constant phase space density in two-dimensional velocity space and the lower panels show B_z and parallel cuts through two distributions. Distribution functions in the upper panels were measured in the MSBL and magnetosheath, where $B_z < 0$. The He^{2+} distribution near $V=0$ (first two panels) is the incident magnetosheath He^{2+} distribution. The second distribution in the middle panel at $2V_A$ along the magnetic field is the reflected magnetosheath distribution. Concurrent with this reflected distribution is the transmitted He^+ distribution (third panel).

distributions in Figure 4 are in a plane approximately tangent to the subsolar magnetopause viewed from the sun with the V_x direction approximately perpendicular to the ecliptic plane and the V_y direction approximately in the ecliptic plane toward dusk.

The distribution in the left hand panel was measured in the magnetosphere well away from the LLBL. It is a low energy, highly anisotropic He^+ distribution often found in the outer magnetosphere [e.g., Fuselier et al., 1991] and it is convecting very slowly toward the magnetopause (~ 10 km/s in the V_x direction). The He^+ distributions in the middle panel were measured in the LLBL very near the magnetopause current layer. The same incident magnetospheric distribution in the left hand panel has picked up a substantial perpendicular flow velocity in the V_y direction in the LLBL. The magnetic field direction in the middle panel is drawn through the perpendicular component of the transmitted magnetosheath He^{2+} distribution (and the H^+ distribution (not shown) since the transmitted ion distributions all have the same perpendicular velocity). It is apparent that the incident He^+ distribution picked up the $\mathbf{E} \times \mathbf{B}$ drift of the transmitted magnetosheath plasma in the LLBL. In addition to the incident He^+ distribution in the LLBL, the middle panel shows a second, hotter distribution in the antiparallel direction at approximately twice the local Alfvén velocity in the layer. This is the reflected He^+ distribution predicted in Figure 2. The direction of the reflected distribution in Figure 4 is opposite to the one in Figure 2 because the magnetopause was crossed south and not north of the reconnection

line. The reflected distribution is hotter than the incident one and contains almost 36% of the total He^+ density in the LLBL.

The LLBL He^{2+} and He^+ distributions (right hand and middle panels, respectively) were measured simultaneously. In addition to the transmitted magnetosheath He^{2+} distribution at -260 km/s antiparallel to the magnetic field (open circle), there is some low energy magnetospheric He^{2+} at near zero parallel velocity that, like its He^+ counterpart, acquired the $\mathbf{E} \times \mathbf{B}$ drift of the transmitted magnetosheath population. The transmitted magnetosheath He^{2+} was initially at near zero drift velocity in the magnetosheath but, upon crossing the magnetopause, gained significant energy.

The dHT velocity in Figure 4 bisects the incident and reflected He^+ distributions in the LLBL so that they are at nearly $\pm V_A$ along the magnetic field (see Figure 2). In this frame for this case, the transmitted magnetosheath distribution should be flowing antiparallel to the magnetic field at V_A , the local Alfvén velocity. The right hand panel of Figure 4 shows that the He^{2+} bulk velocity is somewhat less than V_A in the dHT frame. This is also true for the transmitted H^+ distribution (not shown) because it has approximately the same velocity as the transmitted He^{2+} .

Table 1 contains density and temperature ratios of reflected ion distributions reported to date. The 1984 events are from a study of magnetopause crossings from the AMPTE/CCE data [Fuselier et al., 1993]. The reflected to total density ratio (n_r/n_{tot}) and the reflected to incident perpendicular temperature ratio ($T_{r\perp}/T_{i\perp}$) were determined from moments of the incident and reflected dis-

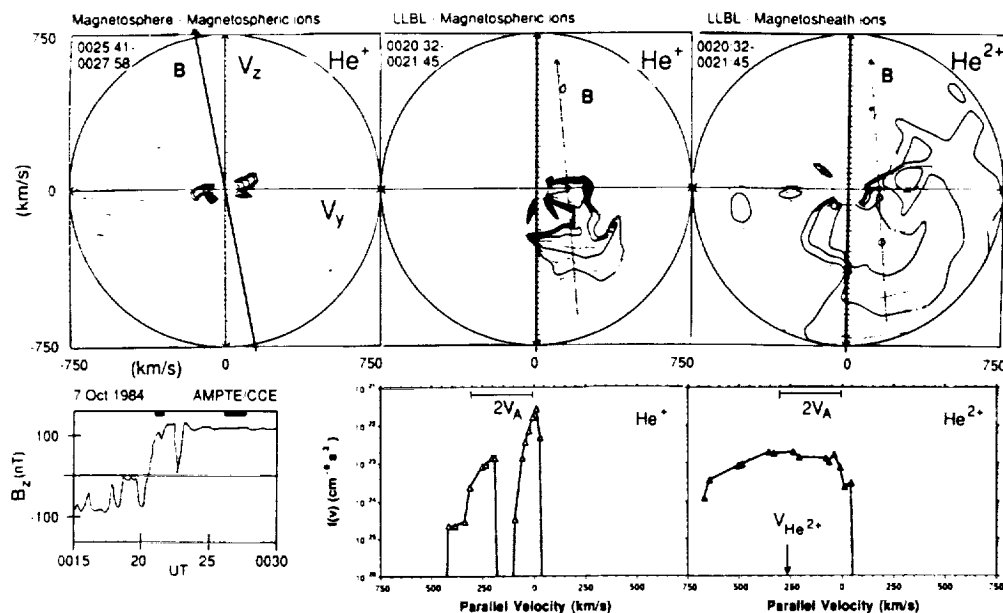


Fig. 4. An example of ion reflection and transmission in the LLBL. The format is similar to Figure 3. The incident cold (few eV) magnetospheric distribution (left hand panel) picks up the $\mathbf{E} \times \mathbf{B}$ drift speed of the transmitted magnetosheath He^{2+} in the LLBL (middle panel). The second distribution in the middle panel at about $2V_A$ along the magnetic field is the reflected He^+ distribution. The transmitted He^{2+} distribution is shown in the right hand panel.

tributions in the MSBL and LLBL. Transmission and reflection at the magnetopause was discussed in detail by Fuselier *et al.* [1991] for one of these events (18 October 1984). The 1978 events are from the ISEE-1 and -2 data sets. The He^{2+} observations from the 8 September 1978 event are in Figure 2 and the H^+ density and temperature ratios for this event were determined from (unpublished) distribution functions from the Los Alamos/Garching Fast Plasma Experiment (M. F. Thomsen, personal communication). Other density and temperature ratios were determined by fitting two temperature Maxwellian functions to published incident and reflected distributions.

Considering individual species, Table 1 shows that ions reflect off the magnetopause in large numbers with reflection coefficients averaging about 30%. Reflected distributions are also about a factor of three hotter than the incident distributions, indicating heating either in the reflection process or after the distributions have reflected (through wave-particle interactions). Although common data for several species are sparse, an intercomparison of columns in Table 1 and their averages shows that reflection coefficients do not vary significantly with species nor are they very different from one side of the magnetopause to the other. All ion species on both sides of the magnetopause appear to respond similarly to the magnetopause current layer.

Time of Flight Effects

As discussed above, time of flight effects have been ignored in the predictions in Figure 2. These effects can be safely ignored so long as observations (such as those in Figures 3 and 4) are

made sufficiently close to the magnetopause current layer. Time of flight effects are the direct result of the finite extent of the reconnection region and are discussed in detail by Gosling *et al.* [1990a]. For example, when the reconnection site is below an observing spacecraft, ions enter the LLBL all along the magnetopause from near the observation point to the magnetic field X line. Plasma convection toward the magnetopause in the LLBL creates a low speed cutoff parallel to the magnetic field in the transmitted distribution because (1) the lower the parallel velocity of the ion, the further south from the observation point the ion crossed the magnetopause and (2) ions cannot come from further away than the magnetic field X line.

For observation points near the magnetopause and for reasonably high dHT velocities, the low speed cutoff due to time of flight effects is below the dHT velocity and therefore does not affect the observed distributions. However, as the observation point moves closer to the boundary between the LLBL and the magnetosphere, the low speed cutoff velocity increases and can become considerably higher than the dHT velocity. In fact, at the separatrix (S2 in Figure 1), the low speed cutoff is at infinite velocity.

Time of flight effects are best seen near this earthward edge of the LLBL by comparing ion and electron distributions in the layer. The extremely high cutoff velocities near the earthward edge of the LLBL and the fact that transmitted magnetosheath electrons have much higher velocities than transmitted ions leads to a layer within the LLBL that contains magnetosheath electrons and no magnetosheath ions. This layer is between I2 and E2 in Figure 1. An excellent example of this layer is described in detail

TABLE 1. Density and Perpendicular Temperature Ratios of Reflected Ions at the Magnetopause

| Date | MP Time | Magnetosheath H ⁺ Reflection | | Magnetosheath He ²⁺ Reflection | | Magnetospheric He ⁺ Reflection | |
|-----------|-------------------|---|-------------------------|---|-------------------------|---|-------------------------|
| | | $n_r/n_{tot}\%$ | $T_{r\perp}/T_{s\perp}$ | $n_r/n_{tot}\%$ | $T_{r\perp}/T_{s\perp}$ | $n_r/n_{tot}\%$ | $T_{r\perp}/T_{s\perp}$ |
| 11 Jun 78 | 2247 ¹ | 30 | 5.8 | - | - | - | - |
| 12 Aug 78 | 1835 ² | 4 | 3.1 | - | - | - | - |
| 8 Sep 78 | 0043 ³ | 9 | 2.6 | 6 | 1.9 | - | - |
| 7 Oct 84 | 0020 | 16 | 2.5 | 23 | 2.6 | 36 | 6.2 |
| 18 Oct 84 | 1302 ⁴ | 37 | 1.2 | 50 | 6.2 | 30 | 1.7 |
| 18 Oct 84 | 1648 | 56 | 1.9 | 55 | 2.8 | - | - |
| 19 Oct 84 | 0810 | 15 | 2.8 | 17 | 2.6 | - | - |
| Average | | 27±18 | 2.8±1.6 | 30±21 | 3.2±1.7 | ~33 | ~3.9 |

¹Gosling et al. [1991].²Gosling et al. [1990] "FTE".³Sonnerup et al. [1981] estimated 20% reflected H⁺ in the MSBL. Scholer and Ipavich [1983] estimated 10-50% reflected ring current H⁺ in the LLBL.⁴Fuselier et al. [1991].

by Gosling et al. [1990a]. There should also be a similar layer of transmitted magnetospheric electrons and no transmitted ions in the MSBL (between I1 and E1 in Figure 1).

DISCUSSION

Observations presented in Figures 3 and 4 and in Table 1 show that reflection (and transmission) of ions occurs at the Earth's magnetopause. These observations are strong evidence in support of the kinetic picture of reconnection at the magnetopause where individual ions either preserve their pitch angle or change it through adiabatic motion in the interaction with the open boundary. Although these observations provide strong evidence for reconnection, they would be difficult to use in a statistical survey of reconnection at the magnetopause. The observations are limited to fairly high dHT drift speeds in the MSBL and require mass resolving detectors (as well as reasonably high dHT drift speeds) in the LLBL. At lower speeds (near the thermal speed of the incident distributions), it is difficult to distinguish incident and reflected distributions.

It is also difficult to distinguish these distributions because of heating of the reflected distribution. Table 1 shows that this heating can be substantial, at least in the perpendicular direction. Parallel heating is more difficult to quantify but does occur (compare the incident and reflected He⁺ distributions in Figure 4). Heating may be the result of scattering of the ions in the current layer (so that near-adiabatic motion is violated) or the result of pitch angle scattering of the reflected distribution by waves.

Although the heating is substantial, it does not dominate the kinematic motion of the ions in the large-scale electric and magnetic fields. This kinematic motion is determined by the change in the ion velocity in the dHT frame. Reflected and transmitted ion distributions provide a relatively easy way to determine the dHT frame [Fuselier et al., 1991]. In the events presented here near the subsolar magnetopause, the dHT frame velocity is simply the velocity that bisects the incident and reflected distributions in the MSBL (Figure 3) and in the LLBL (Figure 4). In this frame, the

incident and reflected distributions are at $\pm V_A$, the local Alfvén velocity in the layer, consistent with predictions of ion interaction with a time stationary, one-dimensional rotational discontinuity.

While predictions for the incident and reflected distributions are nearly in agreement with observations, predicted and observed velocities for the transmitted ion distributions show less agreement. Often, the transmitted distributions on both sides of the magnetopause (Figures 3 and 4) are observed to have velocities less than the predicted V_A in the dHT frame. Since the transmitted protons dominate the LLBL [Fuselier et al., 1993], lower velocities of the transmitted magnetosheath distribution will translate into bulk (or fluid) velocities across the magnetopause that are lower than those predicted by stress balance across a time stationary, one-dimensional rotational discontinuity. The observed bulk flow velocities in the LLBL do average lower than those predicted from stress balance [e.g., Paschmann et al., 1986]. Thus, the fluid treatment (that predicts the velocity through stress balance) and the kinetic treatment (that predicts the transmitted and reflected velocities through single particle motion) both result in higher than observed velocities for the transmitted ions at the magnetopause.

The differences between the observed and predicted velocities are typically not large (~25%) [e.g., Paschmann et al., 1986] and such relatively close agreement is really extraordinary.

These differences may indicate that the magnetopause is not a simple one dimensional discontinuity [e.g., Fuselier et al., 1993]. This suggestion is supported by the fact that the separation between the incident and reflected distributions is both observed and predicted to be $2V_A$ (see Figures 3 and 4) because reflection takes place along essentially the same field line as the incident distribution. Transmitted ion distributions in Figures 3 and 4 are probably not simply connected along a single field line from their origin on one side of the magnetopause to their observation point on the other side.

Time of flight effects in the LLBL also support this suggestion. The finite travel time between the observation point in the LLBL and the entry point where a particle crosses the magnetopause

is best exemplified in the separate ion and electron layers in the LLBL illustrated schematically in Figure 1 (see Gosling *et al.* [1990a]). The much higher speeds of the electrons entering the LLBL allow them to be observed closer to the separatrix between magnetospheric and reconnected field lines. These time of flight effects are not accounted for in the predictions in Figure 2.

Although ion reflection and transmission at the magnetopause and time of flight effects have been observed and several aspects appear to be reasonably well understood, there are other important features of these kinetic processes that are not understood and are open to further research. One feature that is not understood is the amount of reflected ions at the magnetopause. As pointed out in the introduction, the predictions for magnetopause reflection deal with the ion motion upon reflection and do not predict a reflection coefficient. A larger sample of ion reflection and a better understanding of the reflection process itself may allow such a prediction. Along this same line, part of the original motivation for suggesting that ion reflection may occur at the magnetopause was the success in applying this process to the bow shock. It is interesting to compare the results of ion reflection at the two boundaries because, although the physical process is the same, the results are vastly different. The bow shock reflection process [Sonnerup, 1969] produces H^+ ion beams almost uniformly at about 1% of the incident solar wind H^+ density and these beams contain almost no solar wind He^{2+} [e.g., Fuselier and Thomsen, 1992]. In contrast, reflection at the magnetopause produces beams that average ~30% of the total density and all ion species reflect with nearly equal probability (Table 1). An adequate explanation of these differences may include consideration of the very different Mach numbers (very high for the bow shock and very low for the magnetopause) and differences between ion interaction with a supercritical shock and a rotational discontinuity. Finally, some other areas open for research include reflected ions as a source of free energy for waves in the boundary layers and the change in the dHT velocity, the Alfvén velocity, and the low speed cutoff velocity (due to time of flight effects) from the magnetopause to the edge of the boundary layer.

Acknowledgments. The author gratefully acknowledges discussions with B. U. Ö. Sonnerup and J. T. Gosling. The ISEE Fast Plasma Experiment data in Figure 3 were provided by M. F. Thomsen. The ISEE magnetometer data were provided by C. T. Russell through the NSSDC. The CCE magnetometer data were provided by T. A. Potemra through the Applied Physics Laboratory Science Data Center. Research at Lockheed was funded by NASA AMPTE contract NAS5-30565, GI contract NAS5-31213, and SR&T grant NAGW-4049.

REFERENCES

- Beard, D. B., The effect of an interplanetary magnetic field on the solar wind, *J. Geophys. Res.*, **69**, 1159, 1964.
- Cowley, S. W. H., Plasma populations in a simple open model magnetosphere, *Space Sci. Rev.*, **26**, 217, 1980.
- Cowley, S.W.H., The causes of convection in the Earth's magnetosphere: A review of developments during the IMS, *Rev. Geophys.*, **20**, 531, 1982.
- deHoffman, F., and E. Teller, Magnetohydrodynamic shocks, *Phys. Rev.*, **80**, 692, 1950.
- Dungey, J. W., Interplanetary field and the auroral zones, *Phys. Rev. Lett.*, **6**, 47, 1961.
- Fuselier, S. A., and M. F. Thomsen, He^{2+} in field-aligned beams: ISEE results, *Geophys. Res. Lett.*, **19**, 437, 1992.
- Fuselier, S. A., D. M. Klumppar, and E. G. Shelley, Ion reflection and transmission during reconnection at the Earth's subsolar magnetopause, *Geophys. Res. Lett.*, **18**, 139, 1991.
- Fuselier, S. A., D. M. Klumppar, and E. G. Shelley, Mass density and pressure changes across the dayside magnetopause, *J. Geophys. Res.*, **98**, 3935, 1993.
- Gosling, J. T., M. F. Thomsen, S. J. Bame, T. G. Onsager, and C. T. Russell, The electron edge of the low latitude boundary layer during accelerated flow events, *Geophys. Res. Lett.*, **17**, 1833, 1990a.
- Gosling, J. T., M. F. Thomsen, S. J. Bame, R. C. Elphic, and C. T. Russell, Cold ion beams in the low-latitude boundary layer during accelerated flow events, *Geophys. Res. Lett.*, **17**, 2245, 1990b.
- Gosling, J. T., M. F. Thomsen, S. J. Bame, R. C. Elphic, and C. T. Russell, Plasma flow reversals at the dayside magnetopause and the origin of asymmetric polar cap convection, *J. Geophys. Res.*, **95**, 8093, 1990c.
- Gosling, J. T., M. F. Thomsen, S. J. Bame, R. C. Elphic, and C. T. Russell, Observation of reconnection of interplanetary and lobe magnetic field lines at the high-latitude magnetopause, *J. Geophys. Res.*, **96**, 14,097, 1991.
- Paschmann, G., I. Papamastorakis, W. Baumjohann, N. Sckopke, C. W. Carlson, B. U. Ö. Sonnerup, and H. Lüth, The magnetopause for large magnetic shear: AMPTE/IRM observations, *J. Geophys. Res.*, **91**, 11,099, 1986.
- Paschmann, G., S. A. Fuselier, and D. M. Klumppar, High speed flows of H^+ and He^{++} ions at the magnetopause, *Geophys. Res. Lett.*, **16**, 567, 1989.
- Phan, T.-D., G. Paschmann, W. Baumjohann, N. Sckopke, and H. Lüth, The magnetosheath region adjacent to the dayside magnetopause: AMPTE/IRM observations, *J. Geophys. Res.*, **99**, 121, 1994.
- Scholer, M., and F. M. Ipavich, Interaction of ring current ions with the magnetopause, *J. Geophys. Res.*, **88**, 6937, 1983.
- Smith, M. F., and D. J. Rodgers, Ion distributions at the dayside magnetopause, *J. Geophys. Res.*, **96**, 11,617, 1991.
- Sonnerup, B. U. Ö., Acceleration of particles reflected at a shock front, *J. Geophys. Res.*, **74**, 1301, 1969.
- Sonnerup, B. U. Ö., Magnetopause and boundary layer, in *Physics of solar planetary environments*, ed. D. J. Williams, AGU, Washington DC, pp 541-557, 1976.
- Sonnerup, B. U. Ö., G. Paschmann, I. Papamastorakis, N. Sckopke, G. Haerendel, S. J. Bame, J. R. Asbridge, J. T. Gosling, and C. T. Russell, Evidence for magnetic field reconnection at the Earth's magnetopause, *J. Geophys. Res.*, **86**, 10,049, 1981.
- Sonnerup, B. U. Ö., G. Paschmann, and T.-D. Phan, Fluid aspects of reconnection at the magnetopause: In situ observations, this volume.

Stephen A. Fuselier, Dept. 91-20 Bldg. 255, Lockheed Palo Alto Research Laboratory, 3251 Hanover St., Palo Alto, CA 94304. (e-mail: fuselier@space.lockheed.com).

Magnetopause crossings without a boundary layer

T. E. Eastman

Institute for Physical Science and Technology, University of Maryland, College Park

S. A. Fuselier

Lockheed Palo Alto Research Laboratory, Palo Alto, California

J. T. Gosling

Los Alamos National Laboratory, Los Alamos, New Mexico

Abstract. The microstructure of pristine magnetopause crossings has been analyzed by using high-resolution particle and field data obtained by the Active Magnetospheric Particle Tracer Explorers (AMPTE) Charge Composition Explorer (CCE) and ISEE 2 spacecraft. These crossings are pristine in the sense that they exhibit no adjoining magnetospheric boundary layer or, at most, a low-density plateau. The CCE crossings include the low-latitude near-noon region not typically sampled by ISEE 2, which covers all other local time sectors in a complementary way. Magnetopause crossings without a boundary layer are found to occur to all local times, and such crossings constitute about 10% of all magnetopause crossings. Total pressure balance across the magnetopause is observed to within experimental errors; however, electron data, full-energy composition measurements, and occasionally field stress are needed to fully evaluate pressure balance. The microstructure of the magnetopause current layer is also found to depend on local time. Crossings within about 1 hour local time of the noon meridian often exhibit very sharp density gradients on scale lengths down to a few plasma skin depths. These gradients are reduced for crossings farther from local noon such that, for cases near the dawn-dusk meridian, the scale length for density gradients and the magnetopause current are roughly comparable. Magnetopause crossings without a boundary layer impose severe constraints on various theories of boundary layer formation. Pristine magnetopause crossings may be direct cuts through the diffusion region for reconnection. With this interpretation our results are in qualitative agreement with recent simulations of the diffusion region and associated turbulence by *Drake et al.* [1994], who propose the current convective instability as the dominant process for current transport at the magnetopause.

Introduction

Since the discovery of the low-latitude boundary layer by *Eastman et al.* [1976], much work has focused on the structure and characteristics of that region [e.g., *Lundin*, 1988; *Cowley*, 1995]. However, very few magnetopause crossings have been published that do not exhibit the signatures of a boundary layer, and data sets used prior to the late 1970s did not have temporal resolution adequate to clearly separate these two classes of magnetopause crossings, i.e., crossings with versus crossings without an adjoining boundary layer.

The magnetopause is the outermost boundary of the magnetosphere within which charged particle motion is dominated by the geomagnetic field. In general, the magnetopause is marked by a current layer and is usually identified as the innermost major rotation of the magnetic field from local magnetosheath to magnetospheric orientation. However, this operational definition can fail to be sufficiently unambiguous for cases where the magnetosheath and magnetospheric orientations are locally very similar or where rapid, multiple crossings or superimposed flux transfer events (FTEs) may preclude a unique magnetopause identification [*Fuselier et al.*, 1995]. In the present study, only unambiguous magnetopause crossings are used to avoid these problems.

The current layer is well defined in our pristine magnetopause crossings because we avoid similar field orientations across the boundary and there is either no adjoining magnetospheric boundary layer or, at most, a low-density plateau. Our analysis is based on a study of 235 magnetopause crossings sampled by the ISEE 2 spacecraft from October 1977 through December 1978 and 125 magnetopause crossings sampled by the Active Magnetospheric Particle Tracer Explorers (AMPTE) Charge Composition Explorer (CCE) from September 1984 through December 1988. From these data sets, 26 pristine magnetopause crossings for ISEE 2 and 10 such crossings for CCE were identified (see Table 1).

Using high-time resolution plasma and field data, our analysis provides new information on magnetopause microstructure. As documented in the analysis of CCE data by *Eastman et al.* [1994], this microstructure includes particle gradients and some field variations that are sometimes very sharp and on scale lengths much shorter than ion gyroradii, whereas the overall current layer is one or more ion gyroradii in thickness. In the present study we examine basic characteristics of magnetopause crossings without a boundary layer, including pressure balance, local time distributions, and how magnetopause microstructure exhibits a local time variation.

Spacecraft and Data Sets

The AMPTE/CCE spacecraft operated from launch on August 16, 1984 until early 1989. It was in a near-equatorial orbit with

Copyright 1996 by the American Geophysical Union.

Paper number 95JA02757.
0148-0227/96/95JA-02757\$05.00

Table 1. AMPTE/CCE Magnetopause Crossings

| Date | Day of Year | UT | $r(R_E)$ | Latitude (degrees) | MLT | L/R_g |
|----------------|-------------|------|----------|--------------------|------|---------|
| Oct. 6, 1984 | 280 | 0148 | 7.7 | -10.2 | 11.2 | |
| Oct. 19, 1984 | 293 | 0636 | 8.8 | -11.5 | 11.9 | 1.6 |
| Nov. 13, 1984 | 318 | 1613 | 8.8 | 7.6 | 10.0 | 2.2 |
| Nov. 14, 1984 | 319 | 2355 | 8.8 | -11.1 | 10.1 | |
| Nov. 15, 1984 | 320 | 1900 | 7.8 | 3.7 | 11.2 | |
| Nov. 30, 1984 | 335 | 0524 | 6.3 | -15.4 | 11.5 | 3.4 |
| Dec. 26, 1984 | 361 | 0303 | 8.8 | -13.6 | 8.1 | 1.5 |
| Feb. 8, 1986 | 039 | 2250 | 5.2 | 6.5 | 12.9 | |
| Feb. 14, 1986 | 045 | 1530 | 8.6 | 13.3 | 10.8 | |
| April 14, 1987 | 104 | 1334 | 8.8 | 3.4 | 12.6 | 1.4 |

L/R_g is the magnetopause thickness in units of ion gyroradii.

an apogee of $8.8 R_E$ and a 15.6 hour period. During disturbed interplanetary and geomagnetic conditions ($K_p > 5$) the spacecraft sometimes traversed the frontside magnetopause region, although always at low latitude ($<15^\circ$). The spin axis of CCE points roughly sunward and its spin period is about 6 s. A full complement of particle and fields instrumentation was flown as documented by Bryant *et al.* [1985]. The AMPTE/CCE observations presented in this paper were obtained primarily by the hot plasma composition experiment (HPCE) [Shelley *et al.*, 1985] and the magnetic field experiment (MAG) [Potemra *et al.*, 1985]. With this plasma instrument, two-dimensional measurements of electron velocity distributions are made from 50 eV to 25 keV and, for ion distributions, from near spacecraft potential to 17 keV/e. If the electron angular distributions are assumed to be quasi-isotropic, nominal electron densities can be obtained every 155 ms. Such high time resolution data are used in this paper, limited primarily by easily recognized spin modulation as well as by a 50-eV lower-energy cutoff. However, we regard these nominal electron densities to be a proper proxy of total density variations present near the magnetopause, and it is that variation which is of most importance for this paper. Simultaneous MAG measurements are provided every 115 ms, and these together with the high time resolution electron data, provide a closely matched set of plasma and field data for high time resolution studies. The absolute timing accuracy between HPCE and MAG is less than about 0.1 s. Higher-energy particle measurements supporting this study were obtained with the charge-energy-mass (CHEM) spectrometer [Gloeckler *et al.*, 1985] and the medium-energy particle analyzer (MEPA) [McEntire *et al.*, 1985]. The plasma wave experiment (PWE), documented by Scarf [1985], shows some evidence for a weak enhancement in 100-Hz electric wave noise for our magnetopause crossings. However, instrument noise background is

the dominant signature at all channels measured by PWE's short antenna. This background appears to depend on the ambient electron flux (R. J. Strangeway, personal communication, 1995).

The ISEE 1 and 2 spacecraft operated from launch on October 22, 1977, until reentry on September 26, 1987. They flew together with controlled separation distances in a highly eccentric orbit with an apogee of $22.5 R_E$ and approximately 29° inclination. Plasma and field observations used for this paper were obtained by the fast plasma experiment (FPE) [Bame *et al.*, 1978] and the fluxgate magnetometers [Russell *et al.*, 1978]. With the plasma instrument, two-dimensional measurements of ion and electron velocity distributions are made at 16 energies at each of 16 azimuths, integrated over $\pm 55^\circ$ of elevation angle relative to the ecliptic, in one satellite rotation of 3 s. The measurement cycle is repeated every spin in high data rate and every fourth spin in low data rate. The fluxgate magnetometers provide a field vector every 250 ms when in low data rate and 63 ms in high data rate; crossings plotted in this paper are all high data rate.

AMPTE/CCE and ISEE 2 magnetopause crossings used in our study are listed in Tables 1 and 2, respectively, including crossing times and locations. For the CCE data set, all orbits were examined from launch in August 1984 through the end of mission in early 1989. However, for ISEE 2, only magnetopause crossings during the first 15 months of operation were evaluated from launch in October 1977 through December 1978. The CCE spacecraft has a low inclination orbit, which results in crossing latitudes that are all less than 15° . However, local time coverage by CCE is very limited for such crossings, and most occur near local noon under conditions of high dynamic pressure because that is where crossings within its $8.8 R_E$ apogee are most likely. In contrast, the high-inclination, high apogee orbit of ISEE 2 resulted in magnetopause crossings ranging from 8° to 23° latitude for our study, under a wide range of solar wind dynamic pressures. Fortunately, ISEE 2 coverage is excellent at all local times, although crossings close to local noon are typically more than 15° from the magnetic equator. Overall the combined CCE and ISEE 2 crossing sets provide excellent coverage of the magnetopause at relatively low latitudes from local noon to beyond the dawn-dusk meridian. The magnetic field data are all analyzed by a standard minimum variance analysis method developed by Sonnerup and Cahill [1967] and Siscoe *et al.* [1968].

Pristine Magnetopause Crossings

A classic example of a pristine magnetopause crossing is presented in Figure 1 (see 039/86 case in upper left panel). This CCE magnetopause crossing near the subsolar point shows a very clean field rotation in the maximum field component B_t , whereas the normal field component B_n remains constant near zero. However, B_n is not sufficiently steady to specify the type of MHD discontinuity encountered using this component. Further, the intermediate field component B_m exhibits a bimodal pattern, which indicates the presence of a filamentary current structure within the magnetopause. The magnetopause current layer is identified by the field rotation interval from 82,215 s to 82,222.5 s within which the electron density remains at magnetosheath levels. Plotted electron "densities" are only for electrons above 50 eV and are not spin averaged; nevertheless, spin modulation at the 6-s spin period is not noticeable, indicating a relatively isotropic distribution. At the inner edge of the magnetopause the density drops more than 3 orders of magnitude in less than 0.8 s to magnetospheric levels based on data samples taken

every 155 ms. Farther earthward there is no evidence for any magnetosheath-like plasma indicating the presence of a boundary layer. Eastman *et al.* [1994] estimate the magnetopause thickness for such crossings, defined by the magnetic field rotation, to be about 1–4 ion gyroradii based on using boundary sensing with the finite gyroradii of energetic ions. Therefore, the steep density gradient has a scale length less than 1 ion gyroradius.

For all pristine magnetopause crossings observed in the subsolar region we find that the overall magnetopause remains well defined by the shear in magnetic field but that the primary density drop from magnetosheath to magnetospheric levels occurs on the earthward side of the current layer over a scale length that is often less than 20% of the current layer width.

Comparing high-resolution density and magnetic field profiles for various magnetopause crossings reveals important fine structure. Sharp gradients in density extending over 2–4 orders of magnitude within sample times of less than 1–2 s are occasionally observed. For the two crossings presented on the right side of Figure 1 the primary density gradient occurs within about 10% of the current layer interval (0.7 s out of a 7.0-s magnetopause interval for 104/87 and 1.2 s out of a 10-s magnetopause interval for 320/84). The large density change observed for the day 039/86 crossing discussed above occurred within less than 15% of the current layer width. Independent analysis of MEPA data for 35– to 50-keV ions, taking advantage of their finite gyroradii and magnetopause absorption [Fritz and Fahrenstiel, 1982], indicates that the current layer for the 104/87 crossing is approximately 1.4 ion gyroradii thick. Boundary speed relative to the spacecraft is obtained by dividing sounding distance by the time taken to arrive at the remotely sensed boundary. The primary density gradient scale length for this crossing is found to be one tenth the current layer width, or 0.14 ion gyroradii (0.14 times 40 km gyroradius = 5.6 km), which is only a few times the electron plasma skin depth (1.7 km at $n = 10 \text{ cm}^{-3}$). The density gradient scale length is evaluated here as simply the distance covered by the gradient and not an e -folding scale. For the 335/84 case in the lower left panel of Figure 1 the density drops 3 orders of magnitude in 0.2 s within a brief 2.4-s magnetopause crossing. Oscillations in the magnetosheath "density" for this crossing are due to the fact that these samples are not spin averaged and the electrons are not isotropic. Earthward of the magnetopause a brief low-density plateau is observed for 5 s. Such brief plateaus were observed in seven of the 10 CCE magnetopause cases examined and were all highly variable in density. Especially for crossings near local noon we find that magnetopause crossings often exhibit gradients and fine structure on scale lengths much smaller than the scale length of the current layer.

The energetic particle sounding method was applied to the five AMPTE/CCE magnetopause crossings for which all required data were available. The inferred magnetopause thickness in units of plasma ion gyroradii ranged from 1.4 to 3.4. The CCE crossings analyzed in this paper are all cases of high plasma beta in the nearby magnetosheath with beta values ranging from 2 to 40. In a recent survey using ISEE data, Le and Russell [1994] found that magnetopause thickness is smaller for such high-beta conditions. They report magnetopause thicknesses of 2–4 ion gyroradii, essentially the same result as presented here. We found no clear dependence of current layer characteristic with beta for the 10 CCE cases.

For the CCE magnetopause crossings a clear enhancement of low-frequency magnetic fluctuations was observed by the magnetic field experiment (MAG) from about 0.3 to 1.5 Hz (B. J.

Table 2. ISEE 2 Magnetopause Crossings

| Date | Day of Year | UT | r/R | Latitude (degrees) | MLT |
|---------------|-------------|------------------------|-------|--------------------|------|
| Nov. 15, 1977 | 319 | 0614 0627 | 12 | 23 | 10.4 |
| Dec. 9, 1977 | 343 | 0503 | 11 | 22 | 9.1 |
| Dec. 11, 1977 | 345 | 1435 | 11 | 22 | 8.9 |
| Dec. 13, 1977 | 347 | 2134 2151 | 13 | 22 | 8.5 |
| Dec. 25, 1977 | 359 | 2232 | 11 | 21 | 8.0 |
| Dec. 30, 1977 | 364 | 1322 | 14 | 22 | 7.2 |
| Jan. 4, 1978 | 004 | 1312 | 9 | 18 | 7.9 |
| Feb. 15, 1978 | 046 | 0834 | 21 | 22 | ≤3 |
| May 31, 1978 | 151 | 0630 | 20 | 21 | 19.3 |
| June 10, 1978 | 161 | 1358 | 21 | 18 | 19.7 |
| June 30, 1978 | 181 | 0037 | 18 | 15 | 19.0 |
| June 30, 1978 | 181 | 1927 | 10 | 23 | 15.9 |
| Aug. 8, 1978 | 220 | 0243 | 13 | 23 | 14.0 |
| Aug. 14, 1978 | 226 | 1542 | 14 | 10 | 16.7 |
| Aug. 19, 1978 | 231 | 1038 | 14 | 10 | 16.7 |
| Aug. 21, 1978 | 233 | 2109 | 12 | 8 | 16.4 |
| Aug. 24, 1978 | 236 | 0633.0635 0639.0641 | 12 | 8 | 16.3 |
| Aug. 31, 1978 | 243 | 1017 | 13 | 8 | 15.7 |
| Sept. 3, 1978 | 246 | 0708 | 11 | 23 | 12.0 |
| Nov. 15, 1978 | 319 | 2108 | 12 | 4 | 10.8 |
| Dec. 17, 1978 | 351 | 1302 | 13 | 22 | 5.3 |

Anderson, private communication, 1995). The plasma wave instrument (PWE) observed a weak enhancement of 100-Hz electric wave noise near the magnetopause. Unfortunately, its short antenna gives a high background for observation conditions near the magnetopause, and this background tends to mask any other, naturally occurring, signals (R. J. Strangeway, personal communication, 1995).

Local Time Dependence

The local time distribution of ISEE 2 pristine magnetopause crossings is shown in Figure 2. Only ISEE data are used for this purpose because that spacecraft provides the most uniform local time coverage at nominal solar wind dynamic pressure values. Pristine magnetopause crossings are observed at all local times and constitute between 3% and 23% of total crossings observed within different local time sectors. In support of these ISEE results, pristine magnetopause crossings are observed by CCE at all local times at which the spacecraft crossed the magnetopause, from 8 to 13 hours MLT. For the ISEE 2 results, occurrence ra-

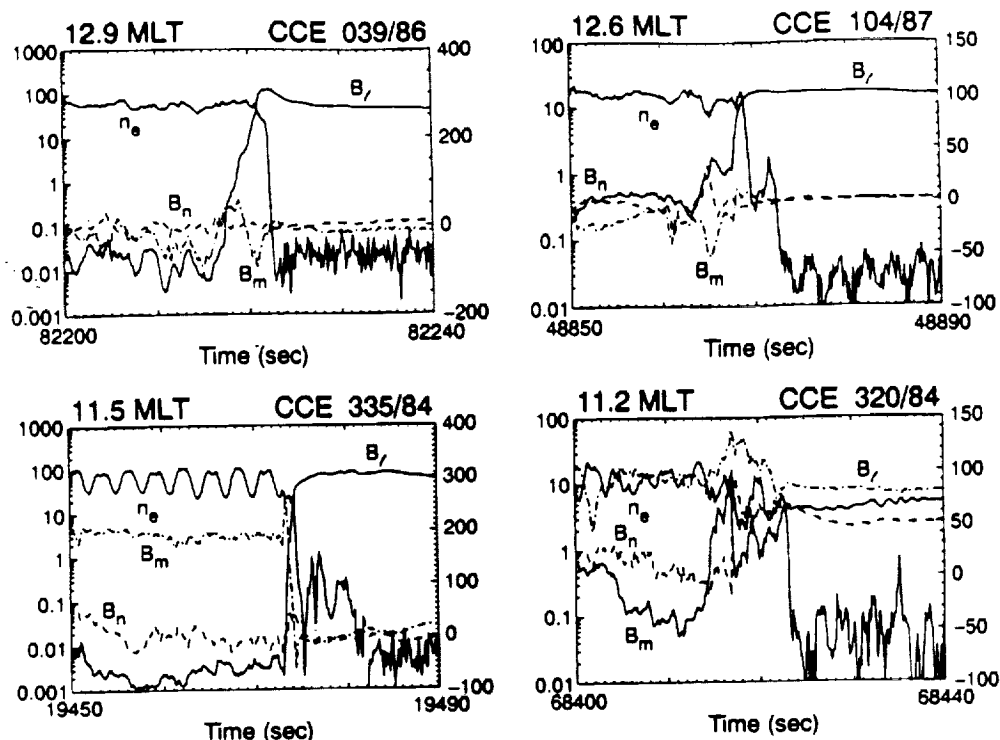


Figure 1. These pristine magnetopause crossings demonstrate the difference in current and density gradient scale lengths observed near local noon by the AMPTE/CCE spacecraft. Electron "density" values are integrated above 50 eV and are not spin averaged; spin modulation reflecting CCE's 6-s spin period is present in the bottom two panels. B_l , B_m , and B_n are the maximum, intermediate, and minimum variance components, respectively, of magnetic field derived from a minimum variance analysis across the magnetopause. (Density scale in particles per cubic centimeter on left side; magnetic field scale in γ ($= 10^{-5}$ g) on right side; each tic mark on the horizontal axes represents 1 s.)

tios peak near 9 and 17 hours MLT and have a minimum near 13 hours MLT. Statistics are best on the frontside from 8 to 18 hours MLT, and within this region the likelihood of pristine magnetopause crossings is lowest near noon or slightly post noon. On

average, over the frontside magnetosphere, pristine magnetopause crossings occur for 10% of all crossings. For 75% of pristine magnetopause crossings when the average magnetosheath field is well defined, 60% are associated with $-B_z$ in the nearby mag-

ISEE 2 MAGNETOPAUSE CROSSINGS

Nov. 1977 - Dec. 1978

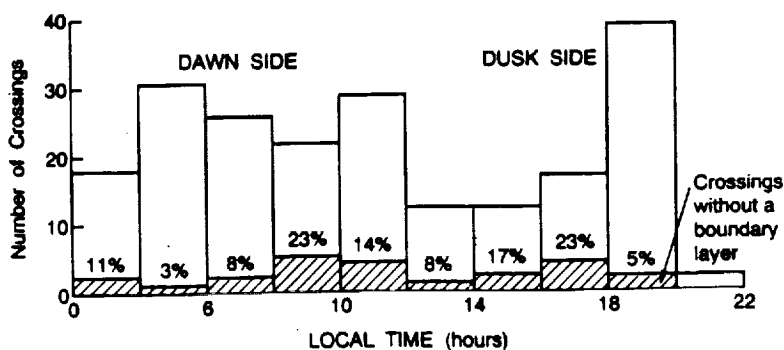


Figure 2. Magnetopause crossings without a boundary layer are found at all local times covered by the ISEE 2 satellite, as shown here for magnetopause crossings sampled during its first 15 months of operation. Percentages of pristine magnetopause crossings are shown along with their crossing numbers (shown crosshatched) for each local time bin compared to total magnetopause crossings.

netosheath, whereas only 15% are associated with $+B_z$. Some of this difference may be due to a selection effect because magnetopause crossings are most distinct for high field shear even though such shear was not a criteria for selection. Most important, pristine magnetopause crossings occur at all local times and are not limited to the subsolar region.

We have compared magnetic field and density profiles for all of the pristine magnetopause crossings listed in Tables 1 and 2 and have found a systematic difference in magnetopause microstructure with local time. This local time dependence is illustrated in Figure 3, which shows log-scale densities and magnetic field profiles in linear scale for eight sample magnetopause crossings displayed sequentially in magnetic local time. These plots have been scaled to a constant width for the magnetopause to aid in comparing profiles of density and magnetic field. The magnetopause has been identified in each case (and marked with vertical lines) on the basis of all three field components, although only the maximum variance component is plotted here. A time interval of 10 s is shown below each plot for comparison.

As confirmed by inspection of Figure 3, the density gradient scale length is often comparable to and rarely less than one half the current-layer scale length for magnetopause crossings more than 1–2 hours local time away from noon. However, most crossings within 1 hour local time of the subsolar point exhibit a density gradient scale length less than 20% of the current layer scale length. For the first three cases, all near local noon, the density gradient scale length is much shorter than the magnetopause interval, whereas these scale lengths are comparable for the last three cases far from local noon. The CCE and ISEE cases in between at 10.1 and 9.1 MLT are intermediate in this scale length comparison.

Fine structure in the magnetic field profile is often present as well. This is especially dramatic in the CCE magnetopause crossing of day 320/84 where several sharp gradients occur within the overall current layer transition. In this case only, the intermediate variance component B_m is used in Figure 3, because it shows the overall current layer more clearly than the maximum variance component, B_l . The day 343/77 crossing of ISEE 2 has high-speed plasma flow (not shown) near the inner portion of the current layer. This location for the high-speed flow is the same as that reported for accelerated plasma flows by Gosling *et al.* [1986]. Such accelerated flows are often confined to the current layer, consistent with recent hybrid simulations of a reconnection layer along the flank magnetopause [Lin and Lee, 1994]. The other two high data rate ISEE 2 crossings do not have this high-speed flow signature.

Pressure Balance and Ion Composition

We evaluated all plasma and field components of the total pressure across the magnetopause for six AMPTE/CCE crossings having a full set of plasma and field parameters including electrons, energetic ions, and composition. "Hot" electrons are defined as those summed by the electron instrument from 50 eV to 25 keV, and "cold" electron densities are obtained by assuming a quasi-neutral plasma and subtracting the hot electron densities from observed ion densities. Nominal cold electron temperatures of 10 eV and 30 eV were assumed for the magnetosheath and magnetosphere, respectively. All particle data below 17 keV are derived from the HPCE instrument; all data above 17 keV are obtained from the CHEM instrument.

Previous estimates of total pressure near the magnetopause have often failed to yield balance across the magnetopause, al-

though, during any arbitrary crossing one is not likely to observe a brief interval of dynamic imbalance [e.g., Paschmann *et al.*, 1986]. These estimates are usually based on only integrating the magnetic field and low-energy hydrogen components, which usually dominate total pressure. However, Table 3 shows that electrons, He^{+2} , and even field stress can be important in providing detailed balance. For plasma pressure nkT we assume that the perpendicular pressure dominates. In most cases, energetic ions (>17 keV) have very small pressure contributions except for protons on the magnetospheric side in three cases.

We evaluated pressure balance immediately across the sharp density discontinuity which occurs on the inner edge of the current layer. On the magnetosheath side of this discontinuity and within the current layer we found that finite pressure from field stress (the magnetic curvature term $\mathbf{B} \cdot \nabla \mathbf{B}$ from the momentum equation) was important in four crossings. To access the contribution of field stress, we start from a simplified form of the momentum transfer tensor obtained by limiting the analysis "to perturbations of scale length short compared to the lateral (i.e., parallel to the discontinuity plane) extent of the observed tangential forms" [Northrop and Birmingham, 1970]. Writing out $\mathbf{B} \cdot \nabla \mathbf{B}$ explicitly

$$\nabla(P + B^2/2\mu_0) = \frac{1}{\mu_0} \mathbf{B} \cdot \nabla \mathbf{B} \quad (1)$$

and neglecting intermediate field terms B_m (which assumes the plane of rotation in B_n and B_l defined by our minimum variance calculation is optimal), we obtain

$$\mathbf{B} \cdot \nabla \mathbf{B} \approx B_n \nabla_n B_l \hat{l} + B_l \nabla_l B_n \hat{n} \quad (2)$$

We now integrate equation (1) from the magnetospheric (SP) side of the density discontinuity to the magnetosheath side (MS), noting that $\mathbf{B} \cdot \nabla \mathbf{B}$ is negligible on the magnetospheric side. Further, we use only the field stress component along the normal \hat{n} and sum over a distance equal to the perturbation scale length so that scale lengths cancel out in this approximation:

$$(P + B^2/2\mu_0)_{MS} - \frac{1}{\mu_0} B_l \Delta B_n = (P + B^2/2\mu_0)_{SP} \quad (3)$$

Total pressure values first given in Table 3 are based only on the standard $P + B^2$ term. The pressure is systematically higher on the magnetosheath side by 34% on average. Adding in estimates for the field stress term reduces the magnetosheath-side totals, and this corresponds to local release of stress. Stress-corrected pressure estimates lead to pressure totals across the density discontinuity that change by 24% on average.

Percentage contributions to total pressure are shown in Table 4 for both the magnetosheath and magnetospheric side of the magnetopause, based on an average over the six crossings used for Table 3 and not including field stress terms discussed above. About 5% of total magnetosheath pressure derives from hot and cold electrons. Ion species other than hydrogen can contribute an additional 11% on the magnetosheath side (primarily from He^{+2}) and 12% on the magnetospheric side (primarily from high-energy H^+). Pressure anisotropy is neglected in this analysis, and this leads to systematically higher pressure estimates in the magnetosheath by about 10% [Paschmann *et al.*, 1986]. The remaining difference of less than 15%, including field stress corrections, is within experimental errors which, overall, are roughly 25–30%. Except for the 280/84 magnetopause crossing, all cases in Table 3 are inbound crossings which correspond to outward magnetopause motion relative to the spacecraft. Thus the observed higher pressure on the magnetosheath side is not likely

related to inward dynamical acceleration of the magnetopause. Combining all these factors, we find that electron data, full-energy composition measurements, and occasionally field stress are needed in addition to proton and magnetic field magnitudes to fully evaluate pressure balance at the magnetopause.

Summary and Conclusion

Magnetopause crossings without any substantial boundary layer are found to occur at all local times, and such crossings constitute about 10% of all magnetopause crossings sampled

by the CCE and ISEE 2 satellite. The overall magnetopause remains well defined by the shear in magnetic field. When the average magnetosheath field is well defined, 60% of such pristine magnetopause crossings are associated with $-B_z$ in the nearby magnetosheath, whereas only 15% of such crossings are associated with $+B_z$.

Analysis of high-resolution density and magnetic field profiles for various magnetopause crossings reveals important fine structure. The density gradient scale length is often comparable to and rarely less than one half the current layer scale length for magnetopause crossings more than 1–2 hours local time away from

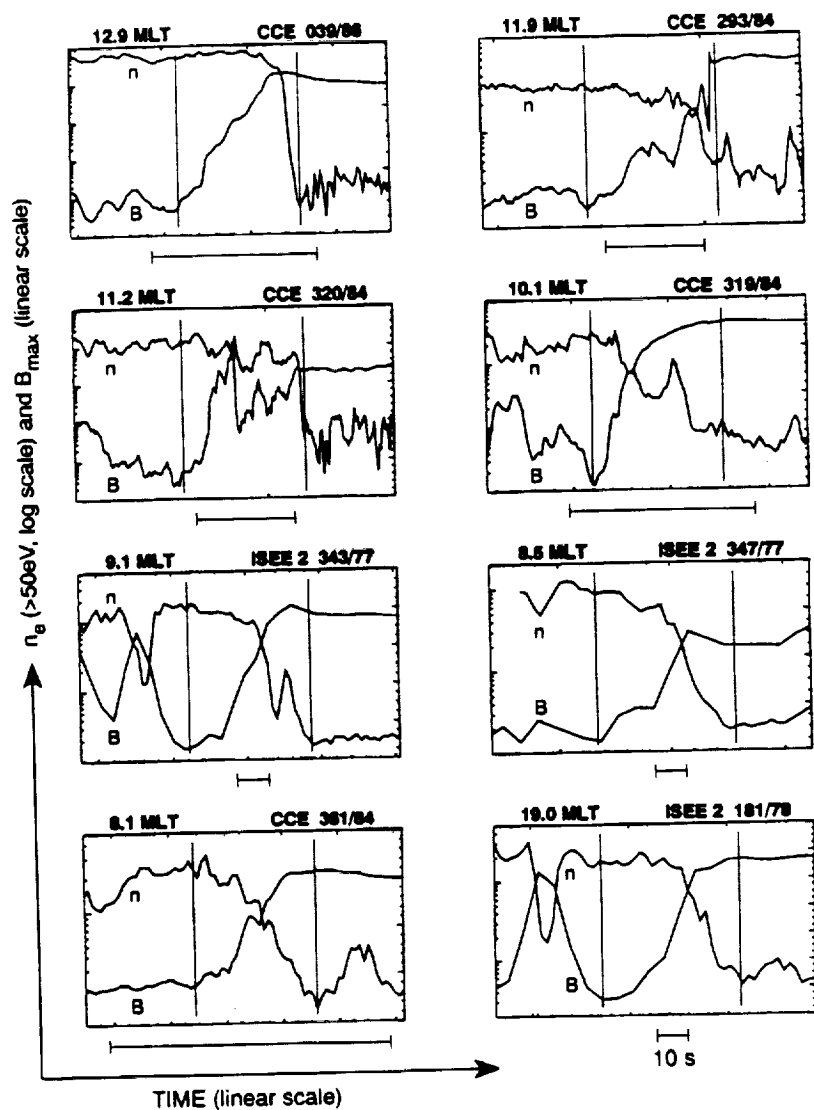


Figure 3. Local time dependence of magnetopause microstructure is illustrated by these eight CCE and ISEE 2 crossings at locations near noon to the dawn-dusk meridian. The magnetopause width is adjusted to be the same on each plot for easy comparison of the basic density versus field structure (vertical scales are relative, and a 10-s baseline is given for each crossing).

Table 3. Magnetopause Pressure Balance Calculations

| | Day of Year / Year | | | | | |
|------------------------------|--------------------|------------|-------------|-------------|-------------|-------------|
| | 280/1984 | 293/1984 | 318/1984 | 319/1984 | 320/1984 | 335/1984 |
| $B^2/2\mu_0$ | 0.4 / 7.2 | 0.4 / 4.6 | 1.0 / 3.2 | 0.6 / 5.4 | 4.0 / 5.7 | 15.9 / 37.0 |
| nkT (H^+) | 13.5 / 6.7 | 6.1 / 0.9 | 4.0 / 0.1 | 6.4 / 0.05 | 8.9 / 0.5 | 30.6 / 0.9 |
| nkT (hot e^-) | 1.6 / 0.3 | 0.9 / 0.02 | 0.4 / 0.05 | 0.4 / 0.1 | 0.2 / 0.01 | 0.6 / 0.01 |
| nkT (cold e^-) | 0.2 / 0.03 | 0.04 / 0 | 0.1 / 0 | 0.2 / 0 | 0.2 / 0.01 | 0.6 / 0.01 |
| nkT (He^{+2}) | 1.3 / 0.2 | 1.1 / 0.01 | 0.6 / 0.01 | 1.0 / 0 | 1.2 / 0.04 | 1.2 / 0.01 |
| nkT (He^+) | 0 / 0.05 | 0 / 0.01 | 0.02 / 0.02 | 0 / 0.01 | 0.01 / 0.04 | 0.02 / 0.01 |
| nkT (O^+) | 0.03 / 0.1 | 0 / 0.09 | 0.01 / 0.03 | 0.01 / 0.05 | 0 / 0.1 | 0.01 / 0.09 |
| H^+ (>17 keV) | 0 / 0.06 | 0.4 / 1.3 | 0.01 / 0.1 | 0.01 / 0.2 | 0.04 / 1.5 | 0.6 / 3.9 |
| O^+ (>17 keV) | 0.01 / 0 | 0.05 / 0.2 | 0 / 0 | 0 / 0.01 | 0 / 0.2 | 0.01 / 0 |
| He^{+2} (>17 keV) | 0 / 0 | 0.1 / 0.1 | 0 / 0 | 0.02 / 0.01 | 0.02 / 0 | 0.08 / 0.5 |
| He^+ (>17 keV) | 0 / 0 | 0 / 0.01 | 0 / 0.01 | 0 / 0 | 0 / 0.06 | 0 / 0.03 |
| Total Pressure | 17.0 / 14.7 | 9.0 / 7.1 | 6.1 / 3.5 | 8.6 / 5.8 | 14.6 / 8.2 | 49.6 / 42.4 |
| $B\Delta B/\mu_0$ | -0.4 / 0 | -0.2 / 0 | -0.3 / 0 | -0.6 / 0 | -4.3 / 0 | -3.1 / 0 |
| Total with $B\Delta B$ added | 16.6 / 14.7 | 8.8 / 7.1 | 5.8 / 3.5 | 8.0 / 5.8 | 10.3 / 8.2 | 46.5 / 42.4 |

All pressure values are in units of 10^{-9} Pa. Each ordered pair (x/y) denotes pressures for the magnetosheath and magnetosphere, respectively.

noon. However, most crossings within 1 hour local time of the subsolar point exhibit a density gradient scale length less than 20% of the current layer scale length.

Energetic ions can be used to scale distances by remotely sensing the magnetopause with their large orbits of gyration. When this method was used, the density gradient scale lengths were often observed to be significantly shorter than 1 ion gyroradius and sometimes close to the electron skin depth. Magnetopause crossings often exhibit fine structure and gradients on scale lengths much smaller than the scale length of the current layer, especially for crossings near local noon. Earthward of the current layer, in seven out of the 10 CCE satellite crossings analyzed, a brief low-density plateau is observed, and these plateaus all have sharp gradients and small-scale structure. These low-density structures are not substantial boundary layers and represent, at most, the incipient formation of boundary layer plasma earthward of the current layer.

Detailed sums of all plasma and field pressure components were calculated for six of the AMPTE/CCE crossings, and the total pressure change observed across the magnetopause is less than about 20% on average, which is within experimental errors.

Pressure balance calculations to date have usually been based on only integrating the magnetic field and low-energy hydrogen components. Our results indicate that such calculations can be low by 15% or more owing to contributions by electrons, field stress, or ions other than low-energy protons. Thus electron data, full-energy composition measurements, and even field stress calculations may be necessary for some crossings in evaluating pressure balance at the magnetopause.

The absence of boundary layers in the present set of observations imposes severe constraints on various theories of boundary layer formation. These theories must explain the absence of the boundary layer in these data. Various processes for solar wind penetration of the magnetopause have been proposed to explain the boundary layer usually observed earthward of the magnetopause [e.g., Lundin, 1988], and such penetration has been unambiguously demonstrated by using ion composition measurements [Eastman et al., 1990]. Impulsive plasma penetration through a tangential discontinuity can result in boundary layer plasma under certain restrictive conditions, as shown by Savoini et al. [1994] in two-dimensional hybrid simulations. Plasma interactions with lower hybrid waves near the magnetopause may lead to localized

Table 4. Percentage Contributions to Average Pressure

| B | H | Hot e^- | Cold e^- | He^{+2} | He^+ | O^+ | H^+ (>17 keV) | O^+ (>17 keV) | He^{+2} (>17 keV) | He^+ (>17 keV) |
|---------------|-----|-----------|------------|-----------|--------|-------|--------------------|--------------------|------------------------|---------------------|
| Magnetosheath | | | | | | | | | | |
| 15 | 69 | 4 | 1.4 | 9 | 0.1 | 0.1 | 1.0 | 0.1 | 0.3 | 0 |
| Magnetosphere | | | | | | | | | | |
| 75 | 12 | 0.9 | 0.1 | 0.4 | 0.3 | 0.8 | 9 | 0.9 | 0.4 | 0.2 |

field structures and enhanced diffusion rates through turbulence [Shapiro et al., 1994]. Whether these theories are consistent with the absence of a boundary layer in the present data is not yet clear.

Reconnection is normally the prime candidate for boundary layer formation. Lin and Lee [1994] used hybrid simulations to determine properties of the outflow region during magnetic reconnection in the presence of shear flow. For all of the AMPTE/CCE cases, magnetosheath flow speeds are small compared to the difference in Alfvén speed across the magnetopause. Under this condition, Lin and Lee's simulations show that the rotational discontinuity is on the magnetosheath side of the outflow region, opposite to conditions observed in the present data. If magnetic reconnection is occurring, the pristine crossings must cut directly through the diffusion region. Such a hypothesis is consistent with the absence of the boundary layer, which would not be expected adjacent to the diffusion region, and would explain why only 10% of all crossings are without a boundary layer [Eastman et al., 1994].

Our observations are also in qualitative agreement with the recent simulations of the diffusion region and associated turbulence by Drake et al. [1994]. They find current convective instability to be the dominant process for current transport at the magnetopause. Whistler waves are driven unstable by the current layer, which maintains an overall width comparable to or larger than an ion gyroradius. Such whistlers cannot be observed with available CCE data but their study with ISEE is possible. The collisionless plasma current layers are not simple laminar structures in the 3-D simulations. Instead they break up into filaments of electron streams with a characteristic transverse width roughly equal to the electron plasma skin depth. Drake et al. suggest that these narrow current layers become turbulent and filamentary. Imbedded filamentary current structures within the magnetopause are common in our AMPTE/CCE no-boundary layer crossings based on the common bimodal signature observed in the intermediate magnetic field values derived from a minimum variance analysis. In some cases, such filamentary currents may offset the prevailing turbulence by linking up to produce FTEs that directly connect the geomagnetic and interplanetary fields, leading to macroscopic changes near the boundary and contributing to formation of the magnetospheric boundary layer [Lee, 1991]. The enhanced presence of magnetopause microstructure with $-B_z$ is also consistent with this model for collisionless reconnection at the magnetopause.

In the Drake et al. [1994] model, extremely sharp density gradient and filamentary current structures are observed at scale lengths less than ion gyroradii and down to electron scale lengths. This feature becomes most clearly resolved by analyzing magnetopause crossings without a boundary layer, because then the short density gradient scale length can be easily compared to the overall magnetopause current layer width. The associated spectrum of electromagnetic waves predicted by the current convective instability is broadband and extends from the ion cyclotron frequency up to the electron cyclotron frequency. Such a spectrum is commonly observed at the magnetopause, as reviewed in detail by Thorne and Tsurutani [1991]. Drake et al. predict that these turbulent fluctuations should be peaked in association with the highest field shear, a result supported by the observations of Song [1994]. Our observations show further that processes transporting current must be much more efficient than processes transporting density, because the scale length for density is often less than that of the current, especially for magnetopause crossings near local noon. Overall, the Drake et al. model for the current convective

instability compares favorably with our high-resolution observations of magnetopause microstructure near the subsolar region.

Acknowledgments. The authors are grateful to Edward Shelley of Lockheed Palo Alto Research Laboratory, Lead Investigator (L.I.) for the CCE HPCE experiment; Thomas Potemra of Johns Hopkins University Applied Physics Laboratory (JHU/APL), L.I. for the CCE MAG experiment; George Gloeckler, University of Maryland, L.I. for the CCE CHEM experiment; and Richard McEntire, JHU/APL, L.I. for the CCE MEPA experiment. McEntire is also CCE Principal Investigator, succeeding S. Krimigis in this capacity. All other instrument "PIs" on CCE are known as Lead Investigators. For the ISEE 2 spacecraft, Chris Russell, UCLA, is P.I. for the ISEE fluxgate magnetometer experiments, and Götz Paschmann, Max Planck Institute in Garching, Germany, is P.I. for the ISEE fast plasma experiment (a cooperative effort of LANL and the Max Planck Institute). We thank James Drake, Surjalal Sharma, and Michael Collier of the University of Maryland, Brian Anderson of JHU/APL, and Robert Strangeway of UCLA for several helpful suggestions. This work has been supported by NASA via JHU/APL contract 601527 and grants NAGW-101, NAGW-1848, and NGR 21-002-316. CCE/CHEM data analysis support at the University of Maryland was supported under NASA grant NAG5-716. Research at Lockheed was supported by NASA AMPTE data analysis contract NAS5-30565 and NASA grant NAGW-4049. Research at the Los Alamos Scientific Laboratory has been supported by NASA grant W-18287. Helpful comments by both reviewers are very much appreciated.

The Editor thanks V. I. Shevchenko and another referee for their assistance in evaluating this paper.

References

- Bame, S. J., J. R. Asbridge, H. E. Felthaus, J. P. Glore, G. Paschmann, P. Hemmerich, K. Lehmann, and H. Rosenbauer, ISEE 1 and ISEE 2 fast plasma experiment and the ISEE-1 solar wind experiment, *IEEE Trans. Geosci. Electron.*, GE-16, 216, 1978.
- Bryant, D. A., S. M. Krimigis, and G. Haerendel, Outline of the active magnetospheric particle tracer explorers (AMPTE) mission, *IEEE Trans. Geosci. Remote Sens.*, GE-23, 177, 1985.
- Cowley, S. W. H., Theoretical perspectives of the magnetopause: A tutorial review, in *Physics of the Magnetopause*, *Geophys. Monogr. Ser.*, vol. 90, edited by P. Song, B. U. Ö. Sonnerup, and M. F. Thomsen, p. 29, AGU, Washington, D. C., 1995.
- Drake, J. F., Jr., J. Gerber, and R. G. Kleva, Turbulence and transport in the magnetopause current layer, *J. Geophys. Res.*, 99, 11,211, 1994.
- Eastman, T. E., E. W. Hones Jr., S. J. Bame, and J. R. Asbridge, The magnetospheric boundary layer: Site of plasma, momentum, and energy transfer from the magnetosheath into the magnetosphere, *Geophys. Res. Lett.*, 3, 685, 1976.
- Eastman, T. E., E. A. Greene, S. P. Christon, G. Gloeckler, D. C. Hamilton, F. M. Ipavich, G. Kremser, and B. Wilken, Ion composition in and near the frontside boundary layer, *Geophys. Res. Lett.*, 17, 2031, 1990.
- Eastman, T. E., B. Anderson, P. Cargill, S. Fuselier, and J. Gosling, Microstructure of the magnetopause, in *The Initial Results From STEP Facilities and Theory Campaigns: Proceedings of the 1992 STEP Symposium/5th COSPAR Colloquium*, edited by D. Baker, V. Papitashvili, and M. Teague, Pergamon, Tarrytown, N. Y., 1994.
- Fritz, T. A., and S. C. Fahnenstiel, High temporal resolution energetic particle soundings at the magnetopause on November 8, 1977, using ISEE 2, *J. Geophys. Res.*, 87, 2125, 1982.
- Fuselier, S. A., B. J. Anderson, and T. G. Onsager, Particle signatures of magnetic topology at the magnetopause: AMPTE/CCE observations, *J. Geophys. Res.*, 100, 11,805, 1995.
- Gloeckler, G. et al., The charge-energy-mass spectrometer for 0.3–300 keV/e ions on the AMPTE CCE, *IEEE Trans. Geosci. Remote Sens.*, GE-23, 234, 1985.
- Gosling, J. T., M. F. Thomsen, S. J. Bame, and C. T. Russell, Accelerated plasma flows at the near-tail magnetopause, *J. Geophys. Res.*, 91, 3029, 1986.
- Le, G., and C. T. Russell, The thickness and structure of high beta magnetopause current layer, *Geophys. Res. Lett.*, 21, 2451, 1994.
- Lee, L. C., The magnetopause: A tutorial review, in *Physics of Space Plasmas (1990)*, *SPI Conf. Proc.*, vol. 10, edited by T. Chang, G. B. Crew, and J. R. Jasperse, p. 33, Scientific, Cambridge, Mass., 1991.

- Lin, Y., and L. C. Lee, Reconnection layer at the flank magnetopause in the presence of shear flow, *Geophys. Res. Lett.*, **21**, 855, 1994.
- Lundin, R., On the magnetospheric boundary layer and solar wind energy transfer into the magnetosphere, *Space Sci. Rev.*, **48**, 263, 1988.
- McEntire, R. W., E. P. Keath, D. E. Fort, A. T. Y. Lui, and S. M. Krimigis, The medium-energy particle analyzer (MEPA) on the AMPTE CCE spacecraft, *IEEE Trans. Geosci. Remote Sens.*, **GE-23**, 230, 1985.
- Northrop, T. G., and T. J. Birmingham, Stability of tangential discontinuities, *Sol. Phys.*, **14**, 226, 1970.
- Paschmann, G., I. Papamastorakis, W. Baumjohann, N. Schopke, C. W. Carlson, B. U. Ö. Sonnerup, and H. Lühr, The magnetopause for large magnetic shear: AMPTE/IRM observations, *J. Geophys. Res.*, **91**, 11,099, 1986.
- Potemra, T. A., L. J. Zanetti, and M. H. Acuna, The AMPTE CCE magnetic field experiment, *IEEE Trans. Geosci. Remote Sens.*, **GE-23**, 246, 1985.
- Russell, C. T., ISEE 1 and 2 fluxgate magnetometers, *IEEE Trans. Geosci. Electron.*, **GE-16**, 239, 1978.
- Savoini, P., M. Scholer, and M. Fujimoto, Two-dimensional hybrid simulations of impulsive plasma penetration through a tangential discontinuity, *J. Geophys. Res.*, **99**, 19,377, 1994.
- Scarf, F. L., The AMPTE/CCE plasma wave investigation, *IEEE Trans. Geosci. Remote Sens.*, **GE-23**, 250, 1985.
- Shapiro, V. D., V. I. Shevchenko, P. J. Cargill, and K. Papadopoulos, Modulational instability of lower hybrid waves at the magnetopause, *J. Geophys. Res.*, **99**, 23,735, 1994.
- Shelley, E. G., A. Ghielmetti, E. Hertzberg, S. J. Battel, K. Altwegg von Burg, and H. Balsiger, The AMPTE/CCE hot-plasma composition experiment (HPCE), *IEEE Trans. Geosci. Remote Sens.*, **GE-23**, 241, 1985.
- Siscoe, G. L., L. Davis Jr., P. J. Coleman Jr., E. J. Smith, and D. E. Jones, Power spectra and discontinuities of the interplanetary magnetic field: Mariner 4, *J. Geophys. Res.*, **73**, 61, 1968.
- Song, P., Observations of waves at the dayside magnetopause, in *Solar Wind Sources of Magnetospheric Ultra-Low-Frequency Waves*, *Geophys. Monogr. Ser.*, vol. 81, edited by M. Engebretson, K. Takahashi, and M. Scholer, p. 159, AGU, Washington, D. C., 1994.
- Sonnerup, B. U. Ö., and L. J. Cahill Jr., Magnetopause structure and altitude from Explorer 12 observations, *J. Geophys. Res.*, **72**, 171, 1967.
- Thorne, R., and B. Tsurutani, Wave-particle interactions in the magnetopause boundary layer, in *Physics of Space Plasmas (1990)*, *SPI Conf. Proc.*, vol. 10, edited by T. Chang, G. B. Crew, and J. R. Jasperse, p. 119, Scientific, Cambridge, Mass., 1991.

T. E. Eastman, Institute for Physical Science and Technology, University of Maryland, College Park, MD 20742. (e-mail: eastman@glue.umd.edu)

S. A. Fuselier, Lockheed Palo Alto Research Laboratory, Palo Alto, CA 94304. (e-mail: fuselier@lockhd.span.nasa.gov)

J. T. Gosling, Los Alamos National Laboratory, Los Alamos, NM 87545. (e-mail: gosling@sstcx1.lanl.gov)

(Received February 17, 1995; revised August 28, 1995; accepted September 5, 1995.)

Electron and ion signatures of field line topology at the low-shear magnetopause

S. A. Fuselier

Lockheed Martin Palo Alto Research Laboratory, Palo Alto, California

B. J. Anderson

Applied Physics Laboratory, The Johns Hopkins University, Laurel, Maryland

T. G. Onsager

Space Environment Center, NOAA, Boulder, Colorado

Abstract. Electrons above 50 eV are a sensitive indicator of field line topology at the magnetopause, particularly when the solar wind dynamic pressure is high and the shear across the boundary is low. AMPTE/CCE electron observations under conditions when these criteria are fulfilled indicate a clear topological transition from the magnetosheath to open field lines threading the magnetopause in the magnetosheath boundary layer (MSBL). Once across the magnetopause and in the low latitude boundary layer (LLBL), the fast moving electrons are no longer a good indicator of magnetic field topology. In particular, the counterstreaming electron observations in this region are not an indicator of a closed magnetic topology. Rather, the field topology continues to be open, and the counterstreaming occurs because electrons from the magnetopause region move rapidly enough along the LLBL magnetic field to make it to the ionosphere, mirror, and return to the observation point. Slower moving ions provide important additional information on magnetic field topology in the LLBL. CCE observations discussed here indicate that two types of solar wind ion distributions are observed in this layer. One type consists of a single, heated distribution which resembles somewhat the electron distribution in the layer. The field-aligned velocity of this distribution is near zero. The other type consists of a unidirectional streaming distribution. The field-aligned velocity of this distribution is higher than in the adjacent magnetosheath. Combining these observations with magnetospheric ion observations (e.g., O^+) in the LLBL and with electron observations in the MSBL, two distinct magnetic field topologies emerge for the low-shear magnetopause. The first, which gives rise to single, low-parallel-velocity and heated solar wind ion distributions in the LLBL, is magnetic reconnection poleward of the cusp. The second, which gives rise to unidirectional streaming solar wind ion distributions in the LLBL, is magnetic reconnection equatorward of the cusp. This type of component reconnection may not be sustained in a quasi-steady fashion.

1. Introduction

Magnetic reconnection is a primary means of transport of mass, energy, and momentum across the magnetopause. There is significant evidence that this process occurs when the shear in the magnetic field across the magnetopause is high. This evidence includes accelerated plasma flows in the low latitude boundary layer earthward of the magnetopause [e.g., Paschmann *et al.*, 1979], separate electron and ion edges in the low latitude boundary layer [Gosling *et al.*, 1990], so-called "D" shaped distributions (i.e., distributions with a low speed cutoff parallel to the magnetic field) in the layer [Smith and Rodgers, 1991; Fuselier *et al.*, 1991a], and a nonzero

normal component to the magnetic field across the magnetopause [e.g., Sonnerup and Ledy, 1979].

Evidence of magnetic reconnection is more difficult to identify at low latitudes when the shear in the magnetic field is low. It is generally believed that under these conditions reconnection occurs at high latitudes in the vicinity of the cusps, where the magnetic shear is high [e.g., Paschmann *et al.*, 1990]. Some direct observations of high-latitude reconnection under high-shear conditions have been reported [e.g., Gosling *et al.*, 1991; Kessel *et al.*, 1996]. The determination of the low-latitude signatures of this high-latitude reconnection is difficult because of the low-shear conditions in the region. One of the primary difficulties in this determination is the identification of the magnetopause itself. When the shear is low, the local magnetopause current layer may be very weak or even nonexistent despite the fact that it may be strong in the vicinity of the reconnection site. Recently, however, a procedure using both plasma and magnetic field data to identify the magnetopause has

demonstrated that a relatively sharp boundary can be identified in the plasma data even when the local magnetic field observations show little or no current layer [Paschmann *et al.*, 1993]. Furthermore, close inspection of these data near low-shear magnetopause crossings indicates that electron fluxes are a sensitive indicator of magnetic field line topology of the boundary [Fuselier *et al.*, 1995] (hereafter called paper 1). Since the focus of this paper is these signatures of reconnection at the low-shear magnetopause, it is important to summarize the findings of paper 1 in detail.

Figure 1 (paper 1, Figure 5) is a schematic representation of magnetic reconnection poleward of the southern cusp for strongly northward interplanetary magnetic field (IMF) conditions. Three regions of distinct magnetic topology are identified in Figure 1. Sunward of the magnetopause current layer, the magnetic field lines in region 1, the plasma depletion layer (PDL), are draped on the dayside subsolar magnetopause but are not magnetically connected to the Earth. Field lines that have reconnected in the cusp region form a second region sunward of the magnetopause, the magnetosheath boundary layer (MSBL) [e.g., Cowley, 1982]. These field lines have one "foot" in the southern ionosphere. Field lines that have convected across the magnetopause form a third region, the low latitude boundary layer (LLBL). In essence, the identification of a high-latitude reconnection

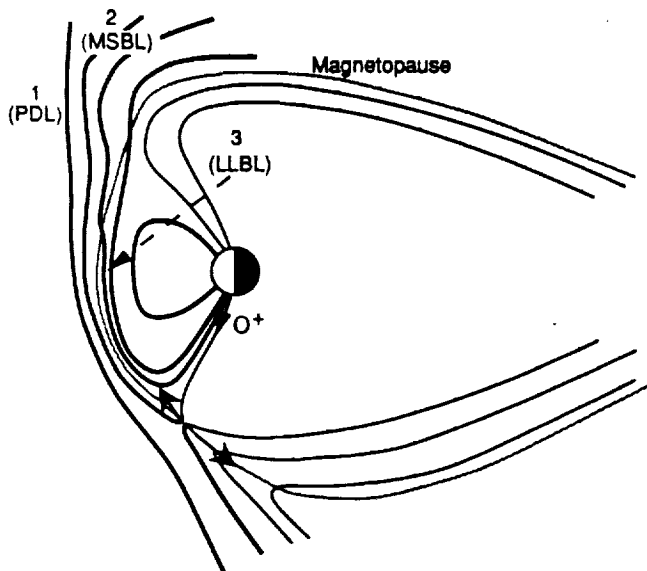


Figure 1. Schematic of the evolution of a solar wind field line consistent with the observations in paper 1. The plasma depletion layer (PDL) (region 1) field line is draped against the magnetopause but still has both ends open to the solar wind. Reconnection occurs poleward of the southern cusp to form an magnetosheath boundary layer MSBL (region 2) field line that is connected to the southern ionosphere and the solar wind. Solar wind electrons heated at the current layer form a population of unidirectional streaming electrons in the MSBL. Finally, the field line convects across the magnetopause into the low latitude boundary layer LLBL (region 3). The source of hot electrons from the current layer stream antiparallel to the magnetic field to the ionosphere, mirror and return to the LLBL. This produces a counterstreaming electron distribution in the layer.

signature at the low-latitude, low-shear magnetopause reduces to the identification of the magnetosheath boundary layer as a topologically distinct region from either the PDL or LLBL. Electron distribution functions are an ideal conveyer of this reconnection signature because of their high parallel speeds. They can provide evidence of reconnection even if it occurs several Earth radii away from a low latitude observation point.

The primary purpose of paper 1 was to demonstrate the existence of signatures in the electron distribution functions near the magnetopause that were consistent with the schematic in Figure 1. Electrons in the energy range from 50 eV to a few keV prove to be sensitive indicators of the magnetic field topology. Electrons at energies of the order of 100 eV are primarily from the magnetosheath, although they are above typical magnetosheath thermal energies of the order of 50 eV or less. Electrons at energies of the order of or greater than a kilovolt are likely from the Earth's magnetosphere.

Electrons in the 50 eV to a few keV energy range are particularly sensitive indicators of magnetic topology when the solar wind dynamic pressure is high. The combination of high dynamic pressure and low magnetic shear produces strong PDL upstream (sunward) of the magnetopause [e.g., Anderson and Fuselier, 1993]. The parallel temperature of the electron distribution is significantly reduced in this strong PDL (region 1 in Figure 1). The reduction in the parallel temperature in the PDL facilitates identification of a heated population of electrons streaming from the magnetopause along reconnected field lines.

When a spacecraft is just sunward of the low-shear magnetopause and on reconnected field lines, the strongly depleted magnetosheath electron distribution and the population of heated electrons from the magnetopause combine to form a unidirectional streaming electron distribution. This streaming distribution is observed throughout the MSBL up to the magnetopause. In paper 1, these streaming distributions and simultaneous solar wind and magnetospheric ion measurements were shown to be consistent with a continuously heated population of solar wind ions and electrons originating from the location where the reconnected field line in the MSBL crosses the magnetopause (region 2 in Figure 1). This MSBL signature is observed in the subsolar region just sunward of essentially all highly compressed, low-shear magnetopause crossings, indicating that the low-shear magnetopause is an open boundary essentially all the time (see paper 1).

Earthward of the low-shear magnetopause, in the low latitude boundary layer (region 3 in Figure 1), bidirectional streaming electron distributions were observed. Previously, these bidirectional streaming distributions were interpreted as evidence for closed magnetic field lines possibly produced by a second reconnection in the northern hemisphere (Figure 1) [e.g., Song *et al.*, 1994]. However, the bidirectional streaming electrons were interpreted differently in paper 1. Simultaneous ion observations suggested that the bidirectional streaming electron distributions were produced by first heating the solar wind electron population at the magnetopause. The heated electron population then propagates to the ionosphere, mirrors, and returns to the spacecraft along the magnetic field thus producing the bidirectional streaming. Round-trip travel times for ~1 keV electrons are of the order of seconds so that bidirectional streaming electron distributions are observed throughout the open low latitude boundary layer.

As a result of this bidirectional streaming, electrons are not useful for determining the topology of field lines once a spacecraft is in the low latitude boundary layer and located between the source of hot electrons (at the magnetopause where the magnetic field line crosses the boundary) and the mirror point (in the ionosphere). However, because ions have a much lower velocity along the magnetic field, they have the potential for providing information on the topology of magnetic field lines in the LLBL.

The purpose of this paper is to extend the results of paper 1 using the ion and electron observations in the subsolar region near low-shear magnetopause crossings with emphasis on the ion observations. Electron observations sunward of the magnetopause in the MSBL and ion observations earthward of the magnetopause in the LLBL from two representative magnetopause crossings are used to distinguish between two distinct open magnetic field topologies. One topology (illustrated in Figure 1) occurs when magnetosheath field lines reconnect with previously reconnected lobe magnetic field lines poleward of the cusp. The second topology occurs when magnetosheath field lines reconnect with previously closed magnetic field lines in the magnetosphere equatorward of the cusp. A survey of the limited number of low-shear magnetopause crossings from the AMPTE/CCE spacecraft shows that both topologies are observed but that the reconnection poleward of the cusp may be somewhat more common.

As in paper 1, this study uses magnetic field, ion, and electron data from the AMPTE/CCE spacecraft. Magnetic field data were from the magnetometer experiment [Potemra *et al.*, 1985]. Electron and ion composition data were from the hot plasma composition experiment (HPCE) [Shelley *et al.*, 1985]. These experiments have been discussed in detail previously (see paper 1 and references therein). The significant difference in time resolution of the electron and ion composition measurements is important for the observations presented here. Whereas the electron instrument required one spin (6 s) for a full two-dimensional distribution over its energy range, the ion mass spectrometer required approximately 2 min for simultaneous, full two-dimensional distributions of each major ion species (H^+ , He^{2+} , He^+ , and O^+) over its energy range.

2. Observations

Event 1: December 13, 1984 (day 348)

An overview of the low-shear magnetopause crossings by the CCE spacecraft on December 13, 1984 is shown in Figure 2. During this 30 min interval, the spacecraft was at 0930 local time, $7.9 R_E$ from the Earth on an inbound trajectory and nearly in the ecliptic plane (the magnetic latitude was -14°). Magnetopause crossings at this local time and at this distance from the Earth require a solar wind dynamic pressure of more than 5 times its nominal value [e.g., Sibeck *et al.*, 1991]. The top panel shows spin averaged (6 s) electron flux at three different energies. High fluxes at 0.151 keV are characteristic of the magnetosheath/plasma depletion layer, while high fluxes at 3.95 keV are characteristic of the magnetosphere. In this event the magnetospheric and solar wind sources contribute approximately equally to the flux at 0.773 keV (see below). Different plasma regions are coded at the top of the electron flux panel. Solid lines identify the plasma depletion

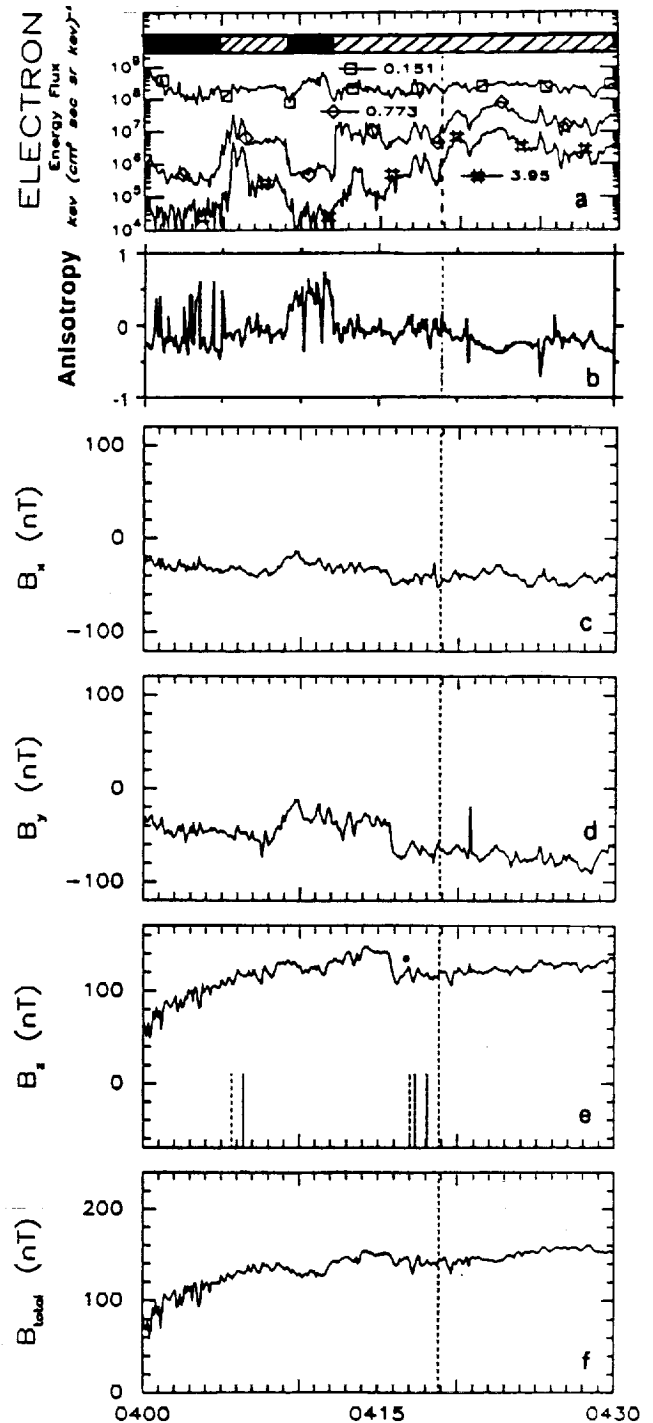


Figure 2. Spin-averaged (6 s) electron fluxes and magnetic field data from an inbound magnetopause crossing on 13 December 1984 (day 348). Solid bars in the top panel show magnetosheath/plasma depletion layer intervals while striped bars show boundary layer intervals on both sides of the magnetopause. Short vertical dashed lines in the panel containing the B_z component of the magnetic field indicate brief encounters with the magnetopause with the final magnetopause crossing occurring at the full vertical dashed line. Encounters with the magnetopause boundary layers are identifiable by increases in the electron flux primarily at 0.773 and 3.95 keV. Magnetopause crossings are not evident in the magnetic field data from these low-shear magnetopause crossings.

layer (PDL) upstream from the magnetopause and striped lines identify boundary layers on both sides of the magnetopause (further distinction of these layers is presented below). The second panel from the top shows the electron anisotropy ($T_{\perp}/T_{\parallel}-1$), with the temperatures calculated using the full energy range of the instrument (50 eV to 25 keV). The lower four panels show the GSE components and total magnitude of the magnetic field, respectively. Short vertical dashed lines in the panel containing the B_z component of the magnetic field indicate brief crossings of the magnetopause with the final inbound crossing occurring at the full vertical dashed line at about 0419 UT. These crossings were determined from high-resolution electron data as discussed below and in paper 1.

The lack of an identifiable rotation in the magnetic field at the magnetopause crossings indicates that there was little or no current layer locally where the spacecraft traversed the boundary. However, ion and electron distributions observed on either side of the magnetopause can originate from locations well removed from the crossing point and may have encountered a magnetopause with larger shear. The general increase in the total magnetic field from 0400 to 0405 UT and the corresponding decrease in the flux of 0.151 keV electrons (indicating a decrease in the magnetosheath electron density) are characteristic of the plasma depletion layer. Prior to 0400 UT, the spacecraft was in the magnetosheath [Anderson and Fuselier, 1993]. After 0400 UT, the spacecraft remained in the PDL except for those intervals of brief magnetopause encounters and extended boundary layer intervals from about 0405 to 0410 UT and after about 0412 UT. These magnetopause encounters and boundary layer intervals are identifiable by the increase in the flux of relatively energetic (0.773 and 3.95 keV) electrons and changes in the anisotropy from greater than zero in the PDL to less than zero in the boundary layers.

An example of the high-resolution electron observations for one of these brief encounters with the magnetopause and its associated boundary layers is shown in Figure 3. The electron energy fluxes (top) at two energies (0.151 and 0.773 keV) at 155 ms time resolution, the highest resolution of the instrument are shown. Again, electrons with 0.151 keV are primarily from the magnetosheath while those at 0.773 keV may have either a magnetosheath or magnetospheric origin. The instantaneous pitch angle (bottom) of the center of the field-of-view of the electron instrument over the 2 min interval is shown. In one 6 s spacecraft spin, the pitch angle cycles through 0° - 180° and 180° - 0° , indicating that the magnetic field was in the field-of-view of the electron instrument.

There are three regions identified (top) in Figure 3. The first region at the left-hand edge is the plasma depletion layer (PDL). This region is characterized by flux minima parallel and antiparallel to the magnetic field and peak fluxes perpendicular to the field. A second region identified as the magnetosheath boundary layer (MSBL) is characterized by peak fluxes along the magnetic field and flux minima antiparallel to the magnetic field. Also, the 0.773 keV flux levels parallel to the magnetic field are significantly higher in the MSBL than in the PDL, and the flux levels for both 0.151 and 0.773 keV antiparallel to the magnetic field in the MSBL are at or below those in the PDL. Finally, the third region, which is identified as the low latitude boundary layer (LLBL), is characterized by enhanced flux levels that peak both parallel and antiparallel to the magnetic field. The enhanced flux levels either parallel or antiparallel to the magnetic field in Figure 3 correspond to the enhanced flux levels at higher electron energies associated with boundary layer intervals in Figure 2, and the enhanced parallel fluxes are responsible for the change in the electron anisotropy in the transition from

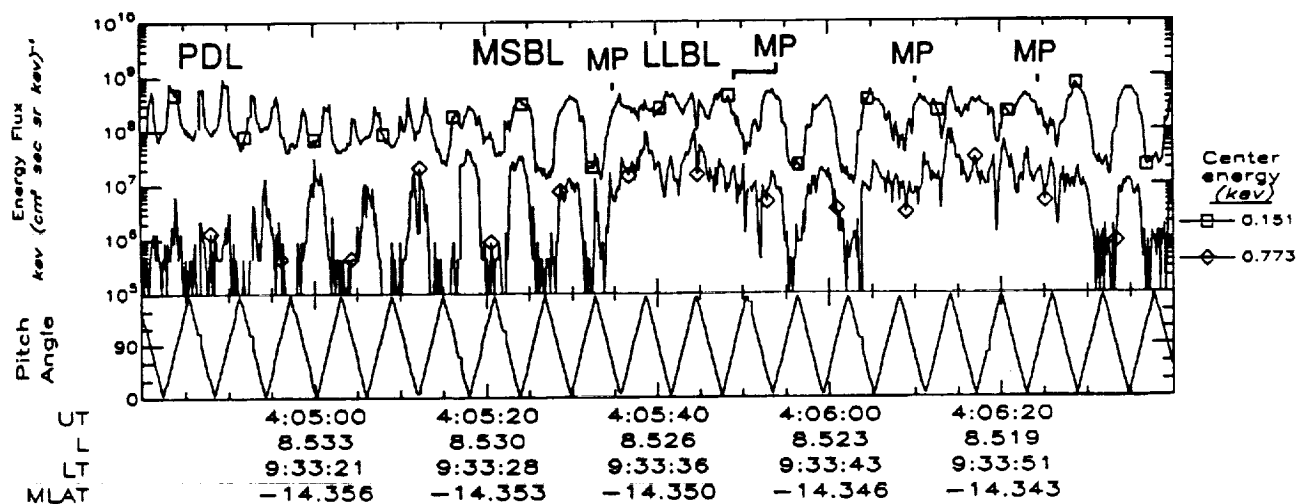


Figure 3. High resolution (155 ms) electron fluxes for a 2 min interval containing a brief encounter with the magnetopause on 13 December 1984 (day 348) starting at 0404:40 UT. (bottom) The instantaneous pitch angle of the measurements is shown. Three regions are identified as plasma depletion layer (PDL), magnetosheath boundary layer (MSBL) sunward of the magnetopause, and low latitude boundary layer (LLBL) earthward of the magnetopause. The PDL is characterized by flux minima parallel and antiparallel to the magnetic field and peak fluxes perpendicular to the magnetic field. The MSBL has peak fluxes parallel to the magnetic field and flux minima antiparallel to the magnetic field. The LLBL fluxes parallel to the field are similar to that in the MSBL but antiparallel fluxes are also nearly as high, indicating a counterstreaming electron population.

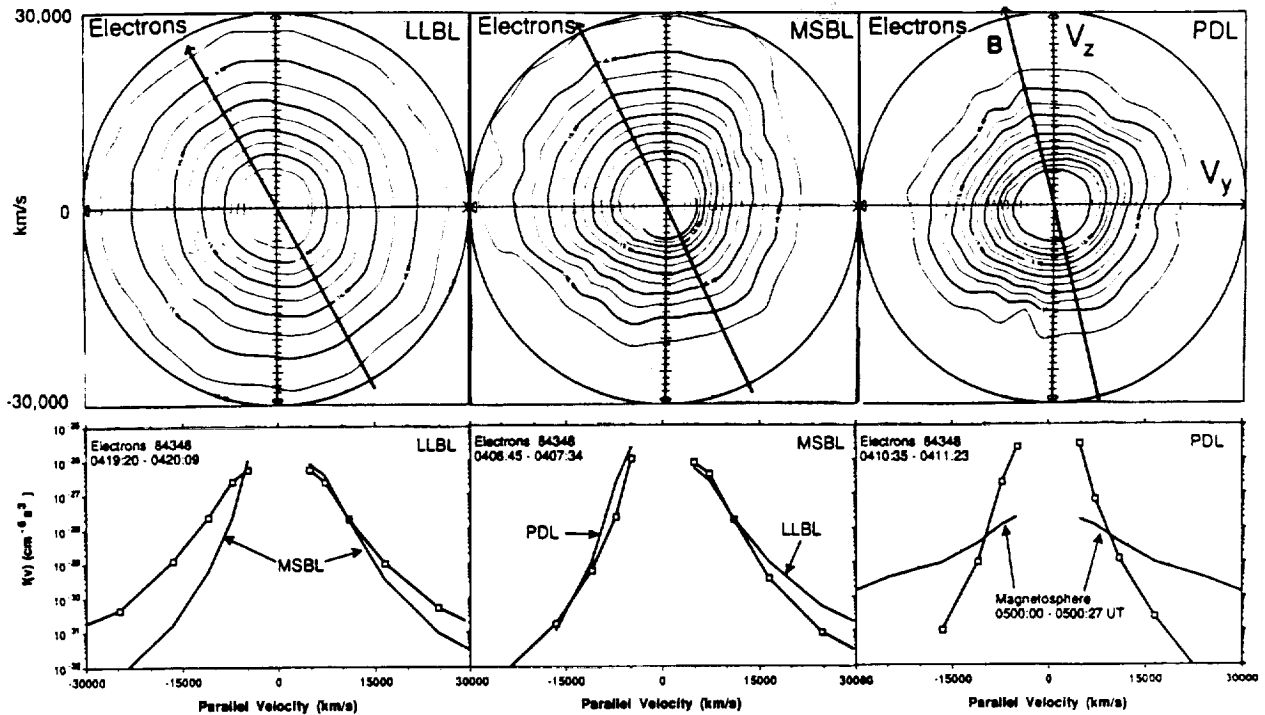


Figure 4. Electron distributions from the three regions (times are different from that in Figure 3). (top) Contours of constant phase space density. (bottom) Cuts parallel to the magnetic field. The V_x velocity is northward and the V_y velocity is duskward in the ecliptic so that the distribution is measured in a plane approximately tangent to the subsolar magnetopause as viewed from the Sun. MSBL electron distributions (middle) are composed of two source populations. Parallel to the field is a population resembling the LLBL electron population while perpendicular to the field is a population resembling the PDL electron population. This combination of two sources and parallel streaming indicates that the MSBL is on open magnetosheath magnetic field lines threading the magnetopause below the spacecraft location.

the PDL to the MSBL or LLBL. Quantitative differences in the 0.151 and 0.773 keV fluxes (for example at 0405:00 UT) in Figure 3 are probably indicative of the fact that the lower energy electrons are almost entirely magnetosheath in origin while the higher energy electrons have a significant magnetospheric contribution.

Figure 4 shows representative two dimensional electron distributions and cuts from each of the three plasma regions. (Time intervals for the three distributions were chosen to correspond to time intervals for the ion observations in Figures 5, 6, and 7.) Contours of constant phase space density with two contours per decade are shown (top). The V_x direction is approximately perpendicular to the ecliptic, and the V_y direction is approximately in the GSE y direction so that the distributions are measured in a plane approximately tangent to the subsolar magnetopause as viewed from the sun. Cuts in the distributions along the ambient magnetic field (bottom) are shown. In the bottom right of Figure 4, the source populations parallel to the magnetic field in the PDL and magnetosphere are compared. These cuts show that electrons at energies below about 0.773 keV (or about 10,000 km/s in Figure 4) are essentially entirely from the magnetosheath. Above this energy, the magnetosphere can contribute significantly to the observed distributions in the MSBL and LLBL.

We interpret the electron distribution in the MSBL (middle) as in paper 1. Although the ultimate source is the

magnetosheath, the electrons at energies below about 0.773 keV in the MSBL behave as if they are from two sources, one source associated with the PDL (right) and the second associated with the LLBL (left). The cooler electron population antiparallel to the magnetic field in the MSBL is nearly the same as the population in the PDL, while the hot electron population parallel to the magnetic field in the MSBL is nearly the same as the population in the LLBL.

The superposition of these two populations indicates that the spacecraft is on reconnected field lines in the MSBL. Furthermore, these unidirectional streaming electrons at energies below 0.773 keV are observed throughout the MSBL up to the magnetopause (see, for example, Figure 3), indicating that the source of the enhanced fluxes of electrons below 0.773 keV is the location where the magnetic field line threading the spacecraft crosses the magnetopause. Thus a heated, streaming population of electrons exists all along the magnetopause and is not confined to the narrow region around the diffusion region as originally suggested in association with impulsive reconnection [e.g., Scudder *et al.*, 1984]. In a study of flux transfer events (FTEs) in the magnetosheath, Thomsen *et al.* [1987] also found that the streaming electron population in FTEs was not confined to a narrow region around the diffusion region. However, they could not conclude that the streaming population was heated magnetosheath electrons. In Figure 4, it is clear that the magnetospheric population contributes only above about 0.151 keV, and

therefore the enhanced fluxes in the parallel direction below this energy are of magnetosheath origin. These enhanced fluxes can be readily identified in the MSBL because the parallel flux decreases significantly from the magnetosheath to the PDL (not shown). Finally, the unidirectional streaming parallel to the magnetic field indicates that the reconnected field line threading the spacecraft in the MSBL crosses the magnetopause southward of the spacecraft.

As the spacecraft crosses the magnetopause from the MSBL to the LLBL, the relatively cool electron population antiparallel to the magnetic field with energies below 0.773 keV is replaced by a heated streaming distribution. This results in a bidirectional streaming distribution in the LLBL. Thus, in the transition from the PDL to the LLBL, the electron distribution changes its anisotropy from $T_{\perp} > T_{\parallel}$ to $T_{\parallel} > T_{\perp}$ [see also Paschmann *et al.*, 1993]. One interpretation of the bidirectional distributions in the LLBL is that this layer is on closed magnetic field lines and the electrons mirror at the two ionospheric mirror points in opposite hemispheres. However, ion observations discussed below suggest that the LLBL is still on open field lines (see also paper 1). The bidirectional streaming is observed in the LLBL because the spacecraft is between the source of hot electrons (the magnetopause) and a mirror point (in the ionosphere). Thus hot electrons from the magnetopause stream down to the ionosphere, mirror and return to the spacecraft.

Simultaneous ion composition measurements in Figures 5, 6, and 7 are consistent with this interpretation of the electron observations. Furthermore, these ion measurements resolve important issues that the electron observations cannot,

including the origin of the heated particles at the magnetopause and the magnetic topology of the LLBL.

Figure 5 shows two-dimensional He^{2+} distributions and cuts from the three regions. (In these and subsequent ion distributions, one count above background was subtracted from the distribution so that phase space densities represent at least two counts above background.) The format is the same as that for the electron distributions in Figure 4 with two exceptions. First, there is a significant change in the velocity scales. The lowest measured electron velocities in Figure 4 are of the order of 5,000 km/s or about 5 times higher than the highest He^{2+} velocities in Figure 5. Second, unlike the electron distributions in Figure 4, the He^{2+} distributions in Figure 5 have essentially no contribution from a magnetospheric source. Evidence for a magnetosheath source for He^{2+} is seen in the comparison of the PDL and magnetospheric populations in the lower right of Figure 5. Despite the significant difference in velocity scales, the He^{2+} distributions in the three regions in Figure 5 are qualitatively similar to the corresponding low energy electron distributions in Figure 4.

The PDL He^{2+} distribution (right) is strongly anisotropic ($T_{\perp} > T_{\parallel}$) with a $-V_y$ flow consistent with the dawnward deflection of the solar wind around the dawnside magnetopause. This flow is shown by the dot along the magnetic field vector in the top right. Compared to the PDL distribution, the MSBL distribution (middle) is cooler in the antiparallel direction and has a heated, streaming component parallel to the magnetic field at velocities greater than 500 km/s. The lower temperature antiparallel to the magnetic field

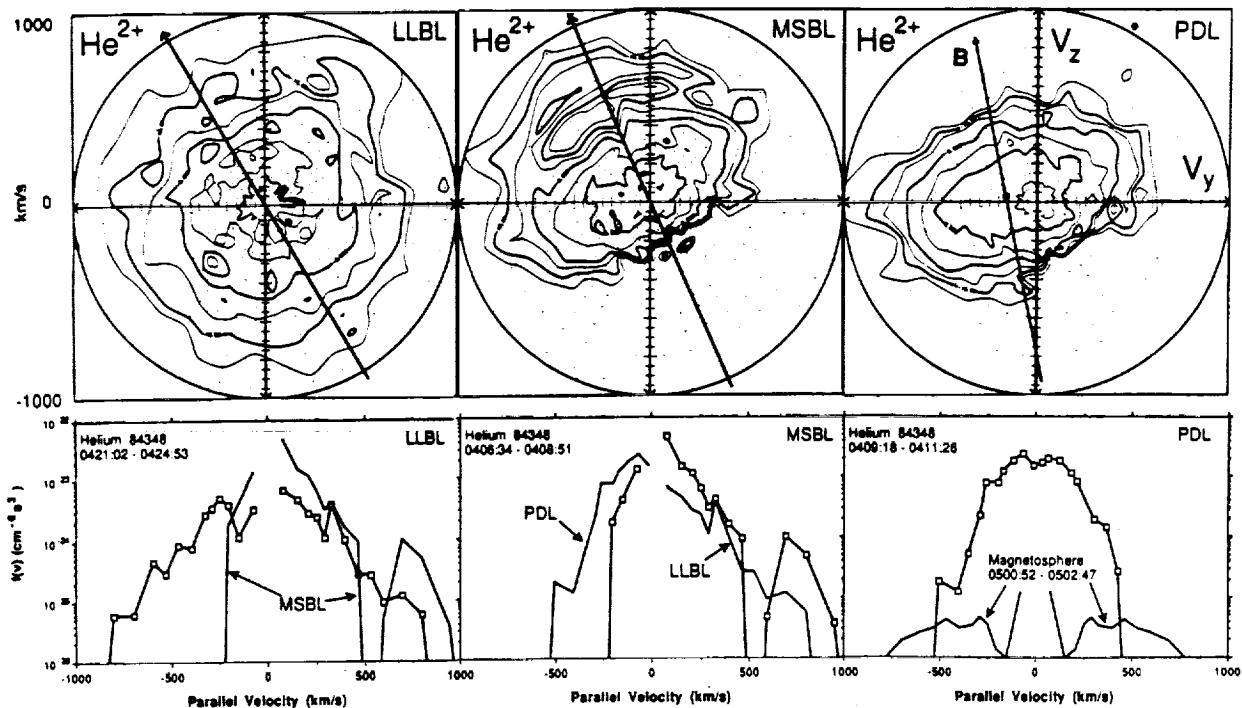


Figure 5. He^{2+} distributions from the three regions. The format is the same as in Figure 4. Qualitatively, the He^{2+} distributions are similar to the electron distributions in Figure 4. In the PDL, (right), the dawnward deflection of the plasma is consistent with that expected for flow around the magnetospheric obstacle. The MSBL distribution (middle) has a parallel streaming component similar to the electron component in Figure 4. In the LLBL (left), the He^{2+} distribution is approximately isotropic with significant flux parallel and antiparallel to the magnetic field down to the lowest velocities measured.

in the MSBL when compared to that in the PDL is consistent with the interpretation that the MSBL is closer to the magnetopause than the PDL. The draping of the magnetic field against the magnetopause causes cooling in the parallel direction [e.g., Fuselier *et al.*, 1991b; Denton *et al.*, 1994] as the plasma convects through the PDL and MSBL up to the magnetopause. The parallel streaming He^{2+} component in the MSBL in Figure 5 is similar to the parallel streaming electron component in the MSBL in Figure 4. The beam-like appearance of the parallel component in the MSBL distribution in Figure 5 may be the result of time aliasing of the distribution (measurement time approximately 2 min) or could be the result of time-of-flight effects in the MSBL. Since the He^{2+} fluxes in the magnetosphere are negligible compared to those in the PDL, the heated, streaming He^{2+} population in the MSBL must have originated in the PDL.

In the LLBL, (top left of Figure 5), the He^{2+} distribution is considerably more isotropic. In particular, there is significant flux in both the antiparallel and parallel directions at all velocities down to the lowest measured. This distribution is similar to the counterstreaming electron distribution in the LLBL in Figure 4. Because of its symmetry, the flow velocity of this distribution parallel to the magnetic field is nearly zero. Thus there is little, if any, change in the parallel flow velocity across the magnetopause.

Figure 6 shows two-dimensional H^+ distributions and cuts from the three regions. The format is the same as that for Figures 4 and 5. The comparison of the PDL and magnetospheric sources in the lower right of Figure 6 indicates the magnetospheric source does not make a significant contribution to the LLBL and MSBL H^+ populations at velocities below about 500 km/s. However, in the

case of H^+ below 500 km/s, a high-latitude ionospheric source may make a direct contribution to the LLBL flux. This ionospheric source would not necessarily be observed in the adjacent magnetosphere (as discussed below). All the features of the He^{2+} distributions in Figure 5 are seen in the H^+ distribution below 500 km/s in Figure 6. The H^+ distribution in the PDL (right) is anisotropic ($T_{\perp} > T_{\parallel}$) with a $-V_z$ flow. The antiparallel component of the H^+ distribution is cooler in the MSBL (middle) than in the PDL. In addition, the MSBL distribution has a heated, streaming component in the parallel direction. Again, this streaming distribution appears beam-like because of time aliasing in the measurement and/or time-of-flight effects in the MSBL. Finally, in the LLBL, the H^+ distribution is approximately isotropic.

Below about 250 km/s along the magnetic field, the LLBL H^+ distribution exhibits a perpendicular anisotropy that is not clearly evident in the He^{2+} distribution in Figure 5. The LLBL O^+ distribution in Figure 7 provides important evidence for an ionospheric origin of this low energy H^+ population. The LLBL O^+ distribution is a unidirectional beam parallel to the magnetic field at about 100 km/s (or approximately the same velocity as the low-energy H^+ in Figure 6). This beam is greater than a factor of 10 above the one count flux level for O^+ . There is no comparable O^+ flux above the one count level in any other region, including the outer magnetosphere (not shown). Therefore, this O^+ beam must have originated in the high-latitude ionosphere. Beams of this type have been reported previously in the LLBL [Fuselier *et al.*, 1989; 1995]. They have also been observed in the auroral zone at low altitudes at significantly lower energies (of the order of a few hundred eV), and these observations indicate that low-energy O^+ outflow is often accompanied by comparable fluxes of low-

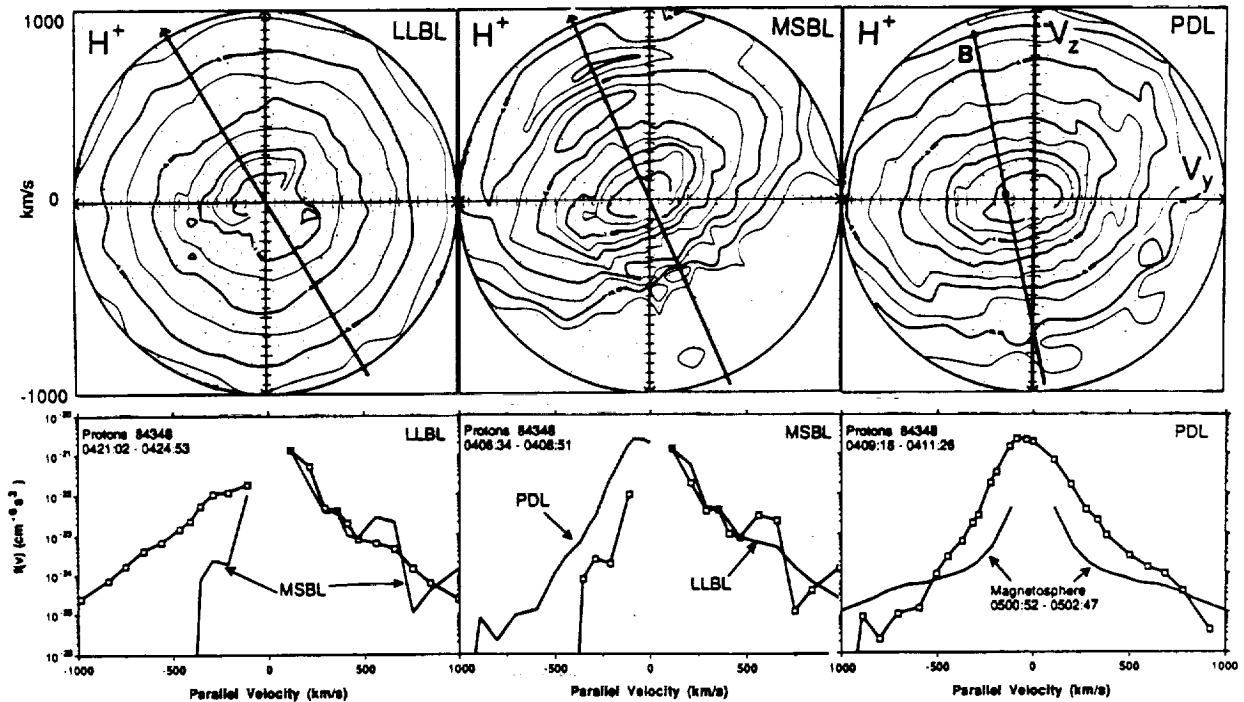


Figure 6. H^+ distributions from the three regions. The format is the same as in Figures 3 and 4. H^+ distributions in the three regions have all the characteristics of the He^{2+} distributions in Figure 5. There is an additional low-energy LLBL H^+ population parallel to the magnetic field at velocities below 250 km/s that is not as evident in the He^{2+} LLBL distribution. This population is from the high-latitude ionosphere.

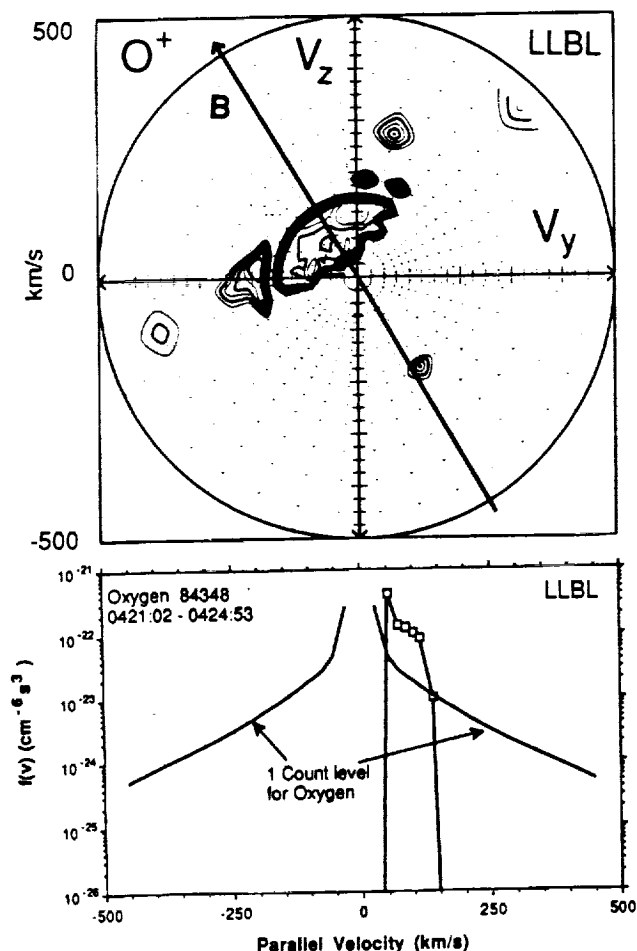


Figure 7. O^+ beam in the LLBL. This O^+ beam parallel to the magnetic field originated in the high latitude southern ionosphere. It has an H^+ counterpart in the LLBL distribution in Figure 5. This beam would have convected tailward, but because of reconnection poleward of the cusp in the southern hemisphere, this beam is observed on reconnected field lines in the LLBL that drape over the dayside magnetosphere.

energy H^+ [Collin *et al.*, 1987]. Thus the auroral ionosphere is the probable origin of both the LLBL O^+ beam in Figure 7 and the low-energy LLBL H^+ population parallel to the magnetic field in Figure 6. The parallel propagation of the beam indicates that it originated in the southern high-latitude ionosphere.

In summary, ion and electron distributions in this event had the following important properties: (1) Both the PDL ion and electron distributions exhibited unidirectional streaming parallel to the magnetic field in the MSBL. The source of the streaming electrons below about 0.773 keV, all of the streaming He^{2+} , and most of the streaming H^+ was the PDL. The streaming, low-energy electron distribution was observed throughout the MSBL. Therefore this population was heated at the location where the magnetic field line crossed the magnetopause. (2) Both the magnetosheath ion and electron distributions exhibited approximately equal fluxes parallel and antiparallel to the magnetic field in the LLBL. The counterstreaming nature of the electron distributions at energies below 0.773 keV is interpreted as evidence that the

spacecraft was between a source of hot electrons (the magnetopause) and a mirror point (the ionosphere). (3) An O^+ beam propagating parallel to the magnetic field was observed in the LLBL. No similar O^+ flux was observed in the adjacent magnetosphere, so the origin of this beam must have been the high-latitude ionosphere. Because of its direction of propagation parallel to the magnetic field, this beam originated in the southern high-latitude ionosphere.

Event 2: November 15, 1984 (Day 320)

An overview of the low-shear magnetopause crossings by the CCE spacecraft for a second representative event on November 15, 1984 is shown in Figure 8. The format is the same as that of Figure 2. During the 30 min interval in Figure 8, the spacecraft was at 1015 local time, $8.8 R_E$ from the Earth on an outbound trajectory and nearly in the ecliptic (the magnetic latitude was -12°). As in the first event, magnetopause crossings at this local time and radial distance require a solar wind dynamic pressure of about 5 times its nominal value. The spacecraft was in the magnetosphere at 0005 UT (indicated by the open bar interval above the top panel) and crossed the magnetopause several times in the 30 min interval (as indicated by the short vertical dashed lines in the panel containing B_z). Some of these crossings (for example near 0014 UT and 0019 UT) had discernible magnetic field rotations associated with them. However, many do not, indicating that little or no current was present locally where the spacecraft crossed the boundary. As in the first example, the magnetopause crossings are identified by high-resolution electron observations discussed below. In general, encounters with the magnetopause and its associated plasma layers are identifiable by energetic (magnetospheric) electron fluxes (e.g., 3.95 keV) that are intermediate between the fluxes in the plasma depletion layer (solid bars) and in the magnetosphere (open bar). In addition, the electron anisotropy changes from greater than zero in the PDL and magnetosphere to less than zero in the MSBL and LLBL.

An example of the high resolution electron observations for one of these brief encounters with the magnetopause and its associated boundary layers is shown in Figure 9. The format is the same as in Figure 3. The PDL in Figure 9 is characterized by enhanced flux parallel to the magnetic field. Unlike the previous example, no peak fluxes perpendicular to the magnetic field are seen. Nonetheless, the contrast between the PDL and MSBL is readily apparent. In the MSBL, the parallel fluxes are an order of magnitude larger than that in the PDL, but the antiparallel fluxes are comparable in the two regions. In the LLBL, the parallel fluxes are comparable to those in the MSBL, but the antiparallel fluxes are also comparable to the parallel fluxes and over an order of magnitude greater than the antiparallel fluxes in the MSBL or PDL. The increase in the parallel flux is responsible for the change in anisotropy from the PDL to the MSBL or LLBL shown in Figure 8.

Figure 10 shows representative electron distributions from each of the three regions. The format is the same as in Figure 4. Some evidence for an anisotropic electron distribution ($T_{\perp} > T_{\parallel}$) in the PDL is seen at low energies. A comparison of the PDL and magnetospheric distributions (bottom right) is shown. In this event, the magnetospheric source population is significant only above about 1 keV or about 15,000 km/s. As in event 1, evidence for a superposition of two populations in the MSBL in event 2 (Figure 10, middle) is readily apparent

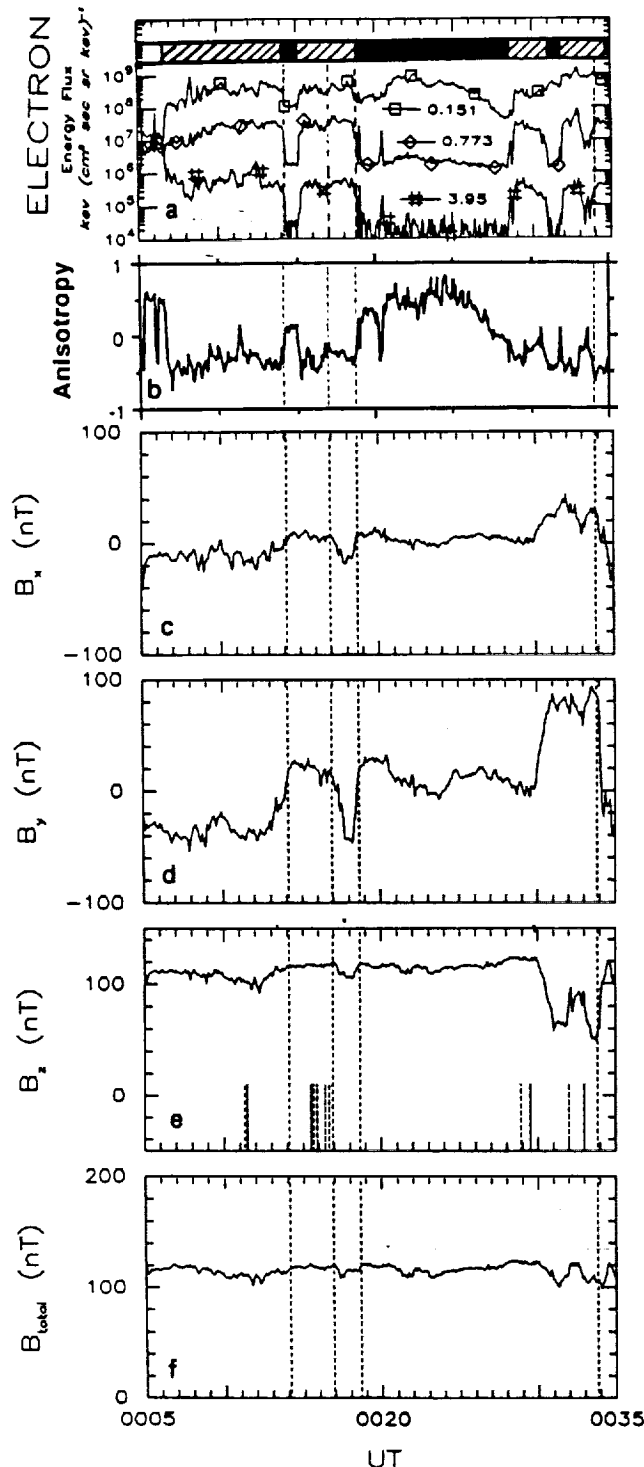


Figure 8. Electron flux and magnetic field data for a 30 min interval around the magnetopause crossings of the second event on 15 November 1984 (day 320). The format is the same as in Figure 2. The spacecraft started in the magnetosphere at the far left (shown by the open bar in the top panel) and crossed the magnetopause and its associated boundary layers many times during the interval.

in the comparison of the MSBL and PDL fluxes in the antiparallel direction and the MSBL and LLBL fluxes in the parallel direction. The parallel streaming in the MSBL

indicates that the reconnected magnetic field line threading the spacecraft crosses the magnetopause southward of the spacecraft location. The transition to a bidirectional or counterstreaming distribution ($T_{\parallel} > T_{\perp}$) from the MSBL to the LLBL is also apparent, and in this event, the low-energy electron distribution in the LLBL show evidence for counterstreaming beams. Qualitatively, the electron distributions for this event have all of the characteristics of the previous event. In particular, there is a well-defined MSBL sunward of the magnetopause where unidirectional electrons parallel to the magnetic field indicate the location of the reconnection site southward of the spacecraft location. Streaming electrons below about 1 keV originated in the PDL and not the magnetosphere. In the LLBL, the electron distribution is bidirectional and therefore provides no information on the topology inside the magnetopause.

Unfortunately, for this event, ion distributions in the MSBL intervals could not be obtained because the spacecraft was in this layer for continuous intervals that were too short (i.e., <2 min). However, there were several LLBL and PDL intervals long enough to obtain ion distributions. Ion distributions in the LLBL show important differences from the first event. Figure 11 shows the He^{2+} distributions in the PDL and LLBL. The format is the same as in Figure 5 except for the absence of an MSBL distribution. The PDL He^{2+} distribution is anisotropic and has a $-V_y$ flow consistent with flow around the magnetospheric obstacle. The parallel cut in the magnetospheric He^{2+} distribution is not shown in the lower right of Figure 11 because the magnetospheric He^{2+} phase space density was below $10^{-26} \text{ cm}^{-6} \text{ s}^3$. Thus He^{2+} at all energies originated in the magnetosheath/PDL. Unlike the nearly isotropic LLBL He^{2+} distribution in event 1 (Figure 5, left), the LLBL He^{2+} distribution in Figure 11 is strongly anisotropic. More importantly, there is a significant flow in the direction parallel to the magnetic field. (The flow velocity is identified by the dot along the magnetic field vector.) The parallel flow is the result of an absence of flux at low velocities (<250 km/s) in the antiparallel direction. This type of "D shaped" distribution (with a sharp cutoff at low velocities along the magnetic field) has been observed at high-shear magnetopause crossings [e.g., Smith and Rodgers, 1991; Fuselier et al., 1991b]. Although there is essentially no flux antiparallel to the magnetic field at the lowest energies measured, there is nonzero flux at somewhat higher energies in the antiparallel direction.

Figure 12 shows the corresponding H^+ distributions in the LLBL and PDL. The PDL H^+ distribution is also highly anisotropic and has the same $-V_y$ flow as the PDL He^{2+} distribution in Figure 11. The LLBL H^+ distribution has less parallel-antiparallel asymmetry compared to the strong asymmetry in the He^{2+} distribution. However, the H^+ distribution is a mixture of magnetospheric and solar wind sources. A comparison of the magnetospheric (measured at 2356 UT on 14 November 1984) and LLBL parallel cuts in the bottom left of Figure 12 shows that the low-energy population is probably from the magnetosphere and may contribute somewhat to the population in the antiparallel direction. At speeds between 100 and 400 km/s, the H^+ distribution, like the LLBL He^{2+} distribution, has significantly lower antiparallel flux than the parallel flux. Another difference between event 2 and event 1 is that no O^+ above background was observed in the magnetosphere, LLBL, or PDL for event 2.

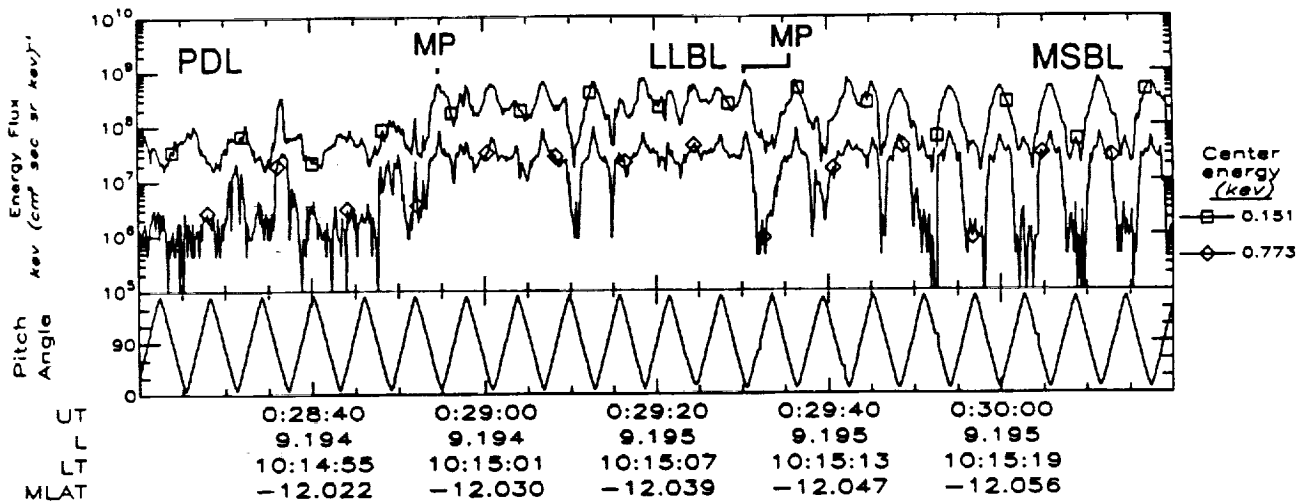


Figure 9. High-resolution electron fluxes for a 2 min interval around one of the brief magnetopause crossings on 15 November 1984 (day 320), starting at 0028:20 UT. The format is the same as in Figure 3. The differences between the PDL, MSBL, and LLBL fluxes are evident, especially the strong parallel flux in the MSBL.

To summarize, the MSBL and LLBL electron distributions for event 2 (Figure 10) were very similar to those of event 1. The unidirectional streaming parallel to the field indicates that the reconnected field lines in the MSBL cross the magnetopause below (southward of) the spacecraft. Bidirectional electron streaming was observed in the LLBL. The principle differences between the first and second events

are in the ion distributions in the LLBL. The solar wind ion distributions in the second event are unidirectional with a streaming velocity parallel to the magnetic field and, at least in the case of He^{2+} , have essentially no flux at low energies in the antiparallel direction (Figure 11, left). In contrast, solar wind ion fluxes parallel and antiparallel flux at low energies were essentially identical for the first event (Figure 5).

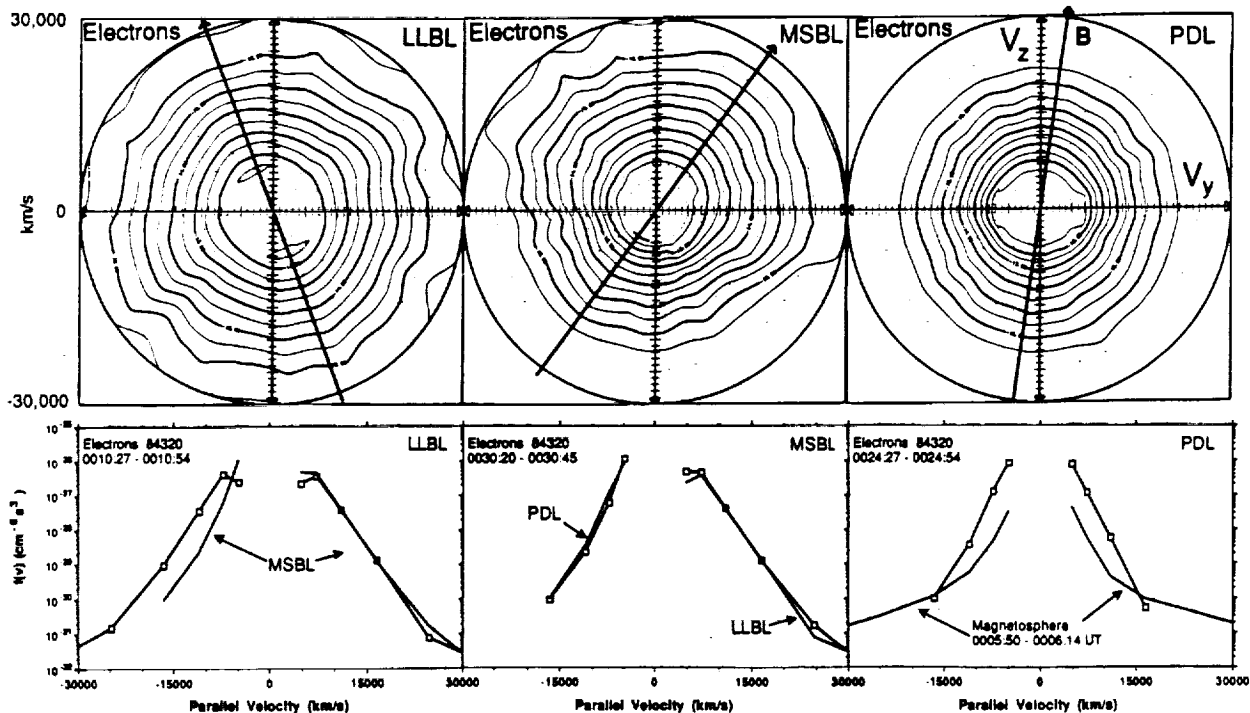


Figure 10. Electron distributions from the three regions. The format is the same as in Figure 4. The two source population of the MSBL is evident in the comparison of MSBL, LLBL, and PDL fluxes (bottom middle). Also evident is the counterstreaming nature of the LLBL distribution. Parallel streaming in the MSBL indicates that the reconnection site is below the spacecraft.

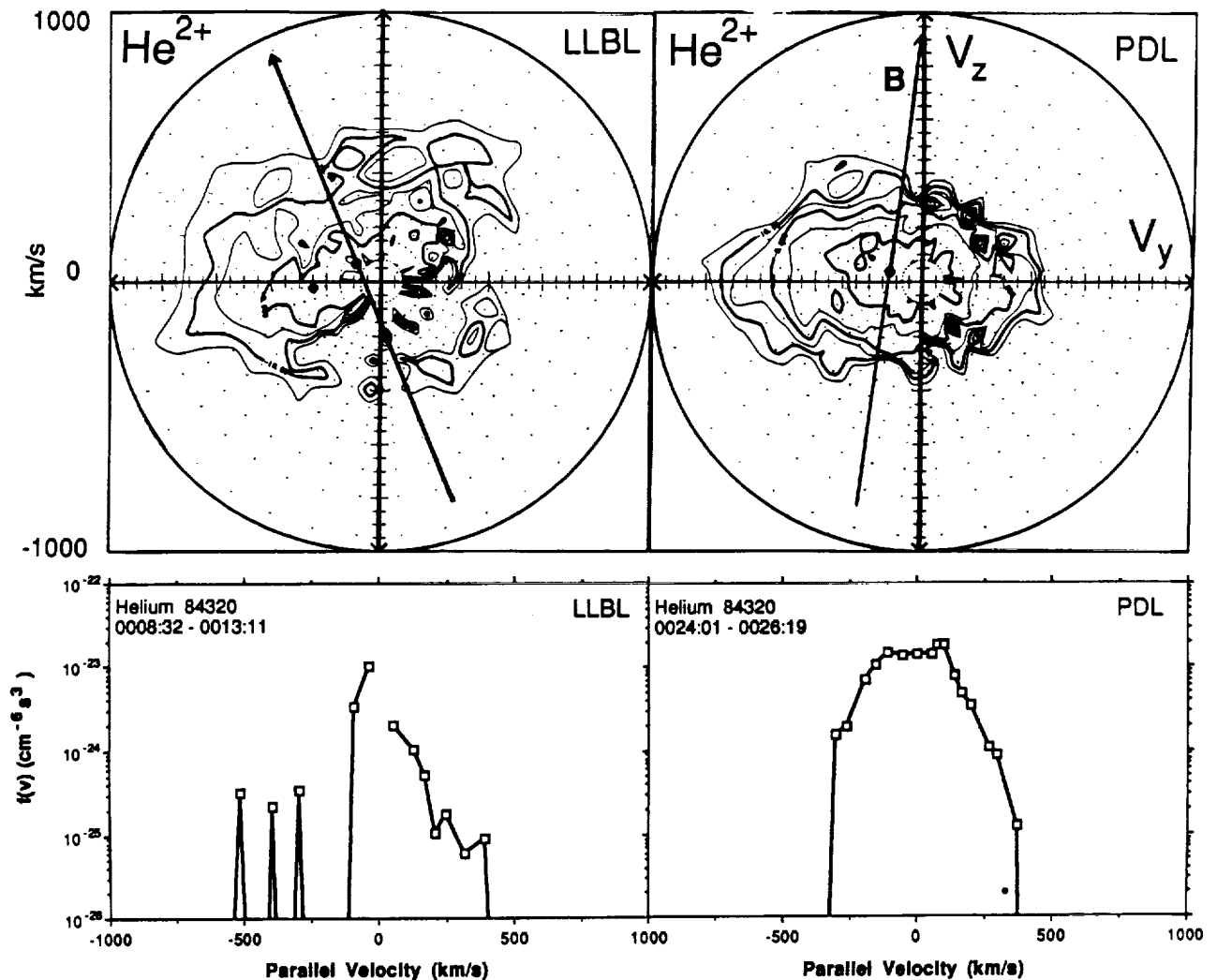


Figure 11. He^{2+} distributions from the LLBL and PDL. In this event, the MSBL intervals were too short to obtain ion distributions, otherwise the format is the same as in Figure 5. The PDL distribution has a downward flow consistent with the downward deflection of the solar wind around the magnetospheric obstacle. The LLBL distribution is strikingly different in this event compared to the one in Figure 5. The unidirectional, parallel streaming of the He^{2+} distribution in this event and the low but measurable return flux at high energies antiparallel to the magnetic field indicate that the magnetic field line in the LLBL crosses the magnetopause southward of the spacecraft location.

Finally, the second event had no measurable O^+ in the LLBL, while the first event had a parallel propagating O^+ beam that originated in the southern high-latitude ionosphere.

3. Interpretation of the Representative Events

In event 1, observations of counterstreaming electrons (and ions) in the LLBL indicate that the spacecraft is between the source of hot solar wind electrons (where the reconnected field line crosses the magnetopause) and the ionospheric foot point (where the solar wind electrons mirror). The direction of the ionospheric O^+ beam (Figure 7) and its H^+ counterpart (Figure 6, left) indicates that the open magnetic field line threading the spacecraft in the LLBL has one foot in the southern auroral ionosphere. With the foot point in the southern hemisphere, the reconnected magnetic field line must therefore cross the

magnetopause above (northward of) the spacecraft location in the LLBL. Sunward of the magnetopause in the MSBL, the unidirectional streaming along the magnetic field in Figures 4, 5, and 6 (middle) indicates that the reconnected magnetic field line crosses the magnetopause below (southward of) the spacecraft location in this region. Thus, in crossing the magnetopause, the spacecraft moves from a field line threading the magnetopause south of the observation point to one threading the magnetopause north of the observation point. The magnetic field topology consistent with this change is shown in the left of Figure 13 (see also Figure 1).

Figure 13 (top left) is a snapshot of the magnetic field configuration as viewed from the Sun for quasi-steady reconnection poleward of the southern cusp. The bottom left shows this snapshot as viewed from the dawnside. In both top and bottom, the circle on the field line indicates where the reconnected field line crosses the magnetopause. Field lines

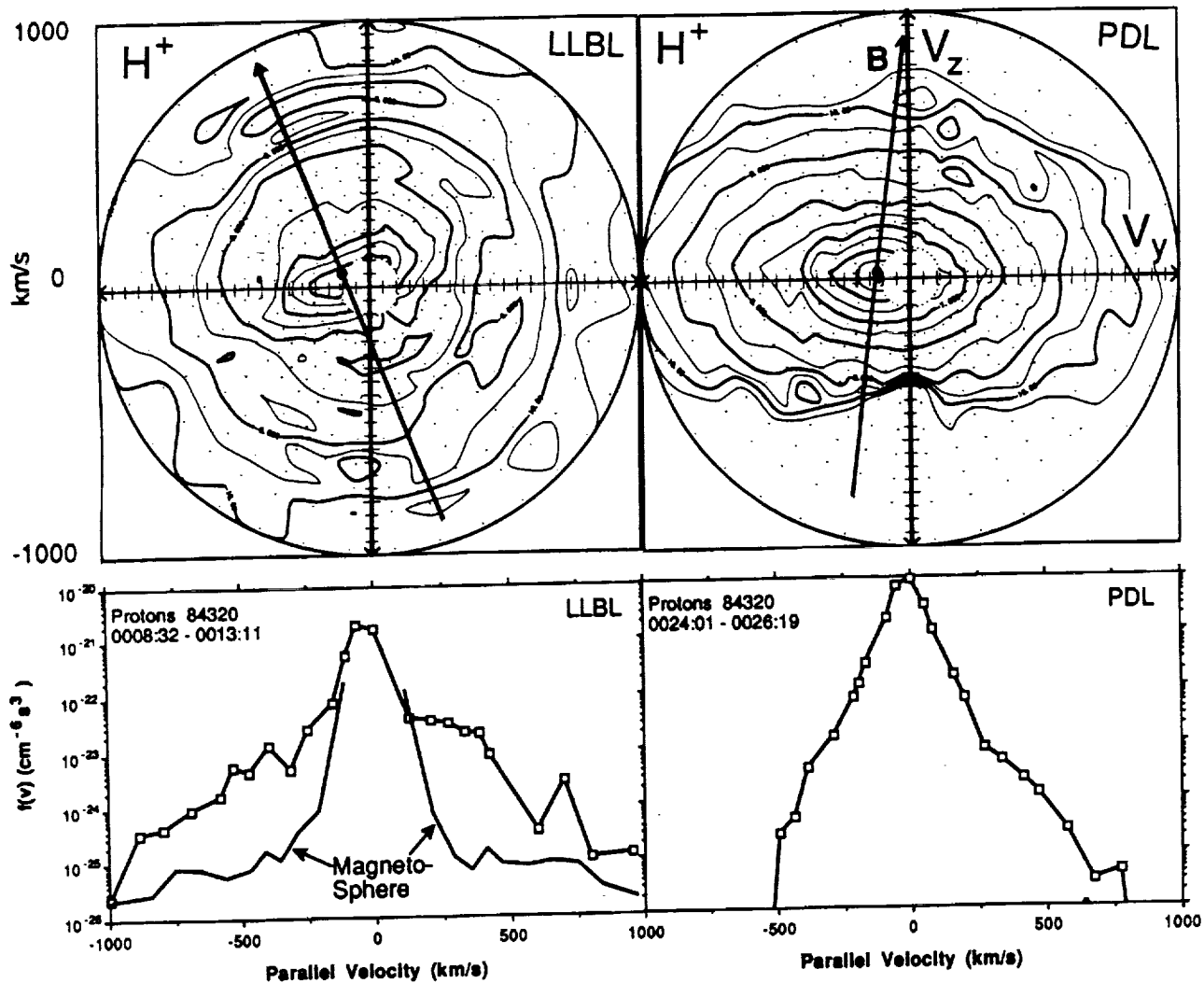


Figure 12. H^+ distributions from the LLBL and PDL. The format is the same as in Figure 6. Parallel streaming of the H^+ distribution is also evident in the LLBL although a measurable flux is seen at low velocities antiparallel to the field. Some of this flux may be due to low-energy magnetospheric H^+ .

in the magnetosphere are solid, while field lines in the magnetosheath are dashed. Reconnection poleward of the cusp for strongly northward IMF (low magnetic shear) occurs when a formerly open lobe field line (in this case in the southern lobe) reconnects with a magnetosheath field line near the cusp [see also Gosling *et al.*, 1991]. This type of reconnection produces two reconnected (or re-reconnected) field line topologies. The first is a completely open lobe field line (i.e., one that has no connection to the Earth's ionosphere) that convects tailward along the southward limit of the magnetopause in Figure 13. The second reconnected field line has one foot point in the southern ionosphere and crosses the magnetopause initially at the southern cusp. The northern part of this field line will also convect tailward, but because it is draped over the dayside magnetopause and the convection velocity in the LLBL is earthward (as illustrated by the open arrow), the location where the field line crosses the magnetopause moves steadily northward as the field line convects around the magnetopause. Crooker [1992] also provides a detailed discussion of this type of reverse convection due to lobe-magnetosheath reconnection.

This type of reconnection is consistent with the observations from event 1. A spacecraft in the subsolar region sunward of the magnetopause (in the MSBL) will observe electron and ion streaming parallel to the magnetic field from the location where the magnetic field line crosses the magnetopause southward of the spacecraft. Earthward of the magnetopause (in the LLBL), the location where the reconnected magnetic field line crosses the boundary will be above the spacecraft. The spacecraft will be located between the source of hot ions and electrons and the ionospheric mirror point in the southern auroral ionosphere. It will observe parallel streaming ionospheric ions from the high-latitude ionosphere (O^+ and H^+). These ions would have convected tailward and ultimately become part of the usual ionospheric contribution to the mantle and ultimately the plasmasheet. However, because the lobe field line was reconnected with a magnetosheath field line draped on the dayside, these ions are now observed on the dayside in the subsolar region. Counterstreaming electrons are observed in the LLBL because their fast motion along the magnetic field allows them to enter the LLBL above the spacecraft, propagate to the ionosphere,

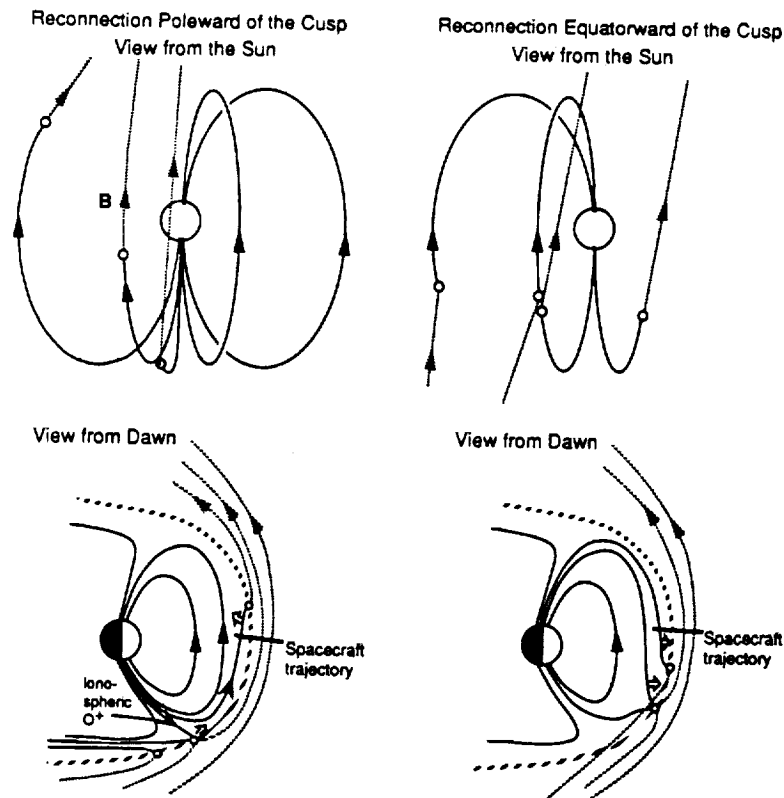


Figure 13. Magnetic field topologies for reconnection poleward of the cusp (left) and equatorward of the cusp (right) for low magnetic shear. (top) Snapshots of the topologies as viewed from the Sun and (bottom) snapshots as viewed from the dawn meridian are shown. Magnetic field lines are solid earthward the magnetopause and dashed sunward of the magnetopause with the locations where the field line crosses the magnetopause identified by the open circles. Reconnection poleward of the cusp occurs when previously open lobe field lines reconnect with magnetosheath field lines. Reconnection equatorward of the cusp occurs when previously closed magnetospheric field lines reconnect with magnetosheath field lines.

mirror, and return to the spacecraft. Solar wind ions move more slowly along the magnetic field. Because the field is convecting earthward in the subsolar region, magnetosheath plasma with low parallel velocities has access to the LLBL (see paper 1 and Figures 5 and 6). Also, the higher velocity solar wind ions observed in the parallel direction entered the magnetosphere below the spacecraft near the cusp, propagated to the ionosphere, and returned along the magnetic field. Solar wind ions moving antiparallel to the magnetic field entered the LLBL from above the spacecraft. Thus, in the LLBL for reconnection poleward of the cusp, somewhat isotropic solar wind ion distributions result from the earthward convection of the field line and ion entry over a broad region of the magnetopause.

It is tempting to suggest that counterstreaming solar wind ion and electron distributions in the LLBL for event 1 are evidence for multiple reconnection above and below the spacecraft, forming a closed magnetic field topology. There are two observations that argue against this more complicated topology. First, in paper 1, it was found that the transition from unidirectional streaming electrons to bidirectional streaming electrons always occurs at the magnetopause current layer when the layer can be identified. For single reconnection, this correlation between the electron streaming and the magnetopause current layer is simply an indication

that the location where the magnetic field line crosses the magnetopause is the site of heating of the solar wind ion and electron distributions. For multiple reconnection, no such correlation is required. For example, there could be events where the magnetic field reconnects in two places, producing a counterstreaming electron distribution sunward of the magnetopause in the MSBL. No such events were identified in paper 1. A second argument against multiple reconnection is the observation of unidirectional streaming O^+ in the LLBL (Figure 7). If reconnection occurs in both hemispheres, then counterstreaming O^+ beams might be observed in conjunction with the counterstreaming solar wind distributions in the LLBL.

Event 2 (Figures 8 through 12) must have an LLBL topology that is distinct from that of event 1. The unidirectional flow parallel to the magnetic field in the LLBL (Figure 11) suggests that the magnetic field line threading the spacecraft crosses the magnetopause below the spacecraft in this region and not above the spacecraft as in the first event. Furthermore, the unidirectional ion flow in the LLBL is in the same direction as the unidirectional electron flow in the MSBL (Figure 10), indicating that the magnetic field lines crosses the magnetopause below the spacecraft in both the MSBL and LLBL. A topology consistent with these observations is shown in the right of Figure 13. Reconnection equatorward of

the cusp is commonly associated with high-shear magnetopause crossing where the IMF and magnetospheric magnetic fields are nearly antiparallel. Under high-shear conditions, this type of reconnection is relatively easy to illustrate in a two-dimensional diagram [e.g., *Gosling et al.*, 1990]. For low-shear conditions, reconnection equatorward of the cusp is inherently three-dimensional and more difficult to illustrate. This topology was recently suggested for a low-shear magnetopause crossing [*Onsager and Fuselier*, 1994] and occurs when a previously closed magnetospheric field line reconnects with a magnetosheath field line. The result is two open magnetic field lines, one connected to the ionosphere in the northern hemisphere and the other connected to the ionosphere in the southern hemisphere (see Figure 13, top right).

This topology is consistent with the observations from event 2. Sunward of the magnetopause (in the MSBL), electrons are observed to stream along the magnetic field. Parallel streaming indicates that the reconnected magnetic field line threading the spacecraft crosses the magnetopause southward of the spacecraft location. Earthward of the magnetopause (in the LLBL), the spacecraft is located between the source of hot ions and electrons (the magnetopause) and the mirror point (in the ionosphere). Because the magnetic field is convecting toward the magnetopause (as well as tailward as in the right of Figure 13), solar wind ions and electrons observed in the antiparallel direction must enter the magnetopause in the parallel direction, propagate to the ionosphere, mirror, and return before the LLBL magnetic field line convects past the spacecraft. This is not difficult for electrons, and they are observed as a bidirectional distribution. However, this is very difficult for ions because of their low parallel speeds. Thus the ion distributions are observed as essentially unidirectional at low energies. Since the unidirectional streaming is parallel to the magnetic field in the LLBL, the reconnected magnetic field line threading the spacecraft in this region also crosses the magnetopause southward of the spacecraft as shown in the right of Figure 13. Ionospheric O^+ could be observed on these field lines, but like the mirroring solar wind ions, these ions may not arrive at the spacecraft before the magnetic field line convects away from the subsolar region. Also, magnetospheric flux tubes on the dayside may not contain significant ionospheric O^+ . Indeed, no O^+ was observed in the magnetosphere for either event 1 or event 2. Finally, while the lowest-velocity solar wind ions cannot return to the spacecraft from their mirror point in the ionosphere, higher-velocity ions can return [see, e.g., *Fuselier et al.*, 1992; *Onsager and Fuselier*, 1994]. These ions are observed at velocities of the order of 500 km/s antiparallel to the magnetic field (Figures 10 and 11). If the cutoff velocity parallel to the field were high enough to be accurately measured, then these mirrored and returning ions could be used to determine the distance from the spacecraft to the reconnection site [see, e.g., *Onsager and Fuselier*, 1994]. However, in the He^{2+} distribution in Figure 11, the cutoff velocity in the parallel direction must be very small (less than 25 km/s), and energy steps of the instrument at very low energies are too coarse to allow an accurate determination of the cutoff velocity. The high-velocity return population antiparallel to the magnetic field fixes the reconnection point below the spacecraft.

The topology illustrated in the right of Figure 13 is consistent with the observations from this second event.

However, this type of reconnection may not be sustained in a quasi-steady fashion, as discussed in section 5.

4. Survey of AMPTE/CCE Low-Shear Magnetopause Crossings

Representative events for reconnection poleward and equatorward of the cusp were discussed in detail in sections 2 and 3. In paper 1, 29 AMPTE/CCE magnetopause crossings (including the two events discussed in section 2) were identified with shear angles $<60^\circ$. Twenty-six of these events had identifiable MSBL electron signatures. The large number of events with MSBL electron signatures indicates that the low-shear, highly compressed magnetopause is open in the subsolar region essentially all the time. For the 14 events listed in Table 1, the LLBL intervals were long enough (i.e., continuous intervals >2 min) to obtain ion distributions from the mass spectrometer on AMPTE/CCE. The first four columns of Table 1 are the event, day, time of one magnetopause crossing (most of these events, like the ones in Figures 1 and 7, contained multiple crossings), and average shear across the magnetopause. In the next four columns, flow directions are identified as parallel (plus) or antiparallel (minus) to the field. Since the magnetosheath and magnetosphere magnetic fields are northward for these events, plus (minus) sign is also northward (southward). The last column shows the location of the reconnection site (poleward or equatorward of the cusp) consistent with the flow directions.

Several features are apparent in this comparison of events. First, all have identifiable MSBL electron signatures with the majority of the MSBL electron flows parallel to the magnetic field. Second, the MSBL electron and solar wind ion flow directions are consistent for the few cases when an ion flow direction could be obtained. Third, only bidirectional LLBL distributions (or somewhat isotropic distributions such as those in Figure 4) are associated with observations of O^+ beams in the LLBL. Fourth, unidirectional solar wind ion flows in the LLBL are always in the same direction as unidirectional electron flows in the MSBL. Finally, the most common magnetic topology identified is reconnection poleward of the cusp (11 of 15 events).

5. Discussion and Conclusions

In paper 1, electron and ion flows in the MSBL sunward of the magnetopause were used to determine if this boundary was open or closed in the subsolar region. These flows indicate a continuous heating of solar wind ions and electrons at the location where the reconnected field line crosses the magnetopause. In this paper, electron and ion flows in the MSBL sunward of the magnetopause and ion flows in the LLBL earthward of the magnetopause were used to determine the open magnetic field topology of the low-shear, highly compressed magnetopause in the subsolar region. Flows of solar wind ions and/or electrons identify where a reconnected field line crosses the magnetopause. For example, electron flows parallel to the magnetic field line in the MSBL indicate that the field line crosses the magnetopause below (south of) the spacecraft. Flows of ionospheric O^+ indicate the hemisphere (northern or southern) of the ionospheric foot point of a reconnected field line. For example, the field-aligned O^+ beam in the LLBL in Figure 7 indicates that the spacecraft is connected to the southern ionosphere.

Table 1. The 15 Magnetopause Crossings With Shear Angles $<60^\circ$ From *Fuselier et al.* [1995]

| Event | Day (1984) | MP Crossing Time, UT | Magnetic Shear, degrees | MSBL Electron Flow Direction | MSBL Solar Wind Ion Flow Direction | LLBL SW Ion Flow Direction | LLBL O ⁺ Beam Direction | Reconnection Location Relative to Cusp |
|-------|---------------|-------------------------|-------------------------------|------------------------------------|--|-------------------------------|--|--|
| 1 | 267 | 0617:30 | 53 | + | | bidirectional | + | poleward |
| 2 | 279 | 1115:10 | 16 | - | | bidirectional | no beam | poleward |
| 3 | 279 | 1521:30 | 35 | - | | unidirectional - | no beam | equatorward |
| 4a | 280 | 0244:45* | 20 | + | | unidirectional + | no beam | equatorward |
| 4b | 280 | 0319:55† | 20 | + | + | bidirectional | + | poleward |
| 5 | 280 | 0425:40 | 48 | + | | bidirectional | no beam | poleward |
| 6 | 280 | 0639:20 | 17 | + | + | bidirectional | + | poleward |
| 7 | 280 | 1843:55 | 25 | + | | bidirectional | no beam | poleward |
| 8 | 280 | 2307:05 | 54 | - | | bidirectional | +/- | poleward |
| 9 | 281 | 1331:20 | 23 | + | | bidirectional | no beam | poleward |
| 10 | 293 | 0706:50 | 11 | + | | unidirectional + | no beam | equatorward |
| 11 | 320 | 0018:40 | 32 | + | | unidirectional + | no beam | equatorward |
| 12 | 320 | 0335:40 | 26 | + | + | bidirectional | + | poleward |
| 13 | 320 | 1446:40 | 38 | + | | bidirectional | no beam | poleward |
| 14 | 348 | 0418:45 | 17 | + | + | bidirectional | + | poleward |

The magnetosheath boundary layer (MSBL) and LLBL flow directions are given relative to the magnetic field with the plus sign indicating propagation parallel to the magnetic field (in all cases, the magnetic field was northward on both sides of the magnetopause). MSBL ion flow directions could be determined in only four of the events because of the low time resolution of the ion mass spectrometer.

*See *Onsager and Fuselier* [1994].

†See *Fuselier et al.* [1995].

In the MSBL, electron and solar wind ion flows are consistent for the events that ion flows could be identified (Table 1). Most of these flows are parallel to the magnetic field, indicating an open magnetic field topology with the reconnected field line crossing the magnetopause southward of the spacecraft. This suggests that the reconnection site is somewhere in the vicinity of the southern cusp. Seasonal conditions are probably the reason for preferential reconnection in the southern cusp for the events in Table 1. These events occurred during the northern hemisphere late fall/early winter when the tilt of the Earth's dipole axis was away from the Sun in the northern hemisphere. This tilt moves the southern cusp sunward, and draped magnetosheath magnetic field lines may preferentially encounter this cusp region first, as suggested by *Crooker* [1992].

This seasonal bias has another implication also discussed by *Crooker* [1992]. This bias can help explain why the MSBL field lines cross the magnetopause for reconnection poleward of the cusp. For reconnection away from the subsolar region, reconnected field lines will be carried anti-sunward against the reconnection flow direction if the antisunward magnetosheath flow is greater than the Alfvén speed at the reconnection site. For reconnection poleward of the cusp therefore one ordinarily expects that the reconnected field line will convect tailward and will not cross the magnetopause on the dayside to become part of an open LLBL. The large dipole tilt near winter solstice moves the southern cusp closer to the subsolar point where the magnetosheath flow is lower. Thus the reconnection flow may be higher than the sheath convection flow even at the cusp reconnection site, and the reconnected field line may actually move sunward initially as shown in the bottom left of Figure 13.

For low shear reconnection, we have used measurements near the subsolar magnetopause to infer whether reconnection occurs poleward or equatorward of the cusp. Since the electrons move rapidly, traveling to the ionospheric mirror point and back to the spacecraft in a matter of seconds, the LLBL electron distributions contain solar wind electrons from

the magnetosheath that are flowing both parallel and antiparallel to the magnetic field. The LLBL electron distributions therefore indicate that the spacecraft is between the location of the heating of the solar wind electrons (the location where the magnetic field crosses the magnetopause) and the mirror point in the ionosphere. However, these electrons do not carry information about whether reconnection occurs poleward or equatorward of the cusp.

The slower moving solar wind and magnetospheric ions do provide information on the magnetic field topology of the LLBL. The essential distinction between reconnection equatorward and poleward of the cusp is that LLBL field lines convect in opposite senses, earthward (sunward) for reconnection poleward (equatorward) of the cusp (see Figure 13). For reconnection poleward of the cusp, the subsolar LLBL field lines are former MSBL field lines convected across the magnetopause and hence are populated by solar wind ions with all velocities down to zero. The solar wind ion distributions in the LLBL are therefore bidirectional or isotropic and extend to very low parallel velocities.

By contrast, for reconnection equatorward of the cusp, the field lines convect more as they do for subsolar high-shear reconnection, earthward in the MSBL and sunward in the LLBL. Hence the only way for solar wind ions to reach the LLBL in this situation is to flow along the field lines across the magnetopause from the MSBL. The competition between their parallel motion and LLBL convection toward the magnetopause leads to velocity filtering in which only ions with sufficiently high parallel velocity are observed at any particular location in the LLBL. The resulting solar wind ion distributions have velocity cutoffs corresponding to the lowest parallel velocity that has access to the observation point. This situation might also be characterized more generally by having solar wind ions flowing in only one direction along the magnetic field if the spacecraft is fairly close to the reconnection site and even the particles with the highest parallel speeds are not fast enough to travel to the ionosphere and back. Thus unidirectional flowing solar wind

ion distributions, especially at low parallel velocities, are indicative of reconnection equatorward of the cusp. In general, the type of solar wind ion distribution in the LLBL should therefore allow one to infer the sense of convection in the LLBL and hence whether the reconnection is poleward or equatorward of the cusp.

Most of the events display bidirectional/isotropic solar wind ion distributions in the LLBL consistent with reconnection poleward of the cusp. Moreover, ionospheric O^+ beams in the LLBL indicate which end of the field line is connected to the ionosphere because the O^+ beams are from the high latitude ionosphere and not from the magnetosphere immediately adjacent to the subsolar LLBL [Fuselier et al., 1989]. Six events in Table 1 have unidirectional MSBL electrons, counterstreaming LLBL solar wind ions, as well as O^+ beams in the LLBL. In five of these six events, the O^+ flow in the LLBL and the electron flow in the MSBL are in the same direction (parallel to the magnetic field) and thus indicate that the foot point of the magnetic field line threading the spacecraft remains connected to the same (southern) hemisphere as the spacecraft crosses the magnetopause from the MSBL to the LLBL. This is consistent with reconnection poleward of the cusp.

The O^+ signature is not always present. This should be expected because their presence may depend on ionospheric conditions and because the slow moving O^+ ions have to travel a considerable distance to reach the spacecraft. Temporal effects should therefore be expected to confuse the O^+ signature on occasion, and, in fact, a number of events with bidirectional/isotropic solar wind ion distributions in the LLBL had no O^+ beams associated with them. For one of the six events with an O^+ beam, the direction of the beam switched. It was observed in one direction for part of the LLBL and in the opposite direction for another part [Fuselier et al., 1989]. This suggests a more complicated topology than the one shown in the left of Figure 13, perhaps associated with reconnection at multiple sites. Nonetheless, the most significant fact is that the O^+ beams were only associated with bidirectional LLBL solar wind ion distributions. This observation is consistent with the interpretation (discussed earlier) that bidirectional or relatively isotropic solar wind ion distributions in the subsolar LLBL are evidence for reconnection poleward of the cusp and earthward convection of the reconnected field line in the LLBL.

Two observations argue against positing that the bidirectional LLBL ion flows are the result of a simultaneous reconnection of the same field line at the opposite, northern cusp (see section 3 and paper 1). First, the transition from unidirectional streaming electrons in the MSBL to counterstreaming electrons in the LLBL is always associated with the local magnetopause current layer when this layer is present (see paper 1). If reconnection were to occur simultaneously in opposite cusps, then the onset of counterstreaming electrons would not necessarily be observed simultaneously with the magnetopause current layer. Second, the O^+ beam in the LLBL is always unidirectional and never bidirectional. One would expect at least some bidirectional O^+ if the reconnection were simultaneous on the same field line in opposite cusps.

There are events which display unidirectional solar wind ion distributions in the LLBL, indicating that the reconnection site is equatorward of the cusp. This type of reconnection is illustrated schematically in the right of Figure 13. There were

four events, including event 4a, with unidirectional solar wind ion flows in the LLBL, and in all cases, the ion flow in the LLBL was in the same direction as the electron flow in the MSBL. For these cases, both unidirectional MSBL electrons and LLBL solar wind ions indicate that the reconnected field line threading the spacecraft crossed the magnetopause southward of the spacecraft. In the LLBL, the counterstreaming electron distributions indicate that the spacecraft was between the site where the magnetic field crosses the magnetopause (i.e., the site of heating of solar wind electrons) and the mirror point in the ionosphere. The presence of some relatively fast ions heading southward along the field is attributed to ions that had time to travel to the ionosphere, mirror, and return before the magnetic field line convects sunward of the spacecraft. These ions are observed as a return population antiparallel to the magnetic field at high velocities (see the LLBL He^{2+} distribution in Figure 11). Thus, for these three events, the combined electron and solar wind ion observations indicate reconnection equatorward of the southern cusp as illustrated in the right of Figure 13. For event 3 in Table 1, the MSBL electron flow and the LLBL ion flow are antiparallel to the field, and the same topology holds except that the reconnection occurs in the vicinity of the northern cusp.

For reconnection equatorward of the cusp, the solar wind ion distributions in the LLBL give the appearance of an accelerated flow. This acceleration results from the absence of ions in one direction along the magnetic field at low velocities. The acceleration is not as great as that observed for high-shear crossings because the change in the velocity across the magnetopause for ions that directly enter the LLBL is proportional to the vector change in the magnetic field [e.g., Onsager and Fuselier, 1994].

In principle, it is possible that even for reconnection equatorward of the cusp, the solar wind ions may appear bidirectional if the magnetic field line convects very slowly. It would then be possible for even low-energy solar wind ions to mirror in the ionosphere and return to the subsolar region. The resulting distribution would be indistinguishable from that associated with reconnection poleward of the cusp.

Therefore some of the five events in Table 1 that have no O^+ beam but bidirectional solar wind ion distributions in the LLBL may be actually events that have reconnection equatorward of the cusp, rather than poleward of the cusp as shown in Table 1. These events will also show little or no accelerated flow in the LLBL. Because of this ambiguity in approximately one third of the events in Table 1, it is difficult to determine which type of reconnection topology is preferred for the low-shear magnetopause. Also, it is clear that the topology can change in less than 1 hour (see events 4a and 4b in Table 1).

For reconnection equatorward of the cusp, important outstanding questions are the orientation of the neutral line and the convection of the reconnected magnetic field lines. For low-shear, component reconnection, the neutral line is nearly north-south. However, for a single neutral line, this orientation implies that a spacecraft will observe unidirectional streaming signatures in the same direction in the MSBL and LLBL (as in Table 1) only when it crosses the magnetopause and the neutral line simultaneously, a highly unlikely occurrence. The fact that 4 of 15 events in Table 1 (counting events 4a and b as separate) have these unidirectional streaming signatures argues against this

unlikely occurrence. Here it is important to remember that events in this study must have had a sufficiently long LLBL interval (at least 2 min long). Thus events in Table 1 are likely representative of magnetopause crossings with clear flow signatures. Nonetheless, the neutral line orientation and convection of the field lines for reconnection equatorward of the cusp remain outstanding questions. One possible scenario is to have a multiple reconnection region equatorward of the cusp that has both time and spatial limitations. Future studies with other spacecraft will hopefully resolve these questions.

In summary, the electron and ion signatures in the MSBL and LLBL indicate that the low-shear magnetopause is open essentially all the time in the subsolar region. Evidence exists for both reconnection poleward and equatorward of the cusp for these conditions. Reconnection poleward of the cusp appears to be somewhat more common, but it is possible that the number of events with reconnection equatorward of the cusp may be underestimated. In one case, the reconnection site apparently moved from poleward of the cusp to equatorward of the cusp during a 1 hour interval between magnetopause crossings.

Acknowledgments. The authors thank both referees for their comments on this paper. Discussions with T. Phan are also greatly appreciated. Research at Lockheed was funded by NASA under Grant NAGW-4049 and Lockheed Independent Research. Support for research at the Johns Hopkins University Applied Physics Laboratory was provided by NSF and ONR.

The Editor thanks T. M. Bauer and R. C. Elphic for their assistance in evaluating this paper.

References

- Anderson, B. J., and S. A. Fuselier, Magnetic pulsations from 0.1 to 4.0 Hz and associated plasma properties in the Earth's subsolar magnetosheath and plasma depletion layer, *J. Geophys. Res.*, **98**, 1461, 1993.
- Anderson, B. J., S. A. Fuselier, S. P. Gary, and R. E. Denton, Magnetic spectral signatures in the Earth's magnetosheath and plasma depletion layer, *J. Geophys. Res.*, **99**, 5877, 1994.
- Collin, H. L., W. K. Peterson, and E. G. Shelley, Solar cycle variation of some mass dependent characteristics of upflowing beams of terrestrial ions, *J. Geophys. Res.*, **92**, 4757, 1987.
- Cowley, S. W. H., The causes of convection in the Earth's magnetosphere: A review of developments during the IMS, *Rev. Geophys.*, **20**, 531, 1982.
- Crooker, N. U., Reverse convection, *J. Geophys. Res.*, **97**, 12,363, 1992.
- Denton, R. E., B. J. Anderson, S. P. Gary, and S. A. Fuselier, Bounded anisotropy fluid model for ion temperatures, *J. Geophys. Res.*, **99**, 11,225, 1994.
- Fuselier, S. A., D. M. Klumppar, W. K. Peterson, and E. G. Shelley, Direct injection of ionospheric O^+ into the dayside low latitude boundary layer, *Geophys. Res. Lett.*, **16**, 1121, 1989.
- Fuselier, S. A., D. M. Klumppar, and E. G. Shelley, Ion reflection and transmission during reconnection at the Earth's subsolar magnetopause, *Geophys. Res. Lett.*, **18**, 139, 1991a.
- Fuselier, S. A., D. M. Klumppar, E. G. Shelley, B. J. Anderson, and A. J. Coates, He^{2+} and H^+ dynamics in the subsolar magnetosheath and plasma depletion layer, *J. Geophys. Res.*, **96**, 21,095, 1991b.
- Fuselier, S. A., D. M. Klumppar, and E. G. Shelley, Counter-streaming magnetosheath ions in the dayside low latitude boundary layer, *Geophys. Res. Lett.*, **19**, 425, 1992.
- Fuselier, S. A., B. J. Anderson, and T. G. Onsager, Particle signatures of magnetic topology at the magnetopause: AMPTE/CCE observations, *J. Geophys. Res.*, **100**, 11,805, 1995.
- Gosling, J. T., M. F. Thomsen, S. J. Bame, T. G. Onsager, and C. T. Russell, The electron edge of the low latitude boundary layer during accelerated flow events, *Geophys. Res. Lett.*, **17**, 1833, 1990.
- Gosling, J. T., M. F. Thomsen, S. J. Bame, R. C. Elphic, and C. T. Russell, Observations of reconnection of interplanetary and lobe magnetic field lines at the high latitude magnetopause, *J. Geophys. Res.*, **96**, 14,097, 1991.
- Kessel, R. L., S.-H. Chen, J. L. Green, S. F. Fung, S. A. Boardsen, L. C. Tan, T. E. Eastman, J. D. Craven, and L. A. Frank, Evidence of high-latitude reconnecting during northward IMF: Hawkeye observations, *Geophys. Res. Lett.*, **23**, 583, 1996.
- Onsager, T. G., and S. A. Fuselier, The location of magnetic reconnection for northward and southward interplanetary magnetic field, in *Solar System Plasmas in Space and Time*, *Geophys. Monogr. Ser. vol. 84*, edited J. L. Burch and J. H. Waite Jr., p. 183, AGU, Washington D. C., 1994.
- Paschmann, G., B. U. Ö. Sonnerup, I. Papamastorakis, N. Sckopke, G. Haerendel, S. J. Bame, J. R. Asbridge, J. T. Gosling, C. T. Russell, and R. C. Elphic, Plasma acceleration at the Earth's magnetopause: Evidence for reconnection, *Nature*, **282**, 243, 1979.
- Paschmann, G., I. Papamastorakis, W. Baumjohann, N. Sckopke, C. W. Carlson, B. U. Ö. Sonnerup, and H. Lühr, The magnetopause for large magnetic shear: AMPTE/IRM observations, *J. Geophys. Res.*, **91**, 11,049, 1986.
- Paschmann, G., B. Sonnerup, I. Papamastorakis, W. Baumjohann, N. Sckopke, and H. Lühr, The magnetopause and boundary layer for small magnetic shear: Convection electric fields and reconnection, *Geophys. Res. Lett.*, **17**, 1829, 1990.
- Paschmann, G., W. Baumjohann, N. Sckopke, T.-D. Phan, and H. Lühr, Structure of the dayside magnetopause for low magnetic shear, *J. Geophys. Res.*, **98**, 13,409, 1993.
- Potemra, T. A., L. J. Zanetti, and M. H. Acuna, The AMPTE CCE magnetic field experiment, *IEEE Trans. Geosci. Remote Sens.*, **GE-23**, 246, 1985.
- Scudder, J. D., K. W. Ogilvie, and C. T. Russell, The relation of flux transfer events to magnetic reconnection, in *Magnetic Reconnection in Space and Laboratory Plasmas*, *Geophys. Monogr. Ser. vol. 30*, edited by E. W. Hones Jr., p. 153, AGU, Washington D. C., 1984.
- Shelley, E. G., A. Ghielmetti, E. Hertzberg, S. J. Batel, K. Altwegg-Von Burg, and H. Balsiger, The AMPTE CCE Hot-Plasma Composition Experiment, *IEEE Trans. Geosci. Remote Sens.*, **GE-23**, 241, 1985.
- Sibeck, D. M., R. E. Lopez, and E. C. Roelof, Solar wind control of the magnetopause shape, location, and motion, *J. Geophys. Res.*, **96**, 5489, 1991.
- Smith, M. F., and D. J. Rodgers, Ion distributions at the dayside magnetopause, *J. Geophys. Res.*, **96**, 11,617, 1991.
- Song, P., R. E. Holzer, C. T. Russell, and Z. Wang, Modeling the low latitude boundary layer with reconnection entry, *Geophys. Res. Lett.*, **21**, 625, 1994.
- Sonnerup, B. U. Ö., and B. G. Ledley, Electromagnetic structure of the magnetopause and boundary layer, in *Magnetospheric Boundary Layers*, edited by B. Battick, *Eur. Space Agency Spec. Publ. ESA SP-148*, European Space Agency, Paris, p. 401, 1979.
- Thomsen, M. F., J. A. Stansberry, S. J. Bame, S. A. Fuselier, and J. T. Gosling, Ion and electron velocity distributions within flux transfer events, *J. Geophys. Res.*, **92**, 12,127, 1987.

B. J. Anderson, Applied Physics Laboratory, Johns Hopkins University, Laurel, MD 20723.

S. A. Fuselier, Lockheed Palo Alto Research Laboratory, 3251 Hanover Street, Department H1-11, Building 252, Palo Alto, CA 04304-1191. (e-mail: fuselier@space.lockheed.com).

T. G. Onsager, Space Environment Center, NOAA, Boulder, CO, 80303.

(Received January 17, 1996; revised November 1, 1996; accepted November 21, 1996.)

Solar wind composition changes across the Earth's magnetopause

S. A. Fuselier, E. G. Shelley, and O. W. Lennartsson

Lockheed-Martin Palo Alto Research Laboratory, Palo Alto, California

Abstract. ISEE 1 and Active Magnetospheric Particle Tracer Explorers/Charge Composition Explorer (AMPTE/CCE) composition measurements are used to investigate the change in solar wind composition across the Earth's magnetopause. The combined data set of 59 magnetopause crossings covers 0500 to 1900 LT and -20° to $+40^\circ$ magnetic latitude. For each magnetopause crossing, the ratio of the $\text{He}^{2+}/\text{H}^+$ density in the magnetosheath and in the low latitude boundary layer (LLBL) were determined. In addition, some crossings on the duskside flank of the magnetosphere were sufficiently long to determine this density ratio in the current layer. Averaged over all local time, the $\text{He}^{2+}/\text{H}^+$ density ratio is observed to decrease by 40% from the magnetosheath to the low latitude boundary layer. The density ratio decreases by its greatest amount (47%) in the dawnside LLBL and decreases by its smallest amount ($16\% \pm 14\%$) in the duskside LLBL. In addition, there is essentially no reduction in the density ratio ($7\% \pm 12\%$) in the duskside current layer. Finally, even those events that show clear signatures of magnetic reconnection at the magnetopause exhibit an average decrease in the density ratio that is comparable to the decrease seen in the entire data set. This decrease in the $\text{He}^{2+}/\text{H}^+$ density ratio across the magnetopause is not due to the presence of a significant magnetospheric H^+ population in the LLBL. One possible explanation for this composition change is a mass dependent reflection coefficient at the magnetopause. To be consistent with the observations, the reflection coefficient for He^{2+} at the magnetopause must be 40-50% higher than that for H^+ . If true, then the He^{2+} concentration must increase by about 20% in the magnetosheath boundary layer (MSBL) just sunward of the magnetopause.

Introduction

Ion mass spectrometers that measure thermal (approximately 1 to several keV/e) ions in the magnetosphere have provided definitive proof that the ionosphere and the solar wind are both important sources of magnetospheric plasma. Extensive study of the Earth's plasma sheet ion populations indicates that this region is most "solar wind-like" in both composition and mean energy during periods of prolonged quiet [Lennartsson, 1992]. Under these conditions, the $\text{He}^{2+}/\text{H}^+$ density ratio is between 2 and 3% with only about 3% of the plasma sheet H^+ of ionospheric origin [Sharp *et al.*, 1982; Lennartsson, 1992]. During active periods, the ionospheric source becomes more important, but solar wind-like conditions can still be observed, especially near the tail lobes [Lennartsson, 1992]. Under these conditions, the plasma sheet $\text{He}^{2+}/\text{H}^+$ density ratio measured between the 0.1 and 16 keV/e range drops to about 1% with 45% of the plasma sheet H^+ of ionospheric origin [Sharp *et al.*, 1982]. Under active conditions, this ratio is affected somewhat by the limited energy/charge range of the instrument used [e.g., Lennartsson, 1992].

Although these studies did not include a detailed comparison of the plasma sheet $\text{He}^{2+}/\text{H}^+$ density ratio with that measured simultaneously in the solar wind, the average $\text{He}^{2+}/\text{H}^+$ density ratio in the solar wind during the intervals studied was

approximately 1.5 to 2 times higher than that observed in the plasma sheet for quiet conditions. Because the ionospheric H^+ contribution to the plasma sheet is negligible for quiet conditions, the decrease in the solar wind He^{2+} concentration (relative to solar wind H^+) in the magnetosphere appears to be a real effect [Sharp *et al.*, 1982].

There are two possible explanations for this decrease. Solar wind He^{2+} may be preferentially excluded from the magnetosphere at or before the magnetospheric boundary and/or it may be preferentially excluded from the plasma sheet through the processes that energize and transport the plasma from the boundary into the region. A possible explanation for the reduction in the solar wind He^{2+} concentration through the latter mechanism was suggested by Lennartsson and Shelley [1982]. Until now, reduction in the solar wind He^{2+} concentration by the former mechanism has not been considered.

Independent of the energization and transport mechanisms in the magnetosphere, solar wind plasma must first cross the Earth's magnetopause. This plasma can cross at high latitudes into the mantle or at low latitudes into the low latitude boundary layer and can cross on the dayside or in the tail. It is not the purpose here to identify the most likely crossing point of the solar wind plasma that populates the plasma sheet. Rather, it is important to investigate the possible change in the solar wind composition at the magnetopause regardless the actual crossing point.

This paper reports observations of solar wind composition changes across the Earth's magnetopause. Solar wind composition measurements in the dayside magnetosphere and in the low latitude boundary layer are used to

the magnetopause preferentially excludes He^{2+} from the Earth's magnetosphere. A possible explanation for this exclusion is a mass dependent reflection coefficient at the magneto-pause.

Observations

Observations in this paper are from the ISEE 1 and -2 spacecraft and the AMPTE/CCE spacecraft. The ISEE spacecraft were launched into a highly elliptical orbit with an apogee of nearly $23 R_E$ in late 1977. Data used here are from 1977 through 1979. The AMPTE/CCE spacecraft was launched in a highly elliptical orbit with an apogee of about $9 R_E$ in late 1984. Data used here are from October to December 1984.

Data from these two missions are complementary in several aspects. The early ISEE operations occurred during the rising phase of the solar cycle, while the early AMPTE operations occurred near solar minimum of the same cycle. The ISEE spacecraft were launched into an orbit with an inclination of 29° and, with their relatively high apogee, explored the Earth's magnetopause over the full range of dayside local time at geomagnetic latitudes up to 40° . The AMPTE/CCE spacecraft was launched into a near-equatorial orbit and, with its relatively low apogee, crossed the near-equatorial magnetopause only under conditions of high solar wind dynamic pressure. These crossings were more restricted in dayside local time and, because of the high solar wind dynamic pressures, they tended to occur during active magnetospheric conditions.

For the ISEE data, observations of solar wind He^{2+} were from the Plasma Composition Experiment on ISEE 1 [Shelley *et al.*, 1978]. This ion mass spectrometer was one of a class of similar mass spectrometers flown on several missions starting with GEOS 1 and 2 and ending with AMPTE/CCE. The ISEE 1 instrument used here had an energy dependent field of view that ranged in polar angles from $\pm 25^\circ$ at low energies (less than 1 keV/e) to $\pm 7.5^\circ$ at high energies (more than 10 keV/e). Since the ISEE spin axis was nearly perpendicular to the ecliptic plane and the center of the field of view was 5° below the spacecraft spin plane, the composition instrument made measurements approximately in the ecliptic plane and good pitch angle coverage was obtained when the magnetic field did not have a large Z component. In addition, the majority of the He^{2+} distribution was in the instrument field of view as long as its bulk flow velocity did not have a significant Z component. These conditions on the magnetic field and bulk velocity were best met along the flanks of the magnetopause where the magnetic field had a significant X component and the bulk flow velocity was mainly in the -X (antisolar) direction. In the typical operation mode used in this study, the instrument measured a He^{2+} spectrum at 12 azimuthal angles from $0 - 360^\circ$ and 16 energies from about 0.1 to 17 keV/e in about 1 min. Essentially all of the He^{2+} distribution in the magnetosheath and magnetopause boundary layers was contained in this energy range. Spectra were usually not measured continuously. Rather, time between successive He^{2+} spectra was used to measure other ion species.

Observations of solar wind H^+ were from the Fast Plasma Experiment on ISEE 1 (and on ISEE 2 after 1978) [Bame *et al.*, 1978]. This instrument had a $\pm 55^\circ$ field of view centered on the spacecraft spin plane. It made snapshots of the total ion distribution (assumed to be protons) in 3 s with spectra separated by 3 s (high data rate), 12 s (low data rate), or 24 s (after 1977 for ISEE 1). One-minute averages of the high time

resolution snapshots are used here. These data were obtained from the PI through the National Space Science Data Center (NSSDC).

In addition to the plasma observations from ISEE 1, magnetic field data from the ISEE 1 and 2 Fluxgate magnetometers [Russell, 1978] are used to help identify the magnetopause crossings. These data were also obtained from the PI through the NSSDC.

For the AMPTE/CCE data, observations of both solar wind He^{2+} and H^+ were from the Hot Plasma Composition Experiment [Shelley *et al.*, 1985]. As discussed above, this instrument was similar in several respects (e.g., field of view and energy range) to the ISEE 1 Plasma Composition Experiment. One important difference in the AMPTE composition measurements was that the He^{2+} and H^+ spectra were measured simultaneously with a time resolution of approximately 2 min. Another difference was that the spin axis of the AMPTE/CCE spacecraft was pointed approximately toward the sun and good pitch angle coverage was obtained when the magnetic field did not have a large X component. In addition, ion distributions were in the instrument field of view as long as their bulk flow velocity did not have a significant X component. These conditions were best met in the subsolar region where the magnetic field did not have a significant X (or normal) component at the magnetopause and the bulk flow velocity also had a very small -X component.

In addition to the composition measurements from AMPTE, electron observations from the electron spectrometer part of the Hot Plasma Composition Experiment and the magnetic field from the magnetometer experiment [Potemra *et al.*, 1985] were used to identify the magnetopause crossings.

In this study, a typical event consisted of multiple magnetopause crossings in which the spacecraft spent sufficient time (i.e., greater than approximately 2 min) in the magnetosheath, low latitude boundary layer (LLBL) and/or current layer to obtain at least one He^{2+} and H^+ spectrum in each region. A total of 55 events have spectra in the LLBL, and magnetosheath. In addition, there were four ISEE 1 flank magnetopause where sufficient time was spent in the current layer to obtain spectra and one case where the spacecraft spent sufficient time in both the current layer and LLBL. These events are considered separately from crossings from the magnetosheath into the LLBL. As a working definition of these two layers, the LLBL is defined here as the region of magnetosheath-like plasma earthward of the major rotation of the magnetic field from its magnetosheath to its magnetospheric orientation. (The magnitude of this rotation may be small if the shear is low.) The (magnetopause) current layer is defined here as the region where the field is in the process of completing its major rotation from magnetosheath to magnetospheric orientation.

The local time and magnetic latitude of the 59 magnetopause crossings (events) are shown in Figure 1. The top panel shows the location of the crossings rotated into the ecliptic plane. The 32 ISEE 1 magnetopause crossings occurred over a wide range of local times and near the location of the nominal magnetopause position. (The nominal magnetopause position shown in Figure 1 is from Sibeck *et al.* [1991].) These ISEE 1 crossings occurred over a wide range of magnetic latitudes but it may be significant that they were all at relatively high magnetic latitudes for local times less than 0800. In contrast, the 27 AMPTE/CCE magnetopause crossings occurred over a restricted range of local times and

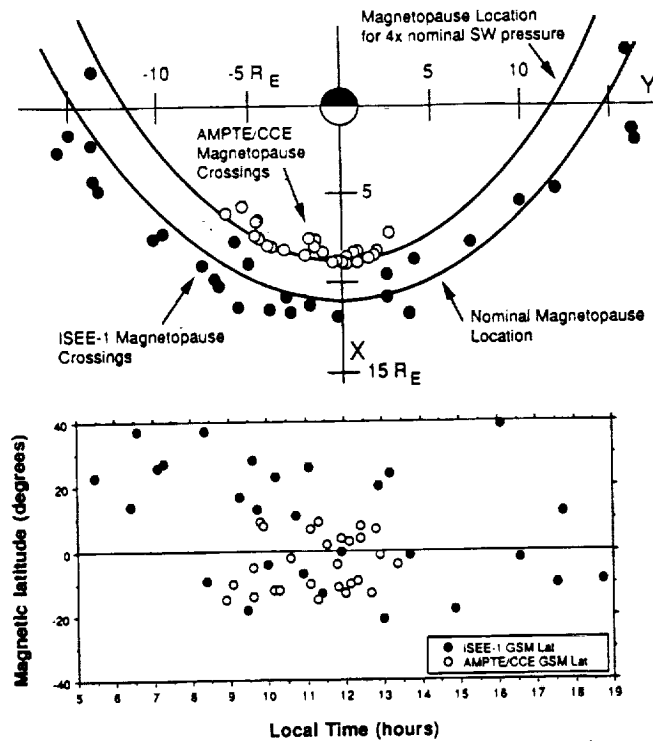


Figure 1. (Top) The location of the magnetopause crossings used in this study rotated into the ecliptic plane. The ISEE 1 magnetopause crossings occurred near the nominal position of the magnetopause while the AMPTE/CCE crossings occurred under highly compressed magnetopause conditions. (Bottom) The magnetic latitude/local time locations of the magnetopause crossings. The latitude ranges from -20 to 40° but only high-latitude crossings occur on the dawn flank.

magnetic latitudes approximately in the subsolar region and occurred under conditions of very high solar wind dynamic pressure. The difference in these two data sets is simply a reflection of the different apogees of the two spacecraft; nearly $23 R_E$ for ISEE 1 and only about $9 R_E$ for AMPTE/CCE.

The 27 AMPTE/CCE magnetopause crossings were used in a study of total mass density changes across the magnetopause [Fuselier et al., 1993]. Identification of the magnetopause and its associated boundary layers are discussed in detail in that study.

The 32 ISEE 1 magnetopause crossings were selected from 1977, 1978, and 1979 data when the ISEE 1 Plasma Composition Experiment was in a mode to detect He^{2+} , there were data from the Fast Plasma Experiment, and the spacecraft remained in the LLBL for ~ 2 min. A combination of plasma (1-min resolution) and magnetic field (4-s resolution) data were used to determine the location of the magnetopause. In addition, high time resolution plasma data for approximately half of the ISEE magnetopause crossings in Figure 1 have been published previously [e.g., Song et al., 1993]. For these crossings, the identification of the magnetopause and its associated layers using the lower time resolution data in this study could be confirmed directly.

An example of one of the ISEE 1 magnetopause crossings in this study is shown in Figure 2. The ISEE spacecraft was located at a radial distance of $11.4 R_E$ and a local time of 10.9 hours. From top to bottom this figure shows a 30-min

interval of 1-min averaged H^+ density, H^+ temperature, He^{2+} density, $\text{He}^{2+}/\text{H}^+$ density ratio, and the Z_{GSE} component of the magnetic field. (During this interval, He^{2+} was measured continuously at approximately 1 min time resolution.) Several magnetopause crossings are identified by the sharp

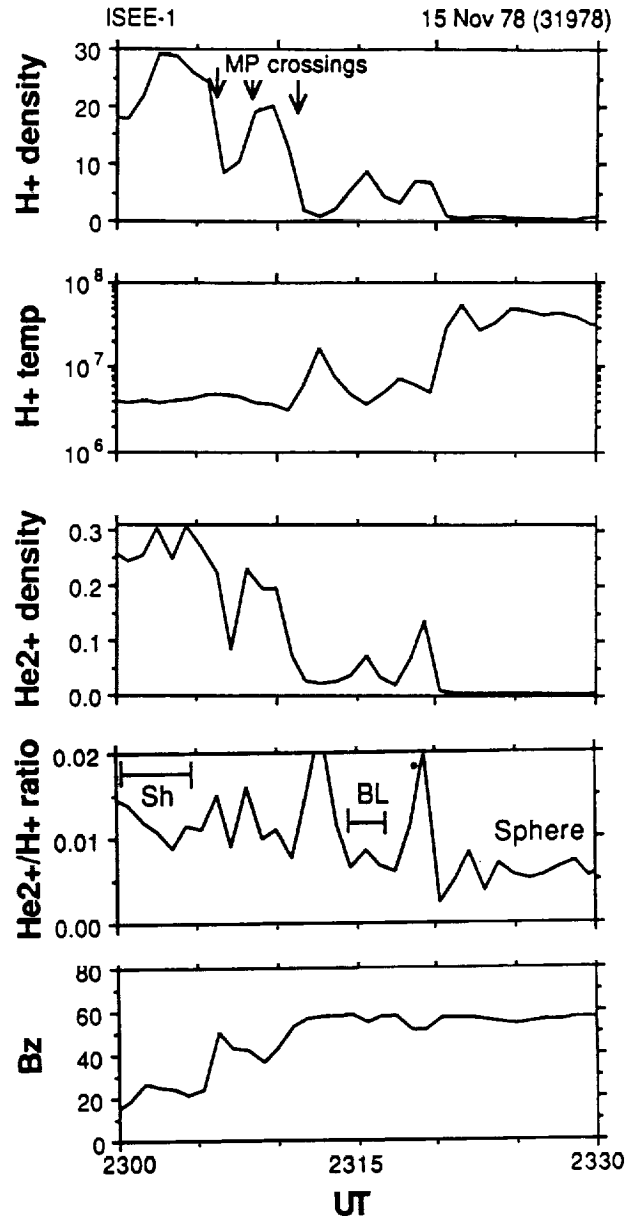


Figure 2. Representative magnetopause crossing from this study. Top to bottom are 1 min averages of the H^+ density, H^+ temperature, He^{2+} density, $\text{He}^{2+}/\text{H}^+$ density ratio and the Z_{GSE} component of the magnetic field. At least three magnetopause crossings occurred between 2305 and 2312 UT. These crossings are identified by the decrease in the solar wind ion densities and the increase in B_z . The crossings were too brief to obtain good measurements of the $\text{He}^{2+}/\text{H}^+$ density ratio across the boundary. However, the $\text{He}^{2+}/\text{H}^+$ density ratio was reasonably well determined in the intervals labeled Sh (magnetosheath), and BL (low latitude boundary layer). The $\text{He}^{2+}/\text{H}^+$ density decreases by about 30% from the magnetosheath to the LLBL and decreases slightly from the LLBL to the magnetosphere.

decrease in the H^+ density (top panel), a corresponding decrease in the He^{2+} density (middle panel), and an increase in the Z component of the magnetic field (bottom panel). In these crossings, the B_z component of the magnetic field was positive in the magnetosheath and the shear at the magnetopause was low (28°). These and other crossings in this data set were identified using higher time resolution magnetic field data than shown in Figure 2. After a brief encounter with the magnetosphere at about 2312 UT, the spacecraft was in the LLBL from about 2315 to 2319 UT. The LLBL is identified as the interval where the He^{2+} and H^+ densities are intermediate between those in the magnetosheath and magnetosphere. After 2320, the significant increase in the H^+ temperature (in the second panel from the top) and the corresponding decreases in the H^+ and He^{2+} densities indicate the final entry into the magnetosphere.

The second panel from the bottom shows the He^{2+}/H^+ density ratio. In the magnetosheath at the left-hand edge of the panel, this ratio is between 1 and 1.5%. This is a factor of 2 to 4 times lower than the typical He^{2+} concentration in the solar wind. The density ratio in the solar wind may have been lower than typical during this interval or this ratio may be low because the Plasma Composition Experiment and the Fast Plasma Experiment were not intercalibrated. Other intervals studied (not shown) do not have lower than typical He^{2+} concentrations in the sheath. In any case, absolute density ratios are not important here, only their relative change across the magnetopause.

Because magnetopause crossings and the crossings of the LLBL-magnetosphere boundary can occur on timescales substantially faster than the 1-min time resolution of the plasma measurements used here, these sharp boundaries must be avoided when computing the change in the He^{2+}/H^+ density ratio from the magnetosheath to the LLBL. For example, in Figure 2 at the relatively brief crossings from the LLBL to the magnetosphere at 2312 UT and 2320 UT, the He^{2+}/H^+ density ratio is a factor of 2 higher than in the magnetosheath. This may reflect an actual change in the composition at these boundaries. However, the acquisition of the He^{2+} and H^+ spectra was different for the two ISEE instruments, and this may have caused significant time aliasing of the density ratio. To minimize possible time aliasing near sharp boundaries, the He^{2+}/H^+ density ratio in the magnetosheath and LLBL was determined during intervals when the density was relatively constant for 2 to 3 min. The density ratios for the AMPTE/CCE events were determined in a similar fashion [Fuselier et al., 1993]. However, time aliasing of the density ratio should be much less for AMPTE/CCE because a single instrument with simultaneous acquisition of H^+ and He^{2+} spectra was used.

For the ISEE 1 event in Figure 2, selected intervals removed from abrupt density changes near the sharp plasma boundaries are shown in the second panel from the bottom. In the magnetosheath (Sh), the He^{2+}/H^+ density ratio was between 0.01 and 0.015, in the LLBL (BL), the ratio was below 0.01, and in the magnetosphere (Sphere), the ratio was somewhat lower than that in the LLBL. Thus, there is a decrease in the He^{2+} concentration relative to H^+ as the spacecraft transitions from the magnetosheath to the LLBL and into the magnetosphere. Taking into account the fluctuations in the density ratio in both the magnetosheath and the LLBL intervals, the relative change in the He^{2+} concentration across the magnetopause for this event, expressed as the He^{2+}/H^+

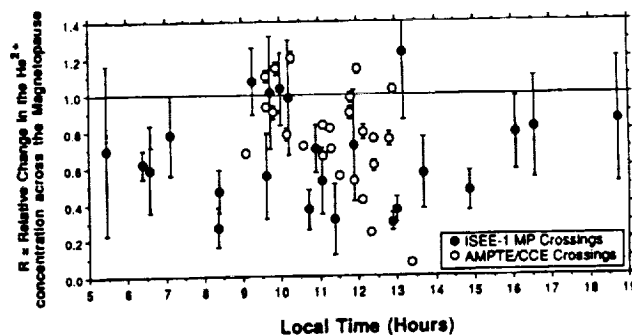


Figure 3. Change in the He^{2+} concentration across the magnetopause (defined as the ratio of the He^{2+}/H^+ density ratios in the LLBL divided by the magnetosheath) as a function of local time. ISEE and AMPTE/CCE observations agree reasonably well and both show that the He^{2+} concentration relative to H^+ most often decreases across the magnetopause.

ratio in the LLBL divided by the ratio in the magnetosheath, is 0.7 ± 0.12 .

The relative changes in the He^{2+} concentration from the magnetosheath to the LLBL for all magnetopause crossings are shown in Figure 3 as a function of local time. A value of 1 indicates no change in the He^{2+} concentration; values greater than (less than) 1 indicate an enrichment (deficit) of He^{2+} relative to H^+ in the LLBL. Error bars on the ISEE 1 values reflect changes in the density measurements during the 2 to 3 min LLBL and magnetosheath intervals. These changes are much larger than the statistical fluctuations in the density measurements from the individual instruments. Error bars on the AMPTE/CCE observations reflect statistical uncertainties in the density measurements because time aliasing in the simultaneous AMPTE/CCE He^{2+} and H^+ measurements is minimal compared to that for ISEE.

Figure 3 shows two important results. First, the relative change in the He^{2+} concentration across the magnetopause is often less than 1, indicating a deficit of He^{2+} in the LLBL. Second, the ISEE and AMPTE/CCE observations agree reasonably well over the same local time range.

Table 1 shows weighted means of the He^{2+} concentration change across the magnetopause for different groupings of the data set. Errors are the standard deviation of the mean, and both the mean and its standard deviation were calculated by weighting the contribution from each measurement to the mean by its uncertainty. Because errors in the AMPTE/CCE values are smaller than those for ISEE, weighting of the mean tends to favor the former values. The first entry in Table 1 shows the mean of the He^{2+} concentration change from the magnetosheath to the LLBL for the LLBL events. The mean value of 0.59 ± 0.01 indicates that, on average, there is a 40% reduction in the He^{2+} concentration relative to H^+ from the magnetosheath to the LLBL.

The second two entries in Table 1 compare the ISEE 1 data and the AMPTE/CCE data over the same local time. Given all the differences in the two data sets discussed at the beginning of this section, it is not surprising that the change in concentration is not exactly the same. However, it is significant that both data sets independently exhibit a decrease in the He^{2+} concentration. The next three entries compare the change in the concentration with local time. The largest decrease occurs on the dawnside, indicating a possible

Table 1. Change in the He^{2+} Concentration Across the Magnetopause

| Data Set | Local Time Coverage | Number of Events | $(\text{He}^{2+}/\text{H}^+)_{\text{Boundary Layer / Sheath}}$ |
|---|---------------------|------------------|--|
| Combined | 0500 - 1900 | 55 | 0.59 ± 0.01 |
| ISEE 1 only | 0900 - 1400 | 14 | 0.43 ± 0.03 |
| AMPTE/CCE only | 0900 - 1400 | 27 | 0.60 ± 0.01 |
| ISEE 1 | 0500 - 0900 | 7 | 0.53 ± 0.05 |
| Combined | 0900 - 1500 | 43 | 0.59 ± 0.01 |
| ISEE 1 | 1500 - 1900 | 5 | 0.84 ± 0.14 |
| ISEE 1 Current Layer | 1400 - 1900 | 5 | 0.93 ± 0.12 |
| ISEE 1 Reconnection Events | 0800 - 1600 | 6 | 0.41 ± 0.05 |
| AMPTE/CCE Reconnection Events | 0900 - 1300 | 13 | 0.72 ± 0.01 |
| Combined with magnetopause shear from 0 to 60° | 0600 - 1800 | 25 | 0.69 ± 0.01 |
| Combined with magnetopause shear from 120 to 180° | 0500 - 1700 | 12 | 0.67 ± 0.01 |
| Combined-Quiet ($AE < 90$ nT) | 0006-1900 | 12 | 0.77 ± 0.03 |
| Combined-Active ($AE > 500$ nT) | 0900-1800 | 16 | 0.67 ± 0.01 |

trend with local time. However, there are few observations on the flanks compared to the subsolar region, and the dawnside observations occurred primarily at high latitude (see Figure 1). The next entry shows that the He^{2+} concentration is relatively constant for the few ISEE 1 events where sufficient time was spent in the duskside flank current layer. The last six entries show that, selecting only events with clear reconnection signatures (such as accelerated flows in the LLBL and reflected/transmitted distributions at the magneto-pause [e.g., Fuselier *et al.*, 1991]), separating high and low shear, or separating active and quiet magnetospheric conditions (with these conditions defined by Sharp *et al.* [1982]), indicate no significant trends. Independent of how the data set is divided, there appears to be a 30-40% decrease in the He^{2+} concentration across the magnetopause from the magnetosheath to the LLBL.

Possible Causes

Possible causes for this apparent reduction in the He^{2+} concentration across the magnetopause include (1) instrumental effects, (2) "contamination" by magnetospheric H^+ in the LLBL, and (3) preferential exclusion of He^{2+} from the LLBL.

Instrumental effects should have minimal impact on the results presented here. By comparing changes in density ratios, difficult problems such as absolute calibration of the different instruments are avoided. Furthermore, both the ISEE and AMPTE data sets exhibit similar reductions in the He^{2+} concentration across the magnetopause (Table 1). With all the differences in the instruments used, spacecraft orbits, upstream solar wind conditions, and magnetospheric activity levels, it is not surprising that the reduction in the He^{2+} concentration is somewhat different for the two data sets. However, it is significant that both data sets independently exhibit a reduction.

Contamination by magnetospheric H^+ in the LLBL lowers the $\text{He}^{2+}/\text{H}^+$ density ratio in that region relative to the magnetosheath. However, this contamination should be negligible in the LLBL. By comparing the $\text{He}^{2+}/\text{H}^+$ density ratio and the H^+ density in the adjacent magnetosphere with the same quantities in the LLBL for all magnetopause crossings in this study, the contribution of the magnetospheric H^+ population to the total H^+ density in the LLBL is estimated to be about 5%. Figure 2 shows an example of this minimal contribution. In the magnetosphere after 2325 UT, the H^+ density is of the order of 0.5 cm^{-3} , while the H^+ density in the LLBL is $5-7 \text{ cm}^{-3}$. Thus a 5-10% concentration of magnetospheric H^+ is possible in the LLBL for this event. However, this magnetospheric H^+ population causes an even smaller reduction in the $\text{He}^{2+}/\text{H}^+$ density ratio in the LLBL because of the presence of magnetospheric He^{2+} in the LLBL (see Figure 2). Furthermore, the magnetospheric $\text{He}^{2+}/\text{H}^+$ concentration in Figure 2 may be underestimated in the magnetosphere because the distribution is hot (of the order of 10 keV/e) and the plasma composition experiment has an energy range of only 17 keV/e [Sharp *et al.*, 1982; Lennartsson, 1992]. Therefore, the possible reduction in the $\text{He}^{2+}/\text{H}^+$ density ratio in the LLBL due to contamination by magnetospheric plasma may be even smaller than 5-10%.

Finally, contamination from magnetospheric H^+ should be a function of magnetospheric activity. By comparing the change in the $\text{He}^{2+}/\text{H}^+$ density ratio across the magnetopause for high and low magnetospheric activity, an estimate of the maximum contamination level from magnetospheric H^+ in the LLBL is obtained. Table 1 shows that there is a reduction in the $\text{He}^{2+}/\text{H}^+$ density ratio in the LLBL for both extreme quiet and extreme active magnetospheric conditions and that the reduction is about 15% greater for extreme active conditions. Thus, assuming essentially no contamination from the magnetospheric H^+ population for quiet conditions, the maximum contribution of magnetospheric H^+ to the $\text{He}^{2+}/\text{H}^+$

density ratio in the LLBL is also about 15%. In Table 1, magnetospheric activity is defined by the maximum hourly AE index from either the interval or 1 hour before, with quiet (active) intervals defined as the maximum hourly AE < 90 nT (>500 nT) [see also Sharp *et al.*, 1982].

Eliminating instrumental and magnetospheric effects, the remaining possible cause for the reduction in the He^{2+} concentration across the magnetopause is preferential exclusion of He^{2+} from the LLBL. Understanding this possible cause requires specification of a mechanism for transfer of solar wind mass across the magnetopause as well as a discussion of the differences between He^{2+} and H^+ distributions in the magnetosheath. Here, magnetic reconnection is the only transfer mechanism considered because this mechanism has been shown to be important at the magnetopause and because the ion distributions on either side of the magnetopause are simply determined, especially for high magnetic shear [e.g., Cowley, 1982]. In addition, consideration is limited to the subsolar region, where most of the observations in Figure 2 are located and where the bulk flow velocity parallel to the magnetic field in the magnetosheath is small. Finally, magnetosheath distributions are assumed to be Maxwellian. In fact, the He^{2+} distribution is better described as a shell in velocity space with bulk flow velocity the same as that for the proton distribution [Fuselier *et al.*, 1988]. If only a limited range of magnetosheath pitch angles and energies crossed the magnetopause and entered the LLBL, then the details of the magnetosheath distribution become very important. This effect is seen in the cusp He^{2+} distributions [Shelley *et al.*, 1976]. However, this is not the case in the LLBL, where the magnetosheath distribution over a wide range of pitch angles and energies is observed at any location except near the inner boundary between the LLBL and magnetosphere. Thus, for the purposes of illustration here, the assumption of a Maxwellian distribution does not lead to serious error.

The remainder of this section is divided into two parts. In the first part, the properties of the solar wind ion distributions incident on the magnetopause and the reflection or transmission of these ions across the boundary are discussed. In the second part, the implications of a mass dependent reflection coefficient at the magnetopause is discussed.

Solar Wind Ion Distributions Incident on the Magnetopause

Solar wind ions incident on the open magnetopause magnetic field topology in the subsolar region will either cross the boundary or reflect off the magnetopause and return to the magnetosheath. The region sunward of the magnetopause that contains the reflected solar wind ions is the magnetosheath boundary layer (MSBL), and the region earthward that contains the transmitted ions is the LLBL. In the deHoffman-Teller frame of reference (i.e., the frame of reference where the $\mathbf{v} \times \mathbf{B}$ electric field vanishes on either side of the magnetopause), the incident, reflected, and transmitted ion distributions will travel either parallel or antiparallel to the magnetic field at approximately the Alfvén velocity [e.g., Cowley, 1982].

Figure 4 shows parallel cuts in the solar wind ion distributions in these layers in the spacecraft frame for reconnection southward of the spacecraft (see also Figure 3 of Cowley [1982]). The deHoffman-Teller velocity (V_{dHT}) is approximately the Alfvén velocity and the bulk flow velocity

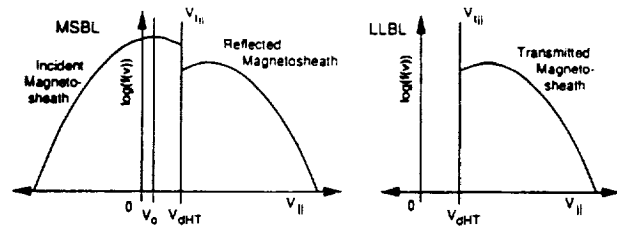


Figure 4. Schematic of parallel cuts in the magnetosheath ion distributions in the MSBL just sunward of the magnetopause and the LLBL just earthward of the magnetopause. These distributions are shown for typical conditions in the subsolar magnetosheath, where the parallel bulk flow velocity (V_0) is small compared to the Alfvén speed (V_A) and the deHoffman-Teller velocity (V_{dHT}) is approximately equal to the thermal velocity (V_{th}) and V_A . The ion reflection coefficient is assumed to be 0.5 so that the reflected distribution is 50% of the incident distribution. The percentage of the distribution incident on the magnetopause depends on the parallel thermal velocity. For a fixed V_{dHT} ion distributions with smaller parallel thermal velocity will have a higher percentage of the distribution incident on the magnetopause (and available for reflection from or transmission through the boundary).

parallel to the magnetic field is small in the subsolar region. Solar wind ions with parallel speeds below V_{dHT} are incident on the magnetopause. Ions with parallel speeds above this velocity will not encounter the magnetopause. Since V_{dHT} is constant for all ion species and the bulk flow velocities of different ion species are approximately the same in the subsolar magnetopause [e.g., Fuselier *et al.*, 1988], Figure 4 shows that the percentage of the solar wind ion distribution incident on the magnetopause (and therefore able to be transmitted across the boundary) is a function of the parallel thermal speed of the distribution. In this simple picture, the reflection and transmission mechanisms are not specified. Instead, a reflection coefficient at the magnetopause is assumed. In Figure 4 this reflection coefficient is assumed to be 50%, approximately consistent with magnetopause H^+ observations [e.g., Fuselier, 1995].

The parallel thermal speed dependence of the percentage of the ion distribution incident on the magnetopause provides a potential mechanism for changing the $\text{He}^{2+}/\text{H}^+$ concentration in the LLBL. Solar wind ion distributions have different temperatures and temperature anisotropies in the magnetosheath [e.g., Fuselier *et al.*, 1991]. In particular, the He^{2+} temperature (where $T = (2T_{\perp} + T_{\parallel})/3$) is about 4 times higher than the H^+ temperature (e.g., Figure 6 of Fuselier *et al.* [1991]). In addition, He^{2+} is more anisotropic than H^+ . Figure 5 shows a comparison of the temperature anisotropies of He^{2+} and H^+ for the 27 AMPTE/CCE events in this study. The average temperature anisotropy for H^+ is about 2. Temperature anisotropies for the two species are well correlated with the He^{2+} anisotropy approximately 1.5 times larger than that for H^+ . With these observations, the ratio of the parallel temperatures of the two ion distributions can be determined.

First, it is assumed that

$$T_{\text{HE}} = 4 T_{\text{H}} \quad (1)$$

and

$$(T_{\perp}/T_{\parallel})_{\text{HE}} = k (T_{\perp}/T_{\parallel})_{\text{H}} \quad (k > 1), \quad (2)$$

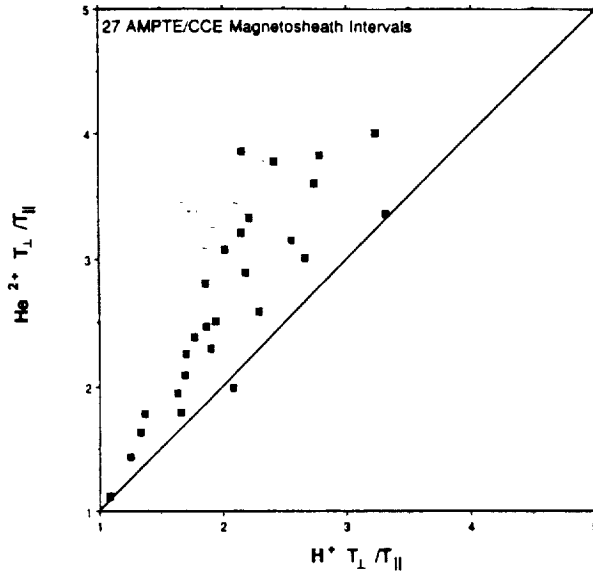


Figure 5. The temperature anisotropies for He^{2+} versus H^+ for the 27 AMPTE/CCE magnetosheath intervals used in this study. The average anisotropy for H^+ is approximately 2, and He^{2+} is consistently more anisotropic than H^+ by a factor of about 1.5.

with

$$T = (2T_{\perp} + T_{\parallel})/3. \quad (3)$$

Equations (1) and (2) are combined and solved for the parallel thermal velocity of He^{2+} ($V_{\parallel\text{He}}$, where $(V_{\parallel\text{He}})^2 \propto T_{\parallel\text{He}}/m$) in terms of the parallel thermal velocity of H^+ and the H^+ temperature ratio.

$$V_{\parallel\text{He}} = V_{\parallel\text{H}} \sqrt{\frac{(2 \frac{T_{\perp\text{H}}}{T_{\parallel\text{H}}} + 1)}{(2k \frac{T_{\perp\text{H}}}{T_{\parallel\text{H}}} + 1)}} \quad (4)$$

Since k is greater than 1, the parallel thermal velocity of He^{2+} will be less than the parallel thermal velocity of H^+ in the magnetosheath. Thus, in general, more of the He^{2+} distribution will be at parallel velocities that are less than the deHoffman-Teller velocity and therefore more He^{2+} than H^+ will be incident on the magnetopause. If the reflection coefficient at the magnetopause is independent of the mass of the incident ion, then the lower parallel temperature of He^{2+} implies that the He^{2+} concentration will go up across the magnetopause.

Assuming Maxwellian distributions incident on the magnetopause, $T_{\perp\text{H}}/T_{\parallel\text{H}} = 2$, $V_{\parallel\text{H}} = V_{\text{dHT}} =$ the Alfvén velocity, V_A , and a bulk flow velocity parallel to the magnetic field of $0.25V_A$ (i.e., small compared to V_A), Table 2 shows how the change in the solar wind He^{2+} concentration across the magnetopause depends on the difference in He^{2+} and H^+ temperature anisotropies in the magnetosheath. Column 1 in the table is k from (2). Column 2 is the ratio of the parallel thermal velocities from (4). Columns 3 and 4 are the percentage of H^+ and He^{2+} incident on the magnetopause, respectively. These percentages were determined from the temperature anisotropy and velocities assumptions above. Column 5 is the ratio of the percentages in columns 4 and 3, which is the change in the He^{2+} concentration from the magnetosheath to the LLBL. Table 2 shows that, assuming magnetic reconnection at the magnetopause and typical magnetosheath conditions in the subsolar region (including $k=1.5$), there should be approximately a 5% increase in the He^{2+} concentration in the LLBL. This is contrary to the approximately 40% decrease in the concentration observed by the ISEE and AMPTE/CCE spacecraft.

Mass Dependent Reflection Coefficient at the Magnetopause

One important free parameter in the above analysis that has the potential to directly affect the He^{2+} concentration in the LLBL is the reflection coefficient at the magnetopause. If the reflection coefficient at the magnetopause is a function of the mass of the incident ion, then more He^{2+} is reflected back into the magnetosheath and less is transmitted into the LLBL. Taking into account that there is a 5% higher percentage of He^{2+} incident on the magnetopause (in Table 2), the bottom panel of Figure 6 shows the relationship between the He^{2+} and H^+ reflection coefficients that would account for the observed change in the He^{2+} concentration from the magnetosheath to the LLBL. Observations of reflected H^+ in the MSBL indicate that the H^+ reflection coefficient is of the order of 0.5 [Fuselier, 1995]. (Note that Fuselier computes the percent of reflected H^+ relative to the total density in the MSBL. This quantity is equal to $R/(1+R)$ where R is the reflection coefficient at the magnetopause.)

With an H^+ reflection coefficient of 0.5, Figure 6 shows that the He^{2+} reflection coefficient must be approximately 0.72 (or about 44% higher) to produce a 40% reduction in the He^{2+} concentration in the LLBL. The ratio of the H^+ to He^{2+} reflection coefficients does not equal the concentration change across the magnetopause because there is 5% more He^{2+} incident on the magnetopause compared to H^+ (as discussed above).

If less He^{2+} enters the LLBL, then there is the potential for excess He^{2+} in the MSBL. The top panel shows the change in

Table 2. Predicted Change in the He^{2+} Concentration Across the Magnetopause for a Constant Reflection Coefficient

| $k = (T_{\perp}/T_{\parallel})_{\text{He}} / (T_{\perp}/T_{\parallel})_{\text{H}}$ | $V_{\parallel\text{He}}/V_{\parallel\text{H}}$ | Percent Sheath H^+ Incident on the Magnetopause | Percent Sheath He^{2+} Incident on the Magnetopause | Change in the He^{2+} Concentration: Sheath to the LLBL |
|--|--|--|--|--|
| 1.0 | 1.00 | 0.76 | 0.76 | 1.00 |
| 1.5 | 0.85 | 0.76 | 0.81 | 1.06 |
| 2.0 | 0.75 | 0.76 | 0.84 | 1.10 |
| 2.5 | 0.67 | 0.76 | 0.86 | 1.12 |
| 3.0 | 0.62 | 0.76 | 0.88 | 1.15 |

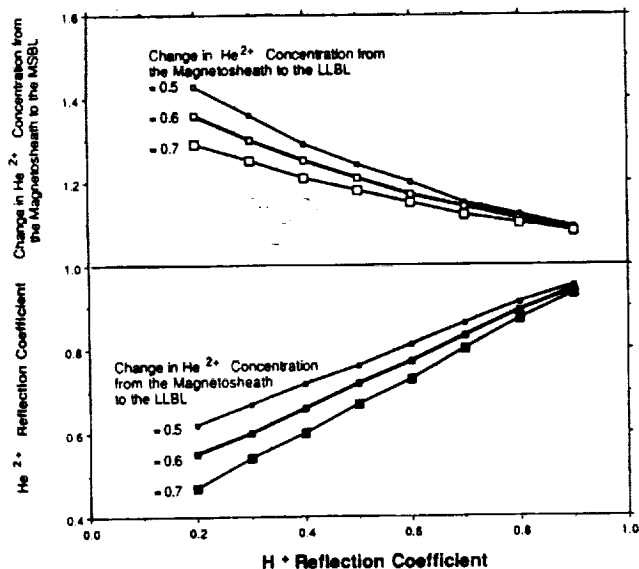


Figure 6. (top) Change in the He^{2+} concentration from the magnetosheath to the MSBL and (bottom) the He^{2+} reflection coefficient as a function of the H^+ reflection coefficient. To account for a 40% change in the He^{2+} concentration from the magnetosheath the LLBL, the He^{2+} reflection coefficient must be approximately 45% higher than the H^+ reflection coefficient (bottom panel, middle curve), and the He^{2+} concentration in the MSBL must increase from 10 to 40% (top panel, middle curve).

the He^{2+} concentration from the magnetosheath to the MSBL as a function of the H^+ reflection coefficient. Again considering an average H^+ reflection coefficient of 0.5, the He^{2+} concentration should be about 20% higher in the MSBL than in the magnetosheath.

Observational confirmation of this increase in the He^{2+} concentration in the MSBL is difficult. Fuselier [1995] shows all published observations of the reflected ion population in the MSBL that include ion composition. While the average percentage of reflected H^+ and He^{2+} appears to be equal for the few published observations, uncertainties in these averages are easily large enough to accommodate a 20% increase in the He^{2+} concentration in the MSBL. Another possibility is that the He^{2+} becomes trapped in the magnetopause current layer. Trapping would result in an increase in the concentration in the current layer but not necessarily in the MSBL. However, this would require specification of a mechanism that would cause this trapping.

Summary and Conclusions

Observations presented here show that there is about a 40% reduction in the He^{2+} concentration (relative to H^+) from the magnetosheath to the LLBL. Instrumental effects and contamination by ionospheric H^+ in the LLBL are ruled out as causes for this reduction. The reduction is independent of magnetic shear, suggesting a single mass transfer process at the magnetopause. There are possible dawn-dusk or latitudinal dependencies in this reduction in the He^{2+} concentration; however, these possible effects require further study at high latitudes.

For magnetic reconnection and a mass independent reflection coefficient at the magnetopause, typical magnetosheath parameters near the subsolar region suggest that the He^{2+} concentration in the LLBL should increase by 5% relative to the magnetosheath and not decrease by 40% as observed. To account for the observed 40% decrease in the He^{2+} concentration, the reflection coefficient for He^{2+} must be approximately 45% higher than that for H^+ . A prediction from this mass dependent reflection coefficient is that the He^{2+} concentration in the MSBL should increase by approximately 20%. Thus far, limited observations in the MSBL neither confirm nor deny this possible increase in the He^{2+} concentration.

Acknowledgments. Discussions with T. Onsager and R. Elphic are gratefully acknowledged. Research at Lockheed was funded under the NASA Supporting Research and Technology program through grant NAGW-4049 and contract NASW-5037.

The Editor thanks T. E. Eastman and another referee for their assistance in evaluating this paper.

References

- Bame, S. J., J. R. Asbridge, H. E. Feldhauser, J. P. Glore, G. Paschmann, P. Hemmerich, K. Lehmann, and H. Rosenbauer, ISEE 1 and -2 fast plasma experiment and the ISEE 1 solar wind experiment, *IEEE Trans. Geosci. Electron.*, GE-16, 216, 1978.
- Cowley, S. W. H., The causes of convection in the Earth's magnetosphere: A review of developments during the IMS, *Rev. Geophys.*, 20, 531, 1982.
- Fuselier, S. A., Kinetic aspects of reconnection at the magnetopause, in *Physics of the Magnetopause*, *Geophys. Monogr. Ser.* vol. 90, edited by P. Song, B. U. Ö Sonnerup, and M. F. Thomsen, p. 181, AGU, Washington D. C., 1995.
- Fuselier, S. A., E. G. Shelley, and D. M. Klumppar, AMPTE/CCE observations of shell-like He^{2+} and O^{6+} distributions in the magnetosheath, *Geophys. Res. Lett.*, 15, 1333, 1988.
- Fuselier, S. A., D. M. Klumppar, E. G. Shelley, B. J. Anderson, and A. J. Coates, He^{2+} and H^+ dynamics in the subsolar magnetosheath and plasma depletion layer, *J. Geophys. Res.*, 96, 21,095, 1991.
- Fuselier, S. A., D. M. Klumppar, and E. G. Shelley, Mass density and pressure changes across the dayside magnetopause, *J. Geophys. Res.*, 98, 3935, 1993.
- Lennartsson, W., A scenario for solar wind penetration of Earth's magnetic tail based on ion composition data from the ISEE 1 spacecraft, *J. Geophys. Res.*, 97, 19,221, 1992.
- Lennartsson, W., and E. G. Shelley, A mechanism for the depletion of He^{++} in the solar wind component of the magnetospheric plasma, *Eos Trans. AGU* 63, 1075, 1982.
- Potemra, T. A., L. J. Zanetti, and M. H. Acuna, The AMPTE CCE magnetic field experiment, *IEEE Trans. Geosci. Remote Sens.*, GE-23, 246, 1985.
- Russell, C. T., The ISEE 1 and -2 fluxgate magnetometers, *IEEE Trans. Geosci. Electron.*, GE-16, 239, 1978.
- Sharp, R. D., W. Lennartsson, W. K. Peterson, and E. G. Shelley, The origins of the plasma in the distant plasma sheet, *J. Geophys. Res.*, 87, 10,420, 1982.
- Shelley, E. G., R. D. Sharp, and R. G. Johnson, He^{2+} and H^+ flux measurements in the day side cusp: Estimates of the convection electric field, *J. Geophys. Res.*, 81, 2363, 1976.
- Shelley, E. G., R. D. Sharp, R. G. Johnson, J. Geiss, P. Eberhardt, H. Balsiger, G. Haerendel, and H. Rosenbauer, Plasma composition experiment on ISEE-A, *IEEE Trans. Geosci. Electron.*, GE-16, 266, 1978.
- Shelley, E. G., A. Ghielmetti, E. Hertzberg, S. J. Batel, K. Alwegg-Von Burg, and H. Balsiger, The AMPTE CCE Hot-Plasma Composition

Experiment (HPCE), *IEEE Trans. Geosci. Remote Sens.*, GE-23, 241, 1985.
 Song, P., C. T. Russell, R. J. Fitzenreiter, J. T. Gosling, M. F. Thomsen, D. G. Mitchell, S. A. Fuselier, G. K. Parks, R. R. Anderson, and D. Hubert, Structure and properties of the subsolar magnetopause for northward interplanetary magnetic field: Multiple-instrument particle observations, *J. Geophys. Res.*, 98, 11,319, 1993.

S. A. Fuselier, O. W. Lennartsson, and E. G. Shelley, Lockheed-Martin Palo Alto Research Laboratory, 3251 Hanover Street, Department 91-20, Building 252, Palo Alto, CA 94304. (e-mail: fuselier@space.lockheed.com)

(Received June 3, 1996; revised July 25, 1996; accepted July 26, 1996.)

Relationships between plasma depletion and subsolar reconnection

B. J. Anderson

The Johns Hopkins University Applied Physics Laboratory, Laurel, Maryland

T.-D. Phan

Space Science Laboratory, University of California, Berkeley, California

S. A. Fuselier

Lockheed Palo Alto Research Laboratory, Palo Alto, California

Abstract. Observations in the subsolar magnetosheath show that the plasma depletion layer (PDL) is less pronounced for southward than for northward IMF. Since subsolar plasma depletion indicates pile-up of magnetic flux, the degree of plasma depletion should depend on the relative rates of flux transport via subsolar reconnection and flux advection by the solar wind flow. To identify the factors affecting plasma depletion, we consider the ratio $D = E_r/E_{sw}$ where E_r is the reconnection electric field and E_{sw} is the imposed solar wind electric field. For a quasi-perpendicular subsolar bow shock D can be expressed in terms of magnetosheath parameters. Since PDL formation is suppressed when the subsolar bow shock is quasi-parallel, we restrict attention to quasi-perpendicular conditions. We show that D increases with increasing reconnection efficiency, magnetic shear at the magnetopause, and the magnetosheath magnetic field but decreases with increasing total perpendicular pressure (particle plus magnetic field) in the magnetosheath. By combining observations of the subsolar quasi-perpendicular magnetosheath from AMPTE/IRM and AMPTE/CCE we verify that the degree of plasma depletion is inversely correlated with D . Furthermore, we show that the greater prevalence of plasma depletion in the CCE data implies that the reconnection efficiency is lower for the CCE events and specifically that the reconnection efficiency depends roughly inversely on magnetosheath β , for $\beta > 1$. Finally, the results show that all of the changes brought about by plasma depletion act to increase E_r so that some subsolar reconnection is likely to occur even for low magnetic shear. Thus the percentage of the magnetosheath magnetic field that participates in reconnection near the subsolar region does not act as a rectifier but remains positive for all shear angles, decreasing monotonically as the magnetic shear at the subsolar magnetopause changes from high to low shear. This implies that the equatorward polar cap convection cells observed during northward IMF and conventionally thought to be driven by a viscous interaction may be due at least in part if not wholly to subsolar low shear reconnection.

1. Introduction

Momentum and energy transfer from the solar wind to the magnetosphere is believed to occur near the subsolar magnetopause via reconnection when the solar wind magnetic field is southward. The magnetosheath plasma imposed on the magnetosphere is therefore of great importance for this transport process. Near the subsolar region the magnetosheath flow can give rise to a region of decreased density and increased magnetic field strength called the plasma depletion layer (PDL) when the subsolar bow shock is quasi-perpendicular. When a PDL forms, it

is the plasma and field in this layer, rather than the magnetosheath proper, that is imposed on the subsolar magnetopause.

There is some variation in the reported prevalence of the PDL. *Anderson and Fuselier* [1993], hereinafter P1, reported a PDL for all orientations of the magnetosheath magnetic field, although the density decrease and field increase were smallest when the field was southward. By contrast, *Phan et al.* [1994], hereinafter P2, found that a PDL was clearly evident only when the magnetosheath field was aligned within 60° of the magnetospheric field. Both P1 and P2 interpreted the dependence of PDL prevalence on IMF orientation as evidence for reconnection flows at the subsolar magnetopause, but the difference in PDL occurrence for high shear between P1 and P2 has not been explained. The issue of PDL formation for southward IMF is important since its formation indicates that mag-

Copyright 1997 by the American Geophysical Union.

Paper Number 97JA00173.
0148-0227/97/97JA-00173\$09.00

netic flux is piling up against the magnetopause despite the reconnection flows and hence that the reconnection electric field has saturated.

The data sets used in P1 and P2 were different. The data of P1 are from the Active Magnetosphere Particle Tracers Explorers (AMPTE) Charge Composition Explorer (CCE) while the data of P2 are from the AMPTE Ion Release Module (IRM) [cf. *Acuña et al.*, 1985]. The geocentric distances of apogee for these spacecraft were significantly different: 8.8 R_E for CCE and 18.8 R_E for IRM. The nominal subsolar magnetopause standoff distance is 11 R_E [Roelof and Sibeck, 1993], so all of the CCE magnetosheath encounters occurred for high solar wind Alfvén Mach number, whereas IRM crossed the magnetosheath under generally more typical solar wind conditions.

The aim of this paper is to understand why CCE and IRM observed a difference in occurrence of plasma depletion. In section 2 we present a model of the relationship between plasma depletion and reconnection to identify the variables that control PDL formation. In section 3 we describe how we combined the two data sets and restricted the data to quasi-perpendicular upstream conditions. Section 4 presents a joint analysis of the databases of P1 and P2 to test the predictions of our model and to deduce the dependence of the reconnection electric field on magnetic shear and magnetosheath plasma β . The implications of the results are discussed in section 5.

The results indicate that the difference in PDL formation between the CCE and IRM data sets is due largely to a reduced reconnection efficiency for the CCE cases attributed to a threefold increase in magnetosheath β for the CCE events relative to the IRM cases. We also point out that the effects of plasma depletion enhance the probability and rate of subsolar reconnection, so that when the magnetosheath conditions are unfavorable for subsolar reconnection, the formation of the PDL acts to restore some subsolar reconnection. Principally, this is due to the fact that the magnetosheath field strength in the PDL increases as the IMF turns northward, implying that subsolar component reconnection remains allowed, albeit at a reduced rate, for all IMF orientations except exactly northward. We therefore propose that subsolar reconnection and plasma depletion should be regarded as dynamically coupled. When conditions in the magnetosheath are unfavorable for subsolar reconnection, plasma depletion occurs and acts to adjust conditions adjacent to the magnetopause so that some subsolar reconnection is likely to occur for almost all upstream conditions and IMF orientations. From this perspective, four-cell convection for IMF $B_z > 0$ can be understood as resulting from the combined effects of cusp reconnection and simultaneous weak subsolar reconnection without recourse to a viscous interaction.

2. Simple Model of Plasma Depletion and Reconnection

In this section we consider the related effects of solar wind and reconnection flows to determine the effect that various parameters should have on PDL formation. Magnetic flux is convected earthward by the solar wind at the rate given by the electric field

$$E_{sw} = B_{sw} V_{sw} \quad (1)$$

where B_{sw} is the magnitude of the solar wind magnetic field transverse to the Earth-Sun line, and V_{sw} is the solar wind velocity. Because the PDL forms preferentially for a quasi-perpendicular subsolar bow shock (e.g., P1), we do not consider the parallel shock case and assume that the solar wind magnetic field is draped in an orderly way. Note that we are not just interested in the southward component of the solar wind magnetic field. Magnetic flux is convected into the reconnection line at a rate given by the reconnection electric field

$$E_r = B_r V_r \quad (2)$$

where B_r is the magnitude of the magnetic field that participates in reconnection and V_r is the inflow velocity from the magnetosheath side into the reconnection line. If we consider the ratio of the E_r and E_{sw}

$$D = \frac{E_r}{E_{sw}} \quad (3)$$

we expect that D is always less than 1. If $D = 0$, then no reconnection occurs and all of the solar wind magnetic field is diverted around the magnetopause via MHD flow. Under these circumstances a plasma depletion layer will form [Midgley and Davis, 1963; Lees, 1964; Zwan and Wolf, 1976]. As D increases, reconnection is able to take up some of the solar wind magnetic flux and the PDL will be correspondingly diminished.

We would like to determine how D depends on the solar wind velocity, density, and magnetic field strength and orientation. We note that V_r depends on the Alfvén speed in the magnetosheath and on the reconnection efficiency, k ,

$$V_r = k V_{A,r} \quad (4)$$

where $V_{A,r} = B_r / \sqrt{\mu_0 \rho_s}$ and ρ_s is the magnetosheath mass density [e.g., *Sonnerup*, 1974]. That is, $V_{A,r}$ is the magnetosheath Alfvén speed using the component of the sheath field that participates in merging. Typically, k is assumed to be around 0.1, and although it is not known how k depends on the properties of the magnetosheath plasma it is expected to go to zero for high β [Sonnerup, 1974].

Denoting the magnetic field in the magnetosheath and in the magnetosphere as \mathbf{B}_s and \mathbf{B}_m , respectively, B_r is the projection of \mathbf{B}_s along the $\mathbf{B}_s - \mathbf{B}_m$ direction:

$$B_r = B_s \cdot \frac{\mathbf{B}_s - \mathbf{B}_m}{|\mathbf{B}_s - \mathbf{B}_m|} \quad (5)$$

When $B_r < 0$, reconnection is geometrically impossible. This is the condition originally discussed by *Sonnerup* [1974]. Because of the PDL, the magnetosheath field strength adjacent to the magnetopause, B_s^* , is not independent of the shear angle, $\Delta\theta$, between \mathbf{B}_s and \mathbf{B}_m . In both P1 and P2 it was found that B_s^* approaches B_m as $\Delta\theta$ goes to zero. Therefore we do not assume that B_r necessarily becomes negative, although it must go to zero for $\Delta\theta = 0$. We write $B_r = S(\Delta\theta) B_s$ where $S(0) = 0$, $S(\pi) = 1$ and $S(\Delta\theta)$ increases monotonically with $\Delta\theta$. Then (2) and (4) give

$$E_r = \frac{k(\beta_s) S(\Delta\theta)^2 B_s^2}{\sqrt{\mu_0 \rho_s}} \quad (6)$$

To express D in terms of solar wind parameters, we must make some assumption about the shock. If we restrict attention to strong, quasi-perpendicular shocks we can write $B_s = \eta B_{sw}$ and $\rho_s = \eta \rho_{sw}$, where η is close to 4 [e.g., Kennel *et al.*, 1985]. The downstream β is determined principally by the solar wind Alfvén Mach number, M_{Asw} . As M_{Asw} increases, η does not change much and approaches 4 asymptotically, but β_s increases like M_{Asw}^2 because the shock heating increases in proportion to the upstream kinetic energy. We therefore write $k(M_{Asw})$ and have

$$D = \frac{k(M_{Asw})S(\Delta\theta)^2 B_{sw} \eta^{1.5}}{\sqrt{\mu_0 P_{ram}}} \quad (7)$$

where P_{ram} is the solar wind ram pressure, $P_{ram} = \rho_{sw} V_{sw}^2$.

This result suggests that the PDL is most favored under low magnetic shear, high solar wind ram pressure conditions consistent with those of P1 and P2. There are two additional important dependencies predicted by (7). First, large B_{sw} should inhibit PDL formation because although higher B_{sw} implies a higher solar wind magnetic flux transport, it also implies both more flux transport via reconnection and a higher reconnection rate because of the higher Alfvén speed in the sheath. Second, the PDL may be favored when M_{Asw} is large because k decreases with increasing β_s which increases with increasing M_{Asw} .

To compare this model with magnetosheath observations, we express D in terms of quantities measured in the sheath. For the cases discussed below, the ram pressure in the sheath is negligible relative to the perpendicular (magnetic plus thermal) pressure, $P_{\perp Tot,s}$, so we have

$$D = \frac{k(\beta_s)S(\Delta\theta)^2 B_s \eta^{0.5}}{\sqrt{\mu_0 P_{\perp Tot,s}}} \quad (8)$$

The parameters in (8) correspond to values in the magnetosheath proper, upstream of the PDL if present. This is the primary expression used below for comparison with the observations.

3. Combining the IRM and CCE Databases

To combine the IRM and CCE databases we first ensured that the events selected from each data set corresponded as nearly as possible to the same region of space sampled under comparable shock geometries. Each event is defined as two adjacent time intervals, one from the magnetosheath proper, denoted 1, and the other from the magnetosheath near the magnetopause, denoted 2. The magnetosheath field in 2 was used to evaluate the magnetic shear, $\Delta\theta$, between the magnetosheath near the magnetopause and the magnetosphere. We adopt the magnetosheath proper/PDL intervals of P1 (CCE) and refer to them here as regions 1 and 2, respectively. For the P2 events (IRM), we associate the magnetosheath proper with the time interval 10 to 20 min before (after) the magnetopause on inbound (outbound) crossings. The corresponding time interval for the near magnetopause region was chosen to be 0 to 5 min. We follow P2 and categorize events according to the magnetic shear. Cases with $\Delta\theta < 60^\circ$ are called low shear, and those with $\Delta\theta > 60^\circ$ we call high shear.

CCE: Equivalence of PDL and Near Magnetopause Region

For CCE the low radial spacecraft velocities required that the region identification in P1 be based on local plasma signatures. In P1 the PDL was shown to be correlated with left-handed proton cyclotron waves occurring above the local He^{2+} gyrofrequency, whereas the magnetosheath proper was indicated by mirror mode like fluctuations. The correspondence of this evolution in spectral signatures from the magnetosheath proper to the plasma depletion layer has been confirmed both observationally and theoretically [Anderson *et al.*, 1994; Denton *et al.*, 1994]. The departure of the ion temperature anisotropy below the mirror instability threshold in the PDL necessarily implies that such a mode changeover occurs and is associated with the magnetosheath proper/PDL transition [P2; Phan *et al.*, 1996b].

It is important to consider whether adopting the events of P1 constitutes preselection of the CCE data set against events without plasma depletion layers. First, we note that P1 showed that for quasi-perpendicular, Q_{\perp} , upstream bow shock conditions, 77% of all magnetopause crossings were associated with transition into a PDL. Second, we consider those CCE magnetopause crossings for which the magnetic field and plasma parameters displayed well-behaved, monotonic profiles in the magnetosheath. For these crossings the upstream conditions did not change suddenly, thus giving the best picture of the magnetosheath structure near the magnetopause for the CCE events. These crossings have been presented previously (Plates 1 and 2 of P1) and displayed the above-mentioned spectral characteristics of proton cyclotron waves regardless of the magnetic shear. Thus the presence of the PDL for southward magnetosheath fields is a persistent feature in the CCE observations. Adopting the events of P1 therefore does not exclude a major population of high shear cases without a PDL because such conditions are in the minority in the CCE data set.

Upstream Shock Geometry

We restricted the IRM events of P2 to ensure that the upstream shock geometries were comparable. The upstream shock condition is important because as found in P1, the PDL forms preferentially for Q_{\perp} upstream conditions. The events in P1 identified as PDL all displayed an absence of energetic, >10 keV, He^{2+} indicating connection to a Q_{\perp} bow shock. Corresponding He^{2+} data are not available for the IRM database of P2, so instead we used the R parameter of Lin *et al.* [1991] to discriminate between Q_{\perp} and quasi-parallel, Q_{\parallel} , upstream shock conditions. This parameter is

$$R = \frac{1}{N} \left| \sum_{\Delta t} \frac{\bar{\mathbf{B}}_i}{B_i} \right| \quad (9)$$

where the \mathbf{B}_i are sequential vector samples of the magnetic field, B_i is the field magnitude, Δt is the summation time interval, and N is the number of samples in the sum. If $R \sim 1$, the field orientation is well ordered and nearly constant but $R < 1$ indicates a variable field direction. As Luhmann *et al.* [1986] and Lin *et al.* [1991] discussed, well-ordered field directions are characteristic of Q_{\perp} up-

stream conditions, whereas Q_{\parallel} conditions are associated with variable downstream field orientations.

To ensure that the intervals from P1 and P2 used here correspond to similar upstream shock orientations, we evaluated R for the CCE events and used only those IRM events that gave R values in the same range as the CCE events. To evaluate R for the CCE events, we used a single time interval for each event which spanned both regions 1 and 2 and for the IRM events we used the full 20-min interval sunward of the magnetopause crossing. We evaluated R during each event at intervals separated by $\Delta t/4$ and calculated the average R value for the event, denoted R_{avg} . Values for Δt of both 2 min and 5 min were used and gave essentially the same results. For the CCE events, no R value was less than 0.7 and R_{avg} was larger than 0.94 in every case. We therefore selected only those IRM events which satisfied $R > 0.7$, and $R_{avg} > 0.9$. Of the original 38 events in P2, 25 events met these criteria and were used in this analysis.

The two data sets therefore both correspond to quasi-perpendicular bow shock conditions. Although the subsolar magnetosheath is not highly sensitive to bow shock geometry for an IMF within 45° of the Y - Z GSE plane [Kennel *et al.*, 1985; Wu, 1992] there may be some variation in PDL severity within the data sets due to the range of subsolar shock orientation within the quasi-perpendicular regime. However, temporal variations in solar wind conditions will probably be a more important complicating factor. In any case, we expect that shock geometry variations and temporal change effects will tend to average out in each data set. We are therefore interested only in average trends.

4. Observational Results and Model Comparison

Total Pressure Consistency Checks

Comparing the total pressure in regions 1 and 2 is useful both to compare conditions for the CCE and IRM events and to examine whether there are any systematic variations in upstream conditions between the time intervals used for the two regions. Such a systematic difference is expected for the CCE events because the CCE magnetosheath observations occurred near CCE apogee. Thus whether the magnetosheath proper or PDL was sampled by CCE depended on the imposed dynamic pressure, and we expect that the magnetosphere must be somewhat more compressed for CCE to sample the magnetosheath proper than for it to sample the PDL.

To estimate the dynamic pressure, we use the total static pressure normal to the magnetopause, $P_{\perp Tot} = P_{\perp part} + B^2/2\mu_0$, that is, the sum of magnetic and perpendicular particle pressures. The IRM ram plasma velocities given in P2 indicate that the ram pressure for the IRM events is ~ 0.02 nPa (using a typical magnetosheath density of 20 cm^{-3}), which is negligible compared to $P_{\perp Tot}$. We therefore ignore the magnetosheath ram pressure and assume that the ram pressure is negligible relative to $P_{\perp Tot}$ for the CCE events as well. The field line curvature near the magnetopause is also a negligible effect, so we consider only the scalar magnetic pressure for approximating force balance. In the case of IRM, all ions are interpreted as H^+ , whereas for CCE the H^+ and He^{2+} contributions

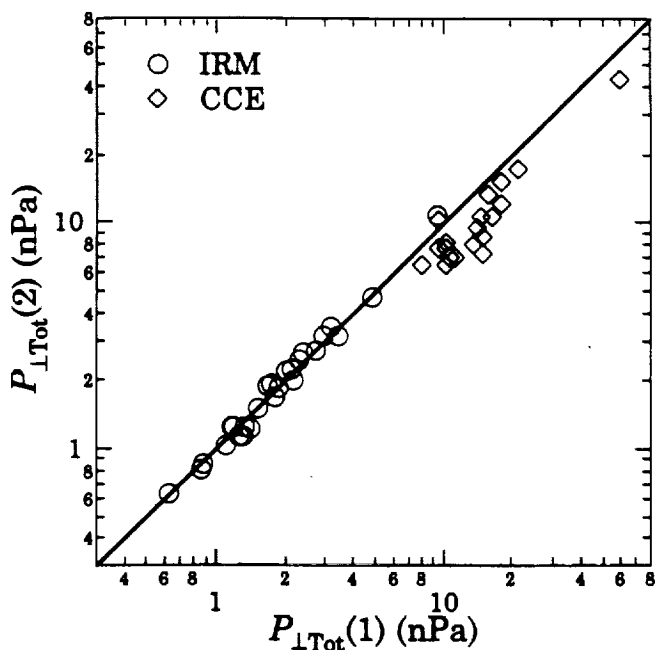


Figure 1. Total perpendicular static pressure, $P_{\perp Tot} = P_{\perp part} + B^2/2\mu_0$, observed near the magnetopause region 2 plotted versus $P_{\perp Tot}$ observed in the magnetosheath proper. That $P_{\perp Tot}(1) = P_{\perp Tot}(2)$ for the IRM events supports the interpretation that IRM traversed a stationary structure. For CCE, $P_{\perp Tot}(2)/P_{\perp Tot}(1) = 0.72$ on average, indicating that the magnetopause was about $0.5 R_E$ more earthward when CCE sampled region 1 than when CCE sampled region 2.

are evaluated separately and added to give $P_{\perp part}$. For CCE the He^{2+} contribution to the pressure was $\sim 10\%$, which is small relative to the difference in pressure between the CCE and IRM data sets.

In Figure 1 we plot $P_{\perp Tot}(2)$ versus $P_{\perp Tot}(1)$. As expected, the pressures during the IRM and CCE events were very different. For IRM the average $P_{\perp Tot}(1)$ was 1.7 (2.8) nPa for low (high) shear whereas for CCE the average $P_{\perp Tot}(1)$ was 9.6 (12.4) nPa for low (high) shear. The comparison of $P_{\perp Tot}$ in regions 1 and 2 is also significant. For the IRM events, $P_{\perp Tot}(2) \sim P_{\perp Tot}(1)$, as expected, if IRM traversed a stationary structure. For the CCE events $P_{\perp Tot}(2) < P_{\perp Tot}(1)$, as expected, if 2 is closer to the magnetopause than 1, since lower $P_{\perp Tot}$ brings CCE closer to the magnetopause when CCE is in the magnetosheath. The average ratio, $P_{\perp Tot}(2)/P_{\perp Tot}(1)$, for CCE is 0.72 which provides a measure of the scale length for the magnetosheath proper to PDL transition. The CCE radial distance at apogee is $8.8 R_E$, so if we take this for the radial distance for 2, $r(2)$, then $r(1)$ for the same dynamic pressure will be given by $r(2)/r(1) \sim 0.72^{1/6} = 0.95$ so that $r(1) - r(2) \sim 0.5 R_E$. Thus the magnetosheath proper/PDL transition occurs over about $0.5 R_E$.

Average Sheath and Inferred Solar Wind Conditions

To quantify the differences between the CCE and IRM events, we compare the average magnetosheath conditions for the data sets. Averages, standard deviations, and minimum and maximum values for $\beta(1)$, $B(1)$, $n(1)$, $P_{\perp Tot}(1)$, and the Alfvén velocity, $V_A(1)$, are given in Table 1. In

Table 1. Average IRM and CCE Parameters in the Magnetosheath Proper Denoted in the Text as Region 1

| | IRM | | CCE | |
|--------------------------------|----------------------------------|---------------|----------------------------------|---------------|
| | Average \pm Standard Deviation | (min, max) | Average \pm Standard Deviation | (min, max) |
| $\beta(1)$ | 2.5 ± 1.4 | (0.51, 5.57) | 8.0 ± 4.1 | (2.71, 14.3) |
| $B(1)$, nT | 39.7 ± 19.5 | (17.2, 119.0) | 67.4 ± 16.5 | (40.1, 120.9) |
| $n(1)$, cm^{-3} | 21.2 ± 18.0 | (5.5, 95.2) | 166 ± 108 | (43.9, 537) |
| $P_{\perp\text{Tot}}(1)$, nPa | 2.15 ± 1.69 | (0.61, 9.26) | 15.8 ± 11.2 | (7.9, 59.5) |
| V_A , km/s | 210 ± 85 | (90, 395) | 130 ± 50 | (70, 250) |

addition to the large difference in $P_{\perp\text{Tot}}(1)$, $\beta(1)$ is roughly three times higher for the CCE events than for the IRM events. The difference in $\beta(1)$ is due principally to the eightfold higher density for the CCE events, which more than compensates for the higher magnetic field strength of the CCE events. Owing to the huge densities for the CCE events, $V_A(1)$ is lower for the CCE than for the IRM events.

It is also useful to estimate the solar wind conditions during the events. We can infer the upstream solar wind conditions to $\sim 20\%$ on the basis of observations in the magnetosheath proper. We estimate the field strength, B_{sw} , solar wind flow speed, V_{sw} , and proton density, n_{sw} , from parameters in region 1 as follows. Across the shock, B_{sw} and n_{sw} increase by a factor, η , which depends on the upstream Mach number and on the angle between \mathbf{B}_{sw} and the shock normal, θ_{Bn} . We then have, $B_{\text{sw}} = B(1)/\eta$ and $n_{\text{sw}} = n(1)/\eta$. The solar wind ram pressure is approximately $n_{\text{sw}} m_p V_{\text{sw}}^2$, where m_p is the proton mass, and we have ignored He^{2+} . The ram pressure is also given by $P_{\perp\text{Tot}}(1)$, so we obtain

$$V_{\text{sw}} = \sqrt{\frac{\eta P_{\perp\text{Tot}}(1)}{m_p n(1)}} \quad (10)$$

From B_{sw} , V_{sw} , and n_{sw} we then calculate E_{sw} and the Alfvén Mach number, M_{Asw} . Note that E_{sw} and M_{Asw} vary only as $\eta^{-1/2}$ so that these estimates are not very sensitive to η . Moreover, for quasi-perpendicular shocks the jump conditions are not highly sensitive to θ_{Bn} and for strong shocks $\eta \sim 4$ [Kennel et al., 1985]. Table 2 presents the statistics of the inferred solar wind parameters assuming $\eta = 4$.

The inferred solar wind parameters for IRM are very close to average solar wind conditions. The differences

in n_{sw} , B_{sw} , and V_{Asw} carry over directly from the magnetosheath values. The inferred solar wind velocities, V_{sw} , are comparable however. As a result, M_{Asw} for the CCE events is higher than for the IRM events. For both data sets, M_{Asw} is always larger than 3.6 and the average M_{Asw} is greater than 5, indicating that these events occurred for strong shocks, consistent with the assumption regarding the jump conditions, that is, $\eta = 4$.

Measure of Plasma Depletion

To measure the degree of plasma depletion for a given event, we use the ratio of plasma β values in region 1 and 2, $\beta(2)/\beta(1)$. As shown in P1 and P2, the transition from the magnetosheath proper to the PDL corresponds to the simultaneous variation of a number of parameters: the density decreases, the average magnetic field strength increases, and the ion temperature decreases. These changes all contribute to a decrease in the plasma β , so we adopt this parameter as a measure of the degree of plasma depletion. To remove variations in $\beta(1)$ from event to event, we restrict attention to the ratio $\beta(2)/\beta(1)$. When $\beta(2)/\beta(1) \sim 1$, little plasma depletion in region 2 is indicated, whereas $\beta(2)/\beta(1) \ll 1$ indicates significant depletion in region 2.

Since the CCE events do not correspond to traversal of a stationary structure, $\beta(1)$ and $\beta(2)$ for the CCE events are not directly comparable in the sense that they necessarily correspond to somewhat different upstream conditions. Specifically, we know that $P_{\perp\text{Tot}}(2) < P_{\perp\text{Tot}}(1)$. Hence for the CCE events we estimate $\beta(2)$ corresponding to conditions near the magnetopause when CCE was in region 1, denoted as $\beta(2)'$. Because the measured $\beta(2)$ is probably lower than $\beta(2)'$, the measured $\beta(2)$ gives a lower limit value for $\beta(2)'$. An upper limit for $\beta(2)'$ is obtained by assuming

Table 2. Inferred Solar Wind Parameters for IRM and CCE Events Evaluated Assuming a Factor of 4 Increase in Density and Magnetic Field Magnitude Across the Shock

| | IRM | | CCE | |
|------------------------------------|----------------------------------|------------|----------------------------------|-------------|
| | Average \pm Standard Deviation | (min, max) | Average \pm Standard Deviation | (min, max) |
| B_{sw} , nT | 9.9 ± 4.9 | (4.3, 30) | 16.9 ± 4.1 | (10, 30) |
| n_{sw} , cm^{-3} | 5.3 ± 4.3 | (1.4, 24) | 42 ± 27 | (11, 135) |
| V_{sw} , km/s | 520 ± 140 | (290, 780) | 490 ± 95 | (380, 720) |
| V_{Asw} , km/s | 100 ± 40 | (45, 200) | 65 ± 25 | (35, 125) |
| M_{Asw} | 5.3 ± 1.0 | (3.6, 7.1) | 8.3 ± 1.9 | (5.6, 11.5) |

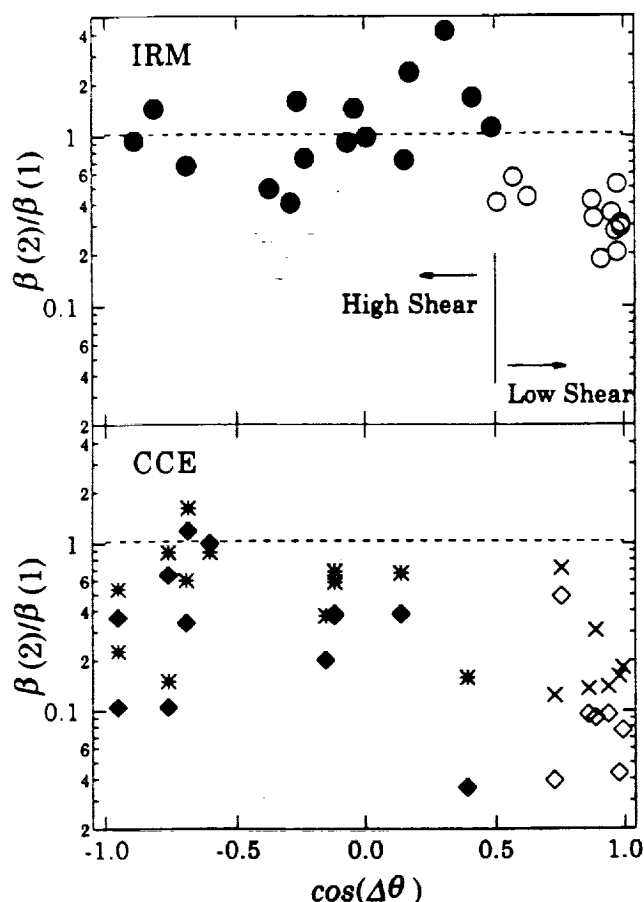


Figure 2. Plot of $\beta(2)/\beta(1)$ versus the cosine of the magnetic shear angle for IRM and CCE. For IRM $\beta(2)/\beta(1)$ are indicated with circles, open for low shear, filled for high shear. For CCE, diamonds indicate $\beta(2)/\beta(1)$, open for low shear, filled for high shear and $\beta(2)*\beta(1)$ are shown with crosses for low shear and asterisks for high shear. See text for definitions of $\beta(1)$, $\beta(2)$, and $\beta(2)*$. Plasma depletion is indicated by $\beta(2)/\beta(1) < 1$. For both IRM and CCE, plasma depletion becomes more prominent as the magnetic shear decreases.

that the change in $P_{\perp \text{Tot}}$, $\Delta P_{\perp \text{Tot}} = P_{\perp \text{Tot}}(1) - P_{\perp \text{Tot}}(2)$, required to move CCE from region 2 to region 1, all goes into particle pressure in region 2. That is, $\beta(2)' \leq (P_{\text{part}}(2) + \Delta P_{\perp \text{Tot}})/P_B(2) = \beta(2)*$.

In the plots of $\beta(2)/\beta(1)$ given below we indicate IRM data with circles, open for low shear, filled for high shear. For CCE we indicate $\beta(2)/\beta(1)$ by diamonds, open for low shear, filled for high shear; and $\beta(2)*\beta(1)$ by crosses for low shear and asterisks for high shear. Note that high and low shear correspond to $\cos(\Delta\theta) < 0.5$ and $\cos(\Delta\theta) > 0.5$, respectively. When referring to $\beta(2)/\beta(1)$ for CCE, we implicitly also refer to $\beta(2)*\beta(1)$ unless otherwise stated.

Plasma Depletion, Shear, Field Strength, and Pressure

Figure 2 shows $\beta(2)/\beta(1)$ plotted versus $\cos(\Delta\theta)$ separately for CCE and IRM. Table 3 gives the average values of $\beta(2)/\beta(1)$ for high and low shear as well as the ratio of the high and low shear averages. Both IRM and CCE observe increased plasma depletion with decreasing shear.

Table 3. Average $\beta(2)/\beta(1)$ for IRM and CCE Events Together With the Ratio for High to Low Magnetic Shear

| | Average $\beta(2)/\beta(1)$ | | |
|-----|-----------------------------|------------|----------|
| | Low Shear | High Shear | High/Low |
| CCE | 0.13 | 0.42 | 3.3 |
| IRM | 0.35 | 1.34 | 3.8 |

This confirms the expectation from the model that shear should have a prominent influence on plasma depletion. However, for a given shear, the plasma depletion is greater for CCE than for IRM. At high shear, most of the CCE events display $\beta(2)/\beta(1) < 0.4$ whereas all of the high shear IRM events have $\beta(2)/\beta(1) > 0.4$. For low shear, plasma depletion for CCE is greater than for IRM and almost all CCE events have $\beta(2)/\beta(1) < 0.1$, whereas the IRM low shear events have $\beta(2)/\beta(1) > 0.15$. These trends are reflected in the average $\beta(2)/\beta(1)$ values. The variations of $\beta(2)/\beta(1)$ with shear for the CCE and IRM data sets are essentially the same, possibly indicating that the shear dependence of plasma depletion is due to the same mechanism but that the different conditions caused uniformly greater plasma depletion for the CCE cases.

The model predicts that plasma depletion occurs even for high shear if either the pressure is high or the reconnection efficiency is low. Even under these conditions, however, increasing $B(1)$ should reduce D , reduce plasma depletion, and hence give increased $\beta(2)/\beta(1)$. To test for this effect we plot $\beta(2)/\beta(1)$ versus $B(1)$ in Figure 3 for the high shear CCE events. We see that $\beta(2)/\beta(1)$ increases as $B(1)$ increases, indicating reduced plasma depletion as predicted by the model.

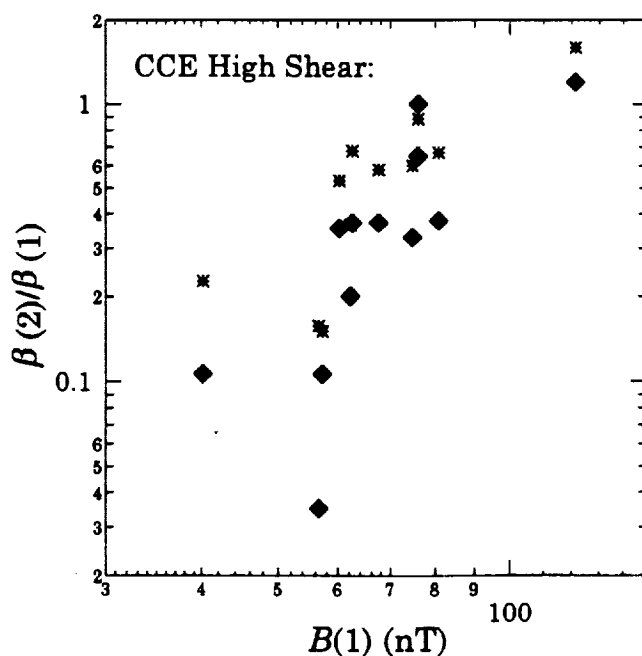


Figure 3. Plot of $\beta(2)/\beta(1)$ versus $B(1)$ for the CCE high shear, $\cos(\Delta\theta) < 0.5$, events showing that plasma depletion is diminished and $\beta(2)/\beta(1)$ increases as the magnetic field strength in the magnetosheath proper, $B(1)$, increases.

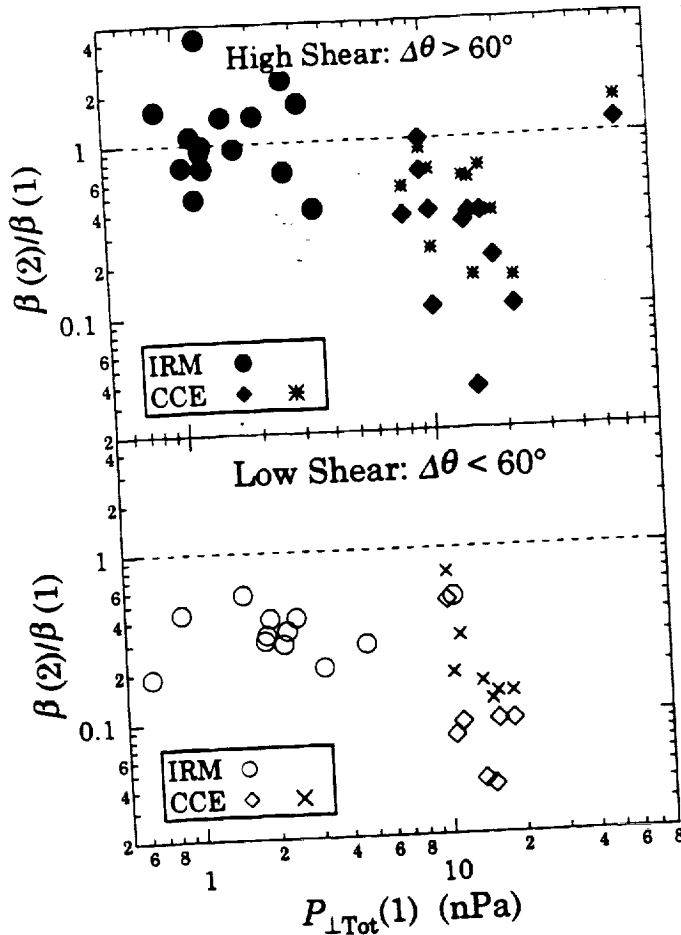


Figure 4. Plot of $\beta(2)/\beta(1)$ versus $P_{\perp Tot}(1)$ for high ($\cos(\Delta\theta) < 0.5$) and low ($\cos(\Delta\theta) > 0.5$) magnetic shear conditions. For both high and low magnetic shear, plasma depletion becomes stronger as the dynamic pressure increases.

Figure 4 shows $\beta(2)/\beta(1)$ plotted versus $P_{\perp Tot}(1)$ separately for high and low magnetic shear. For both high and low shear it is clear that plasma depletion becomes more severe as the applied pressure increases. For low shear the plasma depletion, which is clearly apparent for pressures of ~ 2 nPa, becomes even stronger as the pressure increases so that $\beta(2)/\beta(1)$ decreases by about a factor of five as $P_{\perp Tot}(1)$ increases from 2 nPa to 10 nPa. A similar behavior occurs for high shear. Below about 3 to 4 nPa, no plasma depletion is evident, but $\beta(2)/\beta(1)$ decreases by about a factor of 2 to 3 for pressures of 10 nPa. This shows that for a given magnetic shear the plasma depletion becomes stronger as the pressure increases, also in agreement with the model. Note, however, that Figure 4 reflects the combined effects of $P_{\perp Tot}$ and β , through k , and because $P_{\perp Tot}$ is positively correlated with β , the effect of pressure on plasma depletion is exaggerated in this plot.

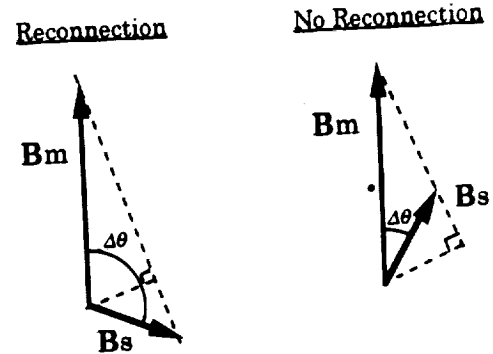
Reconnection Magnetic Field

In order to test whether the difference in $P_{\perp Tot}$ between the CCE and IRM events accounts for the difference in plasma depletion, we need to characterize the shear function, $S(\Delta\theta)$, that appears in (8). This can be done us-

ing (5) given $\Delta\theta$ and the field strengths in the magnetosheath just outside the magnetopause, B_s^* , and in the magnetosphere, B_m . For IRM we determined B_m by averaging the field strength over the +1 to +2 min time interval corresponding to periods inside the magnetopause and just inside the LLBL. We cannot measure B_m for the CCE events because not every event is associated with a magnetopause crossing. Moreover, for the CCE events, magnetopause crossings do not correspond to the same upstream conditions as when CCE observed the magnetosheath proper. Therefore we must use only the IRM data to estimate $S(\Delta\theta)$.

The fact that the magnetic field enhancement in the PDL becomes stronger as the magnetosheath field turns northward implies that component merging may be allowed for nearly all orientations of the magnetosheath field. Figure 5 illustrates this effect. As sketched in Figure 5a, component merging can occur only when there exists a coordinate system in which the field in the magnetosheath, B_s , and in the magnetosphere, B_m , have antiparallel components. This requirement gives the condition $B_s^*/B_m > \cos(\Delta\theta)$ for which reconnection may occur [Sonnerup, 1974]. If B_s^* is independent of $\Delta\theta$, then as the

(a) No PDL: $B_s/B_m = \text{const}$



(b) With PDL: B_s/B_m increases as $\Delta\theta$ decreases

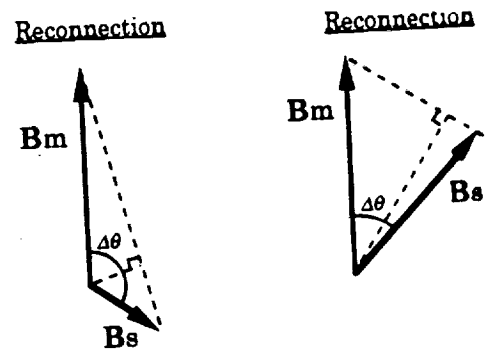


Figure 5. Sketch of relative geometry of magnetospheric magnetic field, vertical arrows, and the magnetosheath magnetic field illustrating the Sonnerup [1974] conditions for reconnection; (a) the turn off of reconnection with shear for magnetosheath field strength independent of $\Delta\theta$ and (b) allowed reconnection for all shear angles if the effects of plasma depletion are included.

shear decreases a point is reached where $B_s^*/B_m = \cos(\Delta\theta)$ and for smaller $\Delta\theta$ there exists no coordinate system in which the fields have antiparallel components and component merging cannot occur (Figure 5a). Because of the PDL, however, B_s^* is not independent of $\Delta\theta$ but increases as the sheath field turns northward. Figure 5b indicates how this affects the merging condition. As $\Delta\theta$ decreases, B_s^* increases, and even as $\Delta\theta$ approaches zero, $B_s^*/B_m > \cos(\Delta\theta)$ may still be satisfied if $B_s^*/B_m \sim 1$. In fact, B_s^*/B_m does approach 1 when $\Delta\theta$ is small [P1; P2; Phan et al., 1996b], implying that the component merging condition can be satisfied in the subsolar region for nearly all shear angles. The quantity of magnetic flux that participates in low shear subsolar reconnection will of course be considerably less than that for high shear. Nonetheless, we expect that plasma depletion facilitates reconnection near the subsolar region for low shear and hence subsolar reconnection should not be regarded as restricted to high shear conditions.

To test this observationally, we calculate B_r using $B(1)$ and B_m and calculate B_r^* using $B(2)$ and B_m . That is,

$$B_r = B(1) \frac{a - \cos(\Delta\theta)}{\sqrt{1 + a^2 - 2a\cos(\Delta\theta)}}, \quad a = \frac{B(1)}{B_m} \quad (11a)$$

$$B_r^* = B(2) \frac{a - \cos(\Delta\theta)}{\sqrt{1 + a^2 - 2a\cos(\Delta\theta)}}, \quad a = \frac{B(2)}{B_m} \quad (11b)$$

Figure 6 shows the ratios $B_r/B(1)$ and $B_r^*/B(1)$ versus $\Delta\theta$. The curves are B_r/B_s calculated from (5) assuming that $B_m/B_s = 1, 2$, and 10. The top panel shows the $S(\Delta\theta)$ one might infer by excluding the effects of plasma depletion. The data closely follow the $B_m/B_s = 2$ curve, and the low shear events have $B_r < 0$. The bottom panel shows the $S(\Delta\theta)$ that is actually observed, since by using $B(2)$ and B_m we have included the field increase in the PDL. In contrast to the top panel, most of the low shear events have $B_r^* > 0$, indicating that component merging does indeed remain allowed for low shear. Thus the observations indicate that we should use an $S(\Delta\theta)$ which does not become negative for $\cos(\Delta\theta) > 0.5$. We therefore adopt the simplest form which gives $B_r = 0$ for $\Delta\theta = 0$: $S(\Delta\theta) = \Delta\theta/\pi$. This relation is used below to remove the general dependence of $\beta(2)/\beta(1)$ on magnetic shear.

This result, that B_r is positive even for low shear with B_r monotonically decreasing as the shear gets smaller, has significant implications for solar wind-magnetosphere interactions when the IMF is northward. The IMF influence on the magnetosphere is often regarded as a half-wave rectifier in the sense that the interaction shuts off when the IMF turns northward [e.g., Crooker et al., 1980]. Our result implies that although the strongest interaction occurs for southward IMF, it is not correct to assume that the interaction disappears for northward IMF. Specifically, it means that some subsolar merging may occur for northward IMF, as in fact reported by Paschmann et al. [1990], and drive convection in the same sense as the dominant pattern when the IMF is southward. Conventionally, this residual convection for $B_z > 0$ has been attributed to a viscous interaction [e.g., Reiff, 1984], but our result suggests that the residual convection may be due to the relatively small degree of subsolar reconnection persisting for $B_z > 0$.

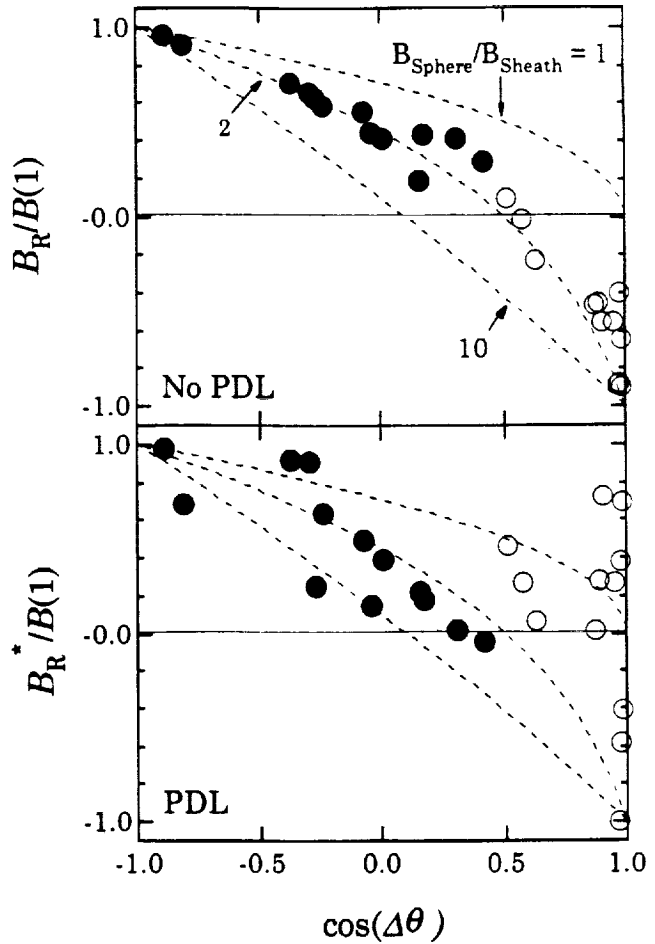


Figure 6. Plot of the magnetosheath field component available for component reconnection, B_r , calculated in two ways and divided by the upstream magnetosheath field, $B(1)$, versus magnetic shear. Upper panel shows B_r calculated using the magnetic field in the magnetosheath proper. Bottom panel shows B_r^* calculated using the magnetosheath field adjacent to the magnetopause.

Reconnection Efficiency

To examine the data for possible dependence on reconnection efficiency, we use (8) to calculate D/k , using $S(\Delta\theta) = \Delta\theta/\pi$, removing the general effects of magnetic shear, field strength, and dynamic pressure and leaving only effects due to changes in k . If k is constant, the same value of D/k for the CCE and IRM cases should give the same value of $\beta(2)/\beta(1)$. Figure 7 shows $\beta(2)/\beta(1)$ plotted versus D/k . Although $\beta(2)/\beta(1)$ generally increases with increasing D/k as we expect, the CCE data are displaced to lower $\beta(2)/\beta(1)$ relative to the IRM data for the same value of D/k . Linear regression of $\log(\beta(2)/\beta(1))$ with $\log(D/k)$ gives $\beta(2)/\beta(1) = g(D/k)^h$, with $g = 1.05$, $h = 0.35$, and a regression coefficient, $r = 0.70$, for IRM and $g = 0.35$, $h = 0.43$, and $r = 0.66$ for CCE. This result implies either that the MHD flow is significantly different for the CCE events or that the reconnection efficiency is lower for the CCE events.

It is unlikely that there is a large difference in the character of the magnetosheath flow around the magnetosphere between the CCE and IRM events. This is because the di-

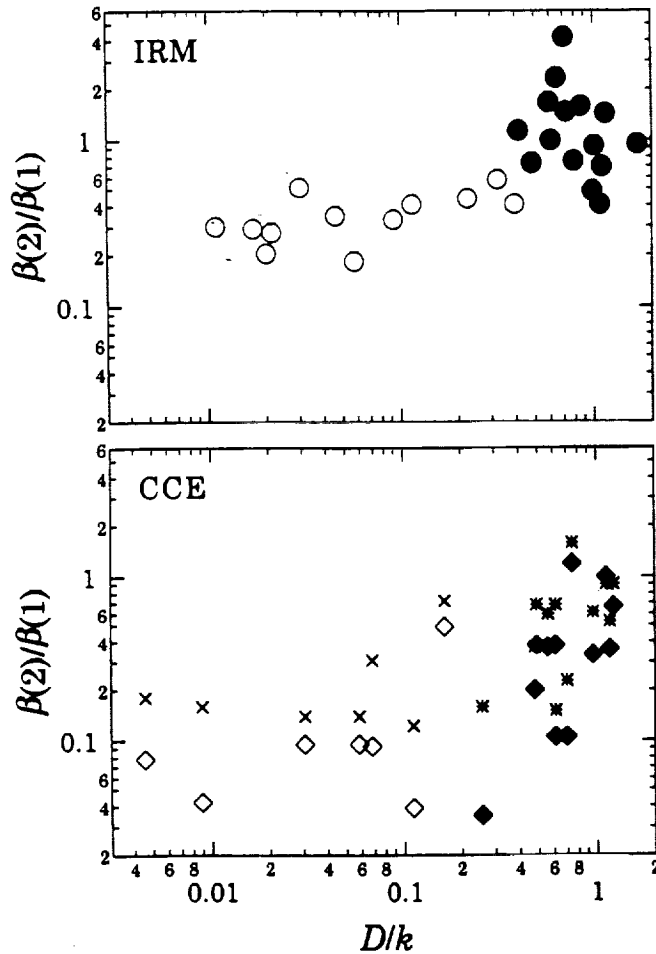


Figure 7. Plot of $\beta(2)/\beta(1)$ plotted versus D/k , where D is the ratio of reconnection to solar wind electric field, that is, $D = E/E_{sw}$, and k is the reconnection efficiency. The IRM and CCE events span the same range of D/k while the CCE values for $\beta(2)/\beta(1)$ are systematically a factor of 3 lower than $\beta(2)/\beta(1)$ for the same D/k .

mensions of the system scale as $P_{ram}^{1/6}$ and the magnetopause and bow shock remain self-similar for different dynamic pressures [Roelof and Sibeck, 1993; Peredo et al., 1995]. The thickness of the magnetosheath relative to the magnetopause standoff distance does not change with P_{ram} and is only weakly dependent on the solar wind Mach number. For a change in M_{Asw} from 2 to 8, the relative thickness of the subsolar magnetosheath changes by +5%; that is, the subsolar magnetosheath relative thickness increases slightly [Peredo et al., 1995]. Thus the magnetosheath cross-sectional area relative to the obstacle size should be larger for the CCE than for the IRM events, so changes in MHD flow should make the PDL more prominent for the IRM events, opposite to what we observe. Hence geometry effects do not explain the observed $\beta(2)/\beta(1)$ difference between IRM and CCE. The results therefore imply $k_{CCE} < k_{IRM}$; the reconnection efficiency must be lower for the CCE events.

5. Discussion

The comparison of IRM and CCE data sets shows that the apparent discrepancy between them, the absence (pres-

ence) of a depletion layer for high shear in the IRM (CCE) data, can be understood as reflecting the difference in balance between the imposed solar wind electric field and the subsolar reconnection electric field. Both data sets display an increase in plasma depletion with decreasing magnetic shear consistent with our model, which predicts the same shear dependence for fixed values of other parameters. The diminution of plasma depletion with increasing sheath field strength for the high shear CCE events is also predicted by our model and results from an increase in the magnetosheath Alfvén velocity and hence in the reconnection rate. The difference in pressure between IRM and CCE events is not sufficient to account for the different in PDL prevalence, however, and indicates that the reconnection efficiency is lower for the CCE than for the IRM events.

To estimate the difference between k_{CCE} and k_{IRM} , we consider how much the CCE data must be moved to the left in Figure 7 so that it makes a good overlap with the IRM data. The regression coefficient between $\log(\beta(2)/\beta(1))$ and $\log(D/k)$ for the combined data set is 0.57. If we allow $k(\beta)$ to have the form $k(\beta) = k_0/(1 + \beta/\beta_c)$ where k_0 and β_c are constants, we can get a rough estimate for β_c by applying the factor $1/(1 + \beta/\beta_c)$ and adjusting β_c to obtain a maximum regression coefficient in the combined data. This form is arbitrary and was chosen simply because it is the simplest form that gives $k \rightarrow 0$ for large β and has no effect on k for small β . Using $\beta_c = 10, 2.0$, and 0.2 gives $r = 0.66, 0.74$, and 0.78 , respectively. Values of $\beta_c < 0.2$ do not change the regression coefficient, probably indicating that the reconnection efficiency first begins to decrease for β smaller than the β values sampled by IRM. Figure 8 shows $\beta(2)/\beta(1)$ plotted versus $(D/k)/(1 + \beta(1)/0.2)$, showing that by allowing for some

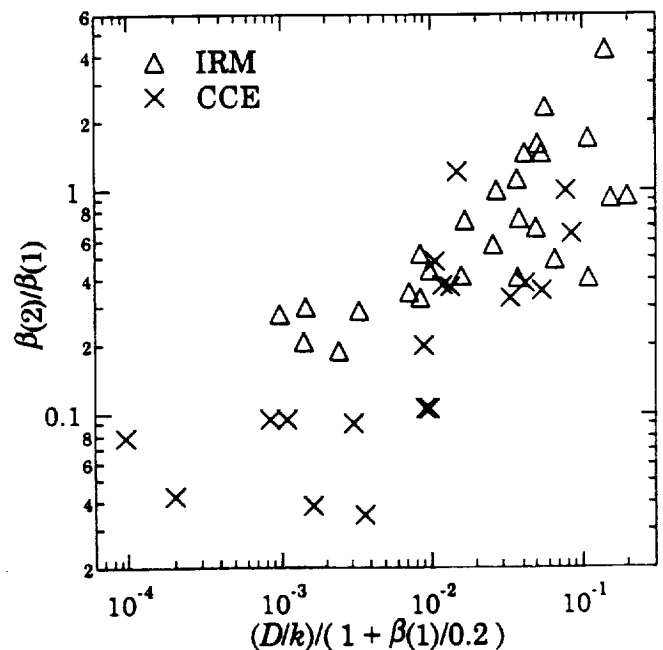


Figure 8. Plot of $\beta(2)/\beta(1)$ versus $D/k/(1 + \beta(1)/0.2)$ showing that the difference in plasma depletion between CCE and IRM can be reconciled if the reconnection efficiency, k , is approximately inversely proportional to β .

decrease in k with β , one can bring the CCE and IRM data to follow similar trends in $\beta(2)/\beta(1)$. Assuming then that k first begins to decrease for $\beta \sim 1$, and given that $k \sim 1/\beta$ brings the CCE and IRM $\beta(2)/\beta(1)$ variations approximately into agreement, we infer that the ratio of the average reconnection efficiencies for CCE and IRM is roughly given by $k_{\text{CCE}}/k_{\text{IRM}} \sim \beta(1)_{\text{IRM}}/\beta(1)_{\text{CCE}} = 2.5/8 = 0.3$.

Previous reports have also found evidence linking increasing β to decreased reconnection efficiency. *Paschmann et al.* [1986] found that the occurrence of reconnection flows is anticorrelated with magnetosheath β and that the magnitude of the reconnection flows decreased as β increased. Using geomagnetic activity as a proxy for reconnection, *Scurry et al.* [1994] inferred that the reconnection efficiency was lower when β was high in the magnetosheath. *Phan et al.* [1996a] also found that reconnection signatures are less prevalent when the magnetosheath β is high, although they point out that direct observation of reconnection flows is more problematical under high β conditions. In the present study we have used the degree of plasma depletion as an indicator of the magnetopause flow boundary condition. This technique therefore provides independent confirmation that the reconnection efficiency decreases with increasing magnetosheath β . Moreover, we have found that the efficiency decreases roughly inversely proportionally to β and that the decrease probably begins for $\beta \sim 1$.

The results imply that reconnection and plasma depletion are closely coupled dynamically. Specifically, when the upstream conditions are unfavorable for reconnection, plasma depletion proceeds and changes conditions near the magnetopause to facilitate some subsolar reconnection. Plasma depletion changes three factors affecting reconnection, and all of them change so as to increase the subsolar reconnection rate. First, the increased magnetic field strength in the PDL implies that the component of magnetosheath field available for reconnection increases. Very significantly, this effect implies that reconnection may remain possible even for very low magnetic shear (see Figure 5). Second, the increased magnetic field and decreased density in the PDL facilitate reconnection by increasing the Alfvén velocity near the magnetopause. Third, the decreased β in the PDL implies that the reconnection efficiency with the plasma in the PDL is higher than it would be with the plasma in the magnetosheath proper. We therefore suggest that the PDL may play an important role in changing the conditions near the subsolar magnetopause to promote subsolar reconnection.

It is clear, however, that the effect of PDL formation is not so great that reconnection flows fully take up the imposed solar wind flow. For high shear and moderate β conditions the subsolar reconnection flows apparently do keep up with the imposed solar wind flow. The simple fact that the PDL forms under low shear and/or high β conditions shows that the reconnection flow does not keep up with the solar wind flow, despite the effect of the PDL to enhance subsolar reconnection. It is clear from Figure 5 that the reconnection rate for high shear will always exceed that for low shear even when the PDL does form. Thus, in our model, PDL formation occurs in response to reductions in the subsolar reconnection rate relative to the solar wind electric field, and the effect of PDL formation on reconnection is to allow somewhat more subsolar

reconnection for moderate shear than would otherwise occur and most importantly allow some subsolar reconnection for low shear when it is impossible otherwise.

It is conventionally assumed that subsolar reconnection does not occur for northward IMF [*Sonnerup*, 1984; *Reiff*, 1984], and this is motivated by the half-wave rectifier analogy for subsolar reconnection which results from the antiparallel merging hypothesis [*Crooker*, 1980]. Under this assumption polar cap convection, which displays a so-called four-cell pattern, two poleward cells giving sunward convection at the center of the polar cap and two equatorward cells giving sunward convection at the equatorward edge of the auroral zone, is understood in terms of the combined effects of cusp reconnection and a viscous interaction [*Maezawa*, 1976; *Reiff*, 1984]. Cusp reconnection is thought to drive the poleward cells, while the viscous interaction drives the equatorward cells [*Burke et al.*, 1979; *Burch et al.*, 1980]. However, owing to the effects of plasma depletion, we expect that subsolar merging does indeed occur for northward IMF, and hence the assumption underlying the conventional understanding of convection for northward IMF may be inaccurate. The low shear magnetopause displays convection and electric field structures consistent with a rotational discontinuity [*Paschmann et al.*, 1990], the subsolar magnetopause appears to generally exhibit a reconnection topology even for northward IMF [*Fuselier et al.*, 1995], and observations of ion velocity dispersion in the subsolar region do indeed indicate that reconnection occurs equatorward of the cusp for northward IMF [*Onsager and Fuselier*, 1994; *Fuselier et al.*, 1997]. Since the equatorward convection cells are in the same sense as convection driven by subsolar reconnection, these cells could be driven by the residual subsolar reconnection facilitated by the PDL. We therefore propose that the four-cell convection pattern observed for northward IMF can be understood as resulting from the combined effects of cusp reconnection and simultaneous weak subsolar reconnection without recourse to a viscous interaction.

That a PDL forms even for high shear indicates that the reconnection electric field fails to keep up with the imposed solar wind flow under high β conditions. We interpret this saturation in terms of a reconnection efficiency which falls off approximately like $1/\beta$ for β larger than about 1. This may account for the observed saturation of the polar cap potential that occurs during periods of high geomagnetic activity [*Wygant et al.*, 1983]. *Reiff et al.* [1981] also noted that the polar cap potential reached a maximum value during active times, and inferred that to achieve the observed convection, the subsolar magnetic field had to be enhanced over its nominal magnetosheath value; that is, a PDL must have formed. As discussed above, PDL formation is intimately related to a reduction of the reconnection rate relative to the solar wind electric field. We find that the reconnection efficiency is reduced under high β , high shear conditions and that this results in PDL formation. The conclusions of *Reiff et al.* and *Wygant et al.* therefore reflect the same underlying phenomenon and are mutually consistent.

It is significant that high β rather than high solar wind ram pressure may be principally responsible for causing PDL formation for the high shear CCE events. The magnetosheath β is $2\mu_0 n_{\text{sh}} k T_{\text{sh}} / B_{\text{sh}}^2$, and for quasi-perpendicular shocks in the strong shock limit, T_{sh} is given by

$$T_{sh} = \frac{2(\gamma - 1)}{(\gamma + 1)^2} m V_{sw}^2 \quad (12)$$

where γ is the ratio of specific heats. Using this together with the compression relations for B_{sh} and n_{sh} we have

$$\beta_{sh} = \frac{4(\gamma - 1)}{\eta(\gamma + 1)^2} \frac{\mu_0 m n_{sw} V_{sw}^2}{B_{sw}^2} \quad (13)$$

Using $\gamma = 5/3$ and $\eta = (\gamma + 1)/(\gamma - 1) = 4$ and recognizing that the second quotient is the square of the solar wind Alfvén speed, we have

$$\beta_{sh} = \frac{3}{32} M_{Asw}^2 \quad (14)$$

Since $M_{Asw}^2 \propto n_{sw} V_{sw}^2 / B_{sw}^2$, it is clear that it is not the solar wind ram pressure alone which principally determines the downstream β . We expect that M_{Asw} rather than ram pressure should be correlated best with low reconnection efficiency and PDL formation. One could then very well have high solar wind ram pressure conditions without a significant plasma depletion layer if the solar wind magnetic field is also enhanced.

6. Conclusions

In this paper we examined the physical mechanisms leading to the different prevalence of plasma depletion in CCE and IRM observations. The ratio of the reconnection electric field to the solar wind electric field, $D = E_r/E_{sw}$, measures the relative rate of magnetic flux transfer by reconnection to the solar wind inflow. Since plasma depletion corresponds to a reconnection flow lower than that required to take up the imposed solar wind flow, this ratio serves as a useful indicator of plasma depletion: $D = 0$ indicates plasma depletion whereas $D \sim 1$ corresponds to no plasma depletion. By expressing D in terms of solar wind or magnetosheath parameters, one can identify the physical variables that influence the occurrence of plasma depletion (see (7) and (8)). Plasma depletion is most sensitive to the magnetic shear at the magnetopause and is most likely for low shear. The model also predicts that plasma depletion decreases as the magnetosheath or solar wind magnetic field strength increases. Increased solar wind dynamic pressure should correspond to increased depletion as well. The reconnection efficiency also has a strong effect on plasma depletion such that plasma depletion should be more prevalent for high magnetosheath β .

The predictions of this model were tested by combining the databases of magnetosheath observations from the CCE and IRM spacecraft. All of the model predictions were borne out observationally, indicating that this simple description captures the essential factors influencing PDL formation. We find that the reconnection efficiency must have been about a factor of three lower for the CCE events than for the IRM events, most probably owing to the threefold higher β for the CCE events. We therefore infer that the reconnection efficiency is roughly inversely proportional to β for β greater than about 1. This conclusion is based on changes in the magnetosheath flow boundary condition as evidenced in the prevalence of plasma depletion. The result provides independent confirmation of the inverse relationship between reconnection ef-

iciency and magnetosheath β predicted by Sonnerup [1974], found in direct observations of accelerated flow at the magnetopause [Paschmann et al., 1986; Phan et al., 1996a], and inferred by variations in geomagnetic activity with upstream conditions [Scurry et al., 1994].

The decrease in reconnection efficiency with β implies that magnetosheath β larger than about 5 or so should correlate with the occurrence of plasma depletion for southward IMF. We therefore expect plasma depletion for high magnetic shear to occur primarily during high solar wind density conditions because although high solar wind velocities produce large increases in solar wind pressure, they do not produce magnetosheath β as high as those observed during high solar wind density conditions.

Because plasma depletion becomes more pronounced for low shear, the magnetosheath magnetic field imposed on the magnetopause is not independent of the shear angle, but increases as the sheath field turns northward. This implies that component merging should remain allowed in the subsolar region for all IMF orientations except purely northward. Plasma depletion also promotes reconnection by increasing the subsolar magnetosheath Alfvén speed and decreasing the subsolar magnetosheath β , thus increasing the reconnection efficiency. The effects of plasma depletion therefore facilitate some subsolar reconnection for northward IMF.

It is conventionally assumed that subsolar reconnection does not occur for northward IMF, and under this assumption four-cell polar cap convection, which occurs for IMF $B_z > 0$, is understood in terms of the combined effects of cusp reconnection and a viscous interaction. Our results suggest that the effects of plasma depletion promote some residual subsolar reconnection even for northward IMF. We therefore suggest that four-cell polar cap convection can be understood as resulting from the combined effects of cusp reconnection and simultaneous weak subsolar reconnection without recourse to a viscous interaction.

Acknowledgments. We thank G. Paschmann for making the data and calibrations for the IRM plasma experiment available to us. Work at the Johns Hopkins University Applied Physics Laboratory was supported by NSF and ONR. Work at the University of California at Berkeley was supported by NASA through grant NAG5-2815. Work at Lockheed Palo Alto Research Laboratory was supported by NASA under grant NAGW-4049.

The Editor thanks T. G. Onsager and another referee for their assistance in evaluating this paper.

References

- Acuña, M. H., G. W. Ousley, R. W. McEntire, D. Bryant, and G. Paschmann, Editorial: AMPTE-Mission Overview, *IEEE Trans. Geosci. Remote Sens.*, 23, 175, 1985.
- Anderson, B. J., and S. A. Fuselier, Magnetic pulsations from 0.1 to 4.0 Hz and associated plasma properties in the Earth's subsolar magnetosheath and plasma depletion layer, *J. Geophys. Res.*, 98, 1461, 1993.
- Anderson, B. J., S. A. Fuselier, S. P. Gary, and R. E. Denton, Magnetic spectral signatures from 0.1 to 4.0 Hz in the Earth's magnetosheath and plasma depletion layer, *J. Geophys. Res.*, 99, 5877, 1994.
- Burch, J. L., P. H. Reiff, R. A. Heelis, R. W. Spiro, and S. A. Fields, Cusp region particle precipitation and ion con-

- section for northward interplanetary magnetic field, *Geophys. Res. Lett.*, **7**, 393–396, 1980.
- Burke, W. J., M. C. Kelley, R. C. Sagalyn, M. Smiddy, and S. T. Lai, Polar cap electric field structures with a northward interplanetary magnetic field, *Geophys. Res. Lett.*, **6**, 21–24, 1979.
- Crooker, N. U., The half-wave rectifier response of the magnetosphere and anti-parallel merging, *J. Geophys. Res.*, **85**, 575–578, 1980.
- Denton, R. E., S. P. Gary, B. J. Anderson, S. A. Fuselier, and M. K. Hudson, Low-frequency magnetic fluctuation spectra in the magnetosheath and plasma depletion layer, *J. Geophys. Res.*, **99**, 5893, 1994.
- Fuselier, S. A., B. J. Anderson, and T. G. Onsager, Particle signatures of magnetic topology at the magnetopause: AMPTE/CCE observations, *J. Geophys. Res.*, **100**, 11,805, 1995.
- Fuselier, S. A., B. J. Anderson, and T. G. Onsager, Electron and ion signatures of field line topology at the low shear magnetopause, *J. Geophys. Res.*, in press, 1997.
- Gary, S. P., M. E. McKean, D. Winske, B. J. Anderson, R. E. Denton, S. A. Fuselier, Proton cyclotron anisotropy instability and the anisotropy/beta inverse correlation, *J. Geophys. Res.*, **99**, 5903, 1994.
- Kennel, C. F., J. P. Edmiston, and T. Hada, A quarter century of collisionless shock research, in *Collisionless Shocks in the Heliosphere: A Tutorial Review*, *Geophys. Monogr. Ser.*, vol. 34, edited by R. G. Stone and B. T. Tsurutani, pp. 1–36, AGU, Washington, D. C., 1985.
- Lees, L., Interaction between the solar plasma wind and the geomagnetic cavity, *AIAA J.*, **2**, 2065, 1964.
- Lin, N., M. J. Engebretson, R. L. McPherron, M. G. Kivelson, W. Baumjohann, H. Lühr, T. A. Potemra, B. J. Anderson, and L. J. Zanetti, A comparison of ULF fluctuations in the solar wind, magnetosheath, and dayside magnetosphere, 2, Field and plasma conditions in the magnetosheath, *J. Geophys. Res.*, **96**, 3455, 1991.
- Luhmann, J. G., C. T. Russell, and R. C. Elphic, Spatial distributions of magnetic field fluctuations in the dayside magnetosheath, *J. Geophys. Res.*, **91**, 1711, 1986.
- Maezawa, K., Magnetic convection induced by the positive and negative z-components of the interplanetary magnetic field: Quantitative analysis using polar cap magnetic records, *J. Geophys. Res.*, **81**, 2289, 1976.
- Midgley, J. E., and L. Davis, Calculation by a moment technique of the perturbation of the geomagnetic field by the solar wind, *J. Geophys. Res.*, **68**, 5111, 1963.
- Onsager, T. G., and S. A. Fuselier, The location of magnetic reconnection for northward and southward interplanetary magnetic field, in *Solar System Plasma Physics: Resolution of Processes in Space and Time*, *Geophys. Monogr. Ser.*, edited by J. L. Burch and J. H. Waite Jr., p. 183, AGU, Washington D. C., 1994.
- Paschmann, G., I. Papamastorakis, W. Baumjohann, N. Sckopke, C. W. Carlson, B. U. O. Sonnerup, and H. Lühr, The magnetopause for large magnetic shear: AMPTE/IRM observations, *J. Geophys. Res.*, **91**, 11,099–11,115, 1986.
- Paschmann, G., B. U. O. Sonnerup, I. Papamastorakis, W. Baumjohann, N. Sckopke, and H. Lühr, The magnetopause and boundary layer for small magnetic shear: Convection electric fields and reconnection, *Geophys. Res. Lett.*, **17**, 1829–1832, 1990.
- Peredo, M., J. A. Slavin, E. Mazur, and S. A. Curtis, Three-dimensional position and shape of the bow shock and their variation with Alfvénic, sonic and magnetosonic Mach numbers and interplanetary magnetic field orientation, *J. Geophys. Res.*, **100**, 7907–7916, 1995.
- Phan, T.-D., G. Paschmann, W. Baumjohann, N. Sckopke, and H. Lühr, The magnetosheath region adjacent to the dayside magnetopause: AMPTE/IRM observations, *J. Geophys. Res.*, **99**, 121, 1994.
- Phan, T.-D., G. Paschmann, and B. U. O. Sonnerup, Low-latitude dayside magnetopause and boundary layer for high magnetic shear, 2, Occurrence of magnetic reconnection, *J. Geophys. Res.*, **101**, 7817–7828, 1996a.
- Phan, T.-D., et al., The subsolar magnetosheath and magnetopause for high solar wind ram pressure: WIND observations, *Geophys. Res. Lett.*, **23**, 1279–1282, 1996b.
- Reiff, P. H., R. W. Spiro, and T. W. Hill, Dependence of polar cap potential drop on interplanetary parameters, *J. Geophys. Res.*, **86**, 7639, 1981.
- Reiff, P. H., Evidence of magnetic merging from low-altitude spacecraft and ground-based experiments, in *Magnetic Reconnection in Space and Laboratory Plasmas*, *Geophys. Monogr. Ser.*, vol. 30, edited by E. W. Hones, pp. 105–113, AGU, Washington, D. C., 1984.
- Roelof, E. C., and D. G. Sibeck, Magnetopause shape as a bivariate function of interplanetary magnetic field B_z and solar wind dynamic pressure, *J. Geophys. Res.*, **98**, 21,421, 1993.
- Scurry, L., C. T. Russell, and J. T. Gosling, Geomagnetic activity and the beta dependence of the dayside reconnection rate, *J. Geophys. Res.*, **99**, 14,811, 1994.
- Sonnerup, B. U. O., Magnetopause reconnection rate, *J. Geophys. Res.*, **79**, 1546, 1974.
- Sonnerup, B. U. O., Magnetic field reconnection at the magnetopause: an overview, in *Magnetic Reconnection in Space and Laboratory Plasmas*, *Geophys. Monogr. Ser.*, vol. 30, edited by E. W. Hones, p. 92, AGU, Washington, D. C., 1984.
- Wu, C. C., MHD flow past an obstacle: Large-scale flow in the magnetosheath, *Geophys. Res. Lett.*, **19**, 87–90, 1992.
- Wygant, J. R., R. B. Torbert, and F. S. Mozer, Comparison of S3-3 polar cap potential drops with the interplanetary magnetic field and models of magnetopause reconnection, *J. Geophys. Res.*, **88**, 5727, 1983.
- Zwan, B. J., and R. A. Wolf, Depletion of solar wind plasma near a planetary boundary, *J. Geophys. Res.*, **81**, 1636, 1976.

B. J. Anderson, The Johns Hopkins University Applied Physics Laboratory, Johns Hopkins Road, Laurel, MD 20723-6099. (e-mail: anderson@ampte.span.nasa.gov)

S. A. Fuselier, Lockheed Palo Alto Research Laboratory, Palo Alto, CA 94304.

T.-D. Phan, Space Science Laboratory, University of California, Berkeley, CA 94720-7450.

(Received August 30, 1996; revised November 15, 1996; accepted January 8, 1997.)